Titre: Title:	Calibration of Machine Tools Using on Machine Probing of an Indigenous Artefact
Auteur: Author:	Md Mizanur Rahman
Date:	2016
Type:	Mémoire ou thèse / Dissertation or Thesis
Référence: Citation:	Rahman, M. M. (2016). Calibration of Machine Tools Using on Machine Probing of an Indigenous Artefact [Ph.D. thesis, École Polytechnique de Montréal]. PolyPublie. https://publications.polymtl.ca/2129/

UNIVERSITÉ DE MONTRÉAL

CALIBRATION OF MACHINE TOOLS USING ON MACHINE PROBING OF AN INDIGENOUS ARTEFACT

MD MIZANUR RAHMAN

DÉPARTEMENT DE GÉNIE MÉCANIQUE

ÉCOLE POLYTECHNIQUE DE MONTRÉAL

THÈSE PRÉSENTÉE EN VUE DE L'OBTENTION

DU DIPLÔME DE PHILOSOPIAE DOCTOR

(GÉNIE MÉCANIQUE)

AVRIL 2016

UNIVERSITÉ DE MONTRÉAL

ÉCOLE POLYTECHNIQUE DE MONTRÉAL

Cette thèse intitulée :

CALIBRATION OF MACHINE TOOLS USING ON MACHINE PROBING OF AN INDIGENOUS ARTEFACT

présenté par : RAHMAN Md Mizanur

en vue de l'obtention du diplôme de : Philosophiae Doctor

a été dûment accepté par le jury d'examen constitué de :

M. BIRGLEN Lionel, Ph. D., président

M. MAYER René, Ph. D., membre et directeur de recherche

M. BARON Luc, Ph. D., membre

M. VELDHUIS Stephen, Ph. D., membre externe

DEDICATION

To my dearest "grandparents", my parents and my little sister

ACKNOWLEDGEMENTS

I would like to express my profoundest gratitude to my research supervisor Professor René Mayer, for his invaluable advice, guidance, support and time (no matter what) whilst encouraging me to pursue my own ideas, allowing me work independently and guiding me at each and every difficult situation throughout all these years. His active research work, ideas, ingeniousness and research methods helped me to complete this research work successfully. He has always been an inspiration to me in all aspects of my life for his wisdom, kindness and trust.

My sincere thanks to the professor Marek Balazinski and Jean-François Châtelain for their valuable advices and suggestions.

I greatly acknowledge Professor Luc Baron, Lionel Birglen and Stephen Veldhuis for the time devoted to evaluate my thesis and for their acceptance to participate in the jury.

I acknowledge the National Science and Engineering Research Council of Canada (NSERC), the Consortium for Research and Innovation in Aerospace in Quebec (CRIAQ), Pratt & Whitney Canada, Meloche Group and SONACA Montreal for their financial support.

I would like to thank Mr. Guy Gironne, Vincent Mayer and François Ménard for the experimental support at Virtual Manufacturing Research Laboratory (LRFV), Ecole Polytechnique de Montreal throughout the completion of this research work.

I would like to thank my colleague, friend and office-mate Mahdi Sabaghi for his constant suggestions, encouragement and assistance. I also express my sincere thanks to Anna Los, Mehrdad Givi, Elie Bitar-Nehme, Maryam Aramesh, Yang Lian Cai, Sebastien Salor, Elisabeth D. Richard and Rachid Guiassa for their friendship, encouragement, suggestions and help during all these years.

A very special thanks to my century old grandfather who always encouraged and supported me for the entire time of this work.

RÉSUMÉ

Les centres d'usinage cinq axes avec deux axes rotatifs facilitent la production des pièces complexes grâce à la capacité de positionnement et d'orientation de l'outil par rapport à la pièce en cours d'usinage. Cependant, le centre d'usinage est vulnérable à de nombreuses sources d'erreurs. L'inspection périodique du centre d'usinage est un élément clé pour obtenir la pièce finie souhaitée dans les limites de tolérances. Les méthodes d'inspection existantes nécessitent un personnel qualifié, un montage spécial et un temps additionnel pour installer les équipements. Par conséquent, l'objectif de cette thèse est de surmonter ces contraintes et développer une nouvelle méthode pour estimer les erreurs paramétrique inter- et intra-axes par palpage d'un artefact indigène directement sur le centre d'usinage. Les palpeurs de déclenchement tactile sont utilisés pour mesurer des facettes de la table de la machine-outil. Un modèle mathématique a été développé pour modéliser les erreurs d'installation de la sonde et des artefacts afin d'enlever leurs effets lors du processus d'étalonnage. Le temps d'étalonnage est de 1 heure et 30 minutes.

La validation de cet étalonnage est effectuée en comparant l'artefact du modèle estimé avec les mesures du même artefact obtenu par mesurage sur une Machine à Mesurer Tridimensionnelle (MMT). La capacité de prédiction des erreurs volumétriques du modèle est également validée en prédisant la position de la touche du stylet dans le repère de la pièce usinée pour d'autres facettes sondées pour fin de validation seulement, et les comparer avec les données mesurées par MMT. La distance résiduelle maximale entre l'artefact prédit par le modèle et l'artefact estimé par le MMT est 139.50 µm sans aucun paramètre estimé, et 6.92 µm avec 86 inter- et intra-axes paramètres estimés par le modèle.

La technique de calibration proposée est appliquée au centre d'usinage intégré avec des tables de formes prismatique et sphérique (Mitsui Seiki HU40T et Huron KX8-five). Un schéma est proposé pour examiner les performances de la machine au cours d'une journée et entre les jours. La qualité du schéma est validée avec les incertitudes des paramètres calibrés venant de la covariance de l'ensemble des résultats de cycles de mesures effectuées pendant des jours consécutifs.

La performance de l'étalonnage est évaluée en examinant la répétabilité de la mesure de la sonde de l'artefact indigène étalonné en fonction de la stratégie de sondage de l’artefact, l’indexation des axes rotatifs, les incertitudes de paramètres et le cycle de montage et démontage de l’artefact.

Une nouvelle technique de mesure avec une sphère unique pour machines cinq axes est proposée pour évaluer directement sur les centres d’usinage leur capacité à prendre des mesures de position. Des facettes, sur une sphère de précision, sont mesurées pour des mouvements des cinq axes et ces mesures exprimées dans le référentiel de la table utilisant le modèle nominal sans erreurs puis le modèle estimé. Les défauts de sphéricité calculés sont analysés pour évaluer les performances de la machine. Les défauts de sphéricité d'un modèle non compensé et compensé sont 268.27 µm et 60.51 µm (HU40-T). Enfin, les performances du processus sont également étudiées en fonction du changement du statut de la machine, la surface mouillée de l’artefact, les irrégularités de surface et la répétabilité de la sonde de déclenchement tactile.

ABSTRACT

Five-axis machine tools with two rotary axes facilitate the production of intricate parts due to the position and orientation capability of the tool with respect to the workpiece but this flexibility also renders the machine tool vulnerable to numerous sources of error. Periodic inspection is the key to obtain finished part within the prescribed tolerance limits. Existing machine tool inspection methods require trained personnel, special setups and additional time to setup the test equipments. Therefore, the aim of this thesis is to overcome these limitations and develop a new method to calibrate inter- and intra-axis error parameters by on-machine probing of an indigenous artefact. A touch trigger probe is used to measure facets on the existing machine tool table. A mathematical model is developed to model the probe and the artefact setup errors and remove their effects from the estimation process. The calibration time is 1 hour and 30 minutes.

The validation of the calibration is done by comparing the model estimated artefact with the Coordinate Measuring Machine (CMM) measured artefact. The volumetric error prediction capability of the model is also validated by predicting the stylus tip positions in the last workpiece branch frame (rigidly connected to the machine table frame) for each facet probing and comparing them with the CMM measurements. The maximum residual distance between the model predicted artefact and CMM artefact is 139.50 μm with no parameters estimated and 6.92 μm with 86 inter- and intra-axis parameters estimated.

The proposed calibration technique is applied to the machine tools integrated with prismatic and cylindrical shape tables (Mitsui Seiki HU40T & Huron KX8-five). A scheme is proposed to investigate the machine performance throughout a day and between days supported by the uncertainties of the calibrated parameters estimated from the pooled covariance of the repeated measurement cycles performed for consecutive days.

The calibration performance is also evaluated by investigating the repeatability of the uncalibrated indigenous artefact probing against artefact probing strategy, rotary axes indexations, parameters' uncertainties and artefact dismount and remount cycle.

Finally, a new technique using a single ball measurement in five-axis is proposed to assess the on machine coordinate measurement capability of the machine tool. Facets on a precision sphere are measured for five-axis positioning and expressed in the machine table frame using in turn nominal and compensated machine models. The out of sphericity of the calculated sphere is analysed to assess the performance of the machine tool. The out of sphericity of the uncompensated and compensated models are 268.27 μm and 60.51 μm respectively (HU40-T). The effects of the machine tool's status change, artefact's surface wetness, surface irregularities and repeatability of the touch trigger probe are also investigated.

TABLE OF CONTENT

LIST OF TABLES

LIST OF FIGURES

LIST OF SYMBOLS AND ABBREVIATIONS

The list of symbols and abbreviations are used in the thesis in alphabetical order along with their meanings.

CMM	Coordinate Measuring Machine
HTM	Homogeneous Transformation Matrices
RUMBA	Reconfigurable Uncalibrated Master Ball Artefact
SAMBA	Scale And Master Ball Artefact
TANGO	Touch ANd GO
CNC	Computer Numerical Control
1D	One Dimensional
2D	Two dimensional
3D	Three dimensional

CHAPTER 1 INTRODUCTION

Manufacturing industries involving metal removal processes are desired to obtain geometrically accurate finish parts within the design tolerance. In order to achieve dimensionally conform part, accuracy of the machine tools is a prior concern to the manufacturer hence periodic inspection is essential. Five-axis machine tools with two rotary axes provide enormous flexibility to fabricate complex geometric parts with a reduced number of setups and higher precision. The downside is the rotary axes bring further sources of errors. Direct calibration techniques attempt to measure the individual error sources. Laser interferometer, electronic level, autocollimator, dial gauge etc. are the most widely used instruments for direct calibration. For the linear axes it is comparatively easy to estimate the error parameters whereas for the rotary axes it is more difficult. Moreover, the estimation process is time consuming, requires trained personnel and is sometimes too difficult to conduct. To avoid these complexities, researchers pursued indirect calibration techniques.

In 1972 David McMurty invented the touch trigger probe (Renishaw plc - 2015) which was only used on CMMs but later on integrated to machine tools as an interchangeable device with the cutting tool mounted in the machine's spindle. Hence, machine tool programmers exploit this device to locate the workpiece prior to the machining operation. Over time indirect calibration techniques have utilized the touch trigger probe for calibration purposes. Indirect approaches measure the combined effect of multiple error sources and use mathematical models to estimate the individual error sources. Indirect approaches have involved either calibrated or uncalibrated artefacts measurements or special instruments (double ball bar) to gather machine's geometric information. Aside from the artefact measurements by touch probe, ball bar is one of the most popular devices that is used for indirect calibration.

Numerous research work has been carried out to calibrate five-axis machine tools in an indirect manner in the past decades (Bringmann and Knapp 2006; Hong and Ibaraki 2013; Ibaraki, Iritani et al. 2012; Lei and Hsu 2002; Mayer 2012; Weikert and Knapp 2004). R-test device, RUMBA or SAMBA technique, 3D probe ball artefact, test piece measurement, non-contact R-test, 2D ball plate artefact, model based chase-the-ball etc. used artefacts and some techniques involve double ball bar device (Abbaszadeh-Mir, Mayer et al. 2002; Zargarbashi and Mayer 2006).

All these research work require artefacts or instruments (externally brought into the machine tool), operator intervention and most cases trained personnel.

1.1 **Problem definition**

Minimizing the production down time, high quality product with accurate geometric dimension, rapid and automated inspection have always been a challenge to the manufacturer thus periodic but automated inspection of the machine tools is needed. Existing inspection techniques involve artefacts/instruments attachment within the machine's working envelop. The artefacts/instruments setup requires time, their handling and storing can be costly, and trained personnel may be required during the inspection process. Consequently, the inspection process no longer remains automated; this increases the chances of human error occurrence. Moreover, handling the artefacts or instruments may require special care causing additional expenses. Additional artefact can also add undesirable geometric errors therefore the question remains, is it possible to calibrate inter- and intra-axis errors of machine tools without human intervention in an automated manner?

The answer to this question involves the following elements:

- an error model to identify the inter- and intra-axis error parameters of five-axis machine tools;
- a technique or strategy to gather machine geometric information, which can be used in the error model to calibrate the parameter, that is fully automated;
- a procedure to validate the proposed error estimation process;
- variables that might influence the calibration quality;
- scheme to evaluate machine tool's measuring performance utilizing the proposed calibration approach;
- repeatability of the calibration performance.

1.2 **Research objectives**

General objective

The substantial drawback in the existing calibration techniques is that, they require brought-in artefacts or special instruments thus hindering the automation of the process. The main objective of this thesis is to "develop a calibration technique by on machine probing of an uncalibrated indigenous artifact in order to rapidly obtain the machine parameters in an automated manner".

Specific objectives

a) Use an existing error model to identify inter- and intra-axis error (link and motion error) parameters by on-machine probing of an uncalibrated indigenous artefact.

Use an error model based on homogeneous transformation matrices to use facet probings on existing machine tool's features considered as indigenous artefact. Facets are distinct features with nominal locations and local nominal normals. Actual position and orientation of the facets are unknown.

b) Propose artefact probing strategy to gather machine tool's data for calibration and artefact geometry estimation.

To gather machine tool data faster and efficiently, different artefact probing strategies need to be studied. The number of measurement points should be greater than the number of unknowns and the probing strategies should be optimized to limit the time taken.

c) Justify the error model and artefact probing strategy by simulation against the numerical stability of the estimation.

Error model and artefact probing strategies need to be numerically validated. The mathematical quantity called condition number[1] of the sensitivity matrix (Jacobian) is observed. Ideally the value is 1 to infinity for a singular matrix.

[1] The idea of the **condition number** was suggested by Wolfgang Knapp during a conversation with Professor Mayer and validated numerically in this work

d) Perform calibration, validate through artefact estimation and model's volumetric position prediction capability.

A well-defined artefact probing strategy with an extensive error model is sought based on the simulated results followed by CNC programming. Artefact measurements provide rich information about the machine tool's geometry for calibration. CMM measurements of the artefact and the estimated artefact can be compared for the validation purposes. Predicted tool position obtained from the estimated model can also be compared with the CMM measurements for additional validation.

e) **Investigate the machine tool's performance for coordinate measurements.**

Calibration results can be used to investigate the machine tool's coordinate measurement performance. Facets on a precision sphere can be measured and data can be analyzed by both the nominal and the calibrated machine model.

f) Evaluate the robustness of the calibration.

Repeatability of the proposed calibration method can be investigated against calibration process variables such as: probing strategies, rotary axes indexations, artefact dismount and remount cycle.

1.3 Hypothesis

a) **A local artifact measurement data can provide the necessary machine tool information to estimated inter- and intra-axis parameters**.

Five-axis machine tool has built-in machine tool table or fixtures that are typically used to attach the workpiece for the machining operation. These table or fixtures can provide necessary machine tool data for calibration.

b) Surface form errors of the artefact have little or no influence on the calibration quality.

The error model is independent to the geometric shape of the artefact since the probing involves measuring facets in a considerably small area where the variation of the shape is negligible.

c) Position and orientation of the artefact is only nominally known.

Actual artefact may depart from nominal values due to the effect of the machine errors and artefact geometric errors. Hence the sensitivity of the probe stylus tip to the artefact is projected along the nominal normal direction.

d) **Constraining the artefact degree of freedom at each machine pose is required to have better estimation**.

To gather machine tool data, the artefact is required to be measured at different machine tool's axes combinations (or at different pose) and at each such pose, artefact's degree of freedom needs to be metrologically constrained i.e. the distribution of the measurement points should be similar to a kinematic set of constraints blocking all six degrees of freedom.

CHAPTER 2 LITERATURE REVIEW

2.1 Introduction

Five-axis machine tool provides better positioning, higher accuracy at higher machining speed with minimum number of setups due to its position and orientation capability of the tool with respect to the workpiece. Geometric errors related to the rotary axes are very difficult to estimate using existing instruments. Additionally, dynamic errors of the rotary axes adds new challenge to the metrologist. Many works in the literature can be found that focused on the linear axes error estimation and different instruments are successfully applied to compute these errors directly. But the interdependent rotary and linear axes errors, axis location and positioning errors of rotary axes still remains a challenge for high speed precision machining. Proper error modelling is required to estimate the error parameters when the calibration is done indirectly. Prior to the error modelling, knowledge of the nature and sources of the errors are important. At the beginning of this section, different types of machine tool errors and their sources will be discussed. Later on, existing calibration approaches will be addressed followed by the inaccuracies induced by the measuring instrument and parameters' uncertainty. Finally a brief conclusion clarifying the limitations of the existing methods will be discussed.

2.2 Errors in machine tool

In a geometrically perfect machine tool, the position and orientation deviation of the tool with respect to the workpiece is zero. But in reality, it is likely impossible to find a geometrically perfect machine tool. Temperature changes, gravitational force of the components, fixtures, workpiece and the motion of the axes yield inaccuracies. For five-axis machine tools, rotary axes provide additional geometric complexities thus machine tools are susceptible to numerous error sources. Some errors are position independent known as link errors or inter-axis errors and some are position dependent known as motion errors or intra-axis errors. Inter-axis error describes the relative position and orientation deviation of the machine's successive joints (prismatic and rotary) which includes joint misalignments, angular offsets and rotary axes separation. Intra-axis error describes the erroneous motion of the machine joints such as scale gain errors, straightness

errors, roll, pitch and yaw of the linear axes and angular positioning errors, tilt errors, radial and axial errors of the rotary axes (Abbaszadeh-Mir, Mayer et al. 2002). Therefore, in the actual machine tools, the combined effects of inter- and intra-axis errors yield position and orientation deviation of the tool with respect to the workpiece. Such deviation is known as the volumetric error (Figure 2-1).

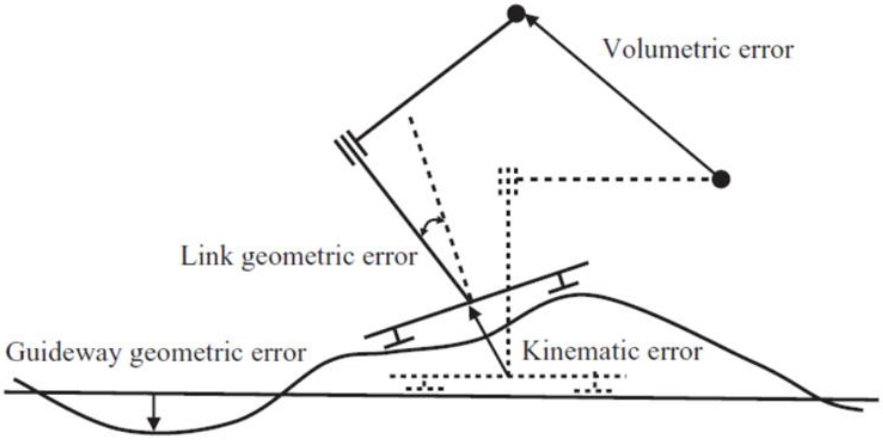

Figure 2-1 Machine error of an X–Y machine with magnified errors on the X-axis guide way (Ekinci and Mayer 2007)

2.2.1 Inter-axis errors

Inter-axis errors or the axis location errors are the deviations of the axes average line from its nominal position and orientation. Rotary axes have five inter-axis errors: two positioning errors, two orientation errors and one zero angular positioning error as shown in Figure 2-2. The linear axes have two orientation errors and one zero positioning error (Figure 2-2).

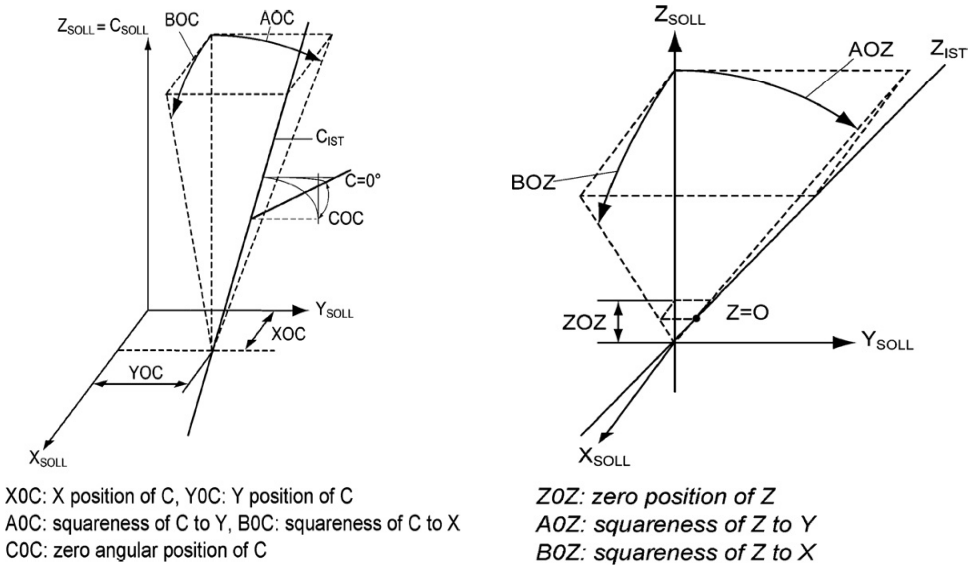

Figure 2-2 Inter-axis errors of C axis (rotary) and inter-axis errors of Z axis (linear) (Schwenke, Knapp et al. 2008)

2.2.2 Intra-axis errors

The intra-axis errors are also known as the motion errors. They describe the deviation of an axis from its perfect motion. Linear axes have six intra-axis errors which include two straightness errors, one positioning error, one pitch, one roll and one yaw error. Rotary axes have two radial errors, two tilt errors, one axial and one angular positioning error (Figure 2-3).

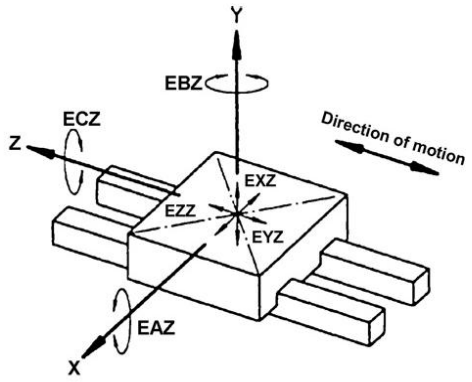

EXZ: horizontal straightness error motion of Z (straightness error motion of Z in X direction)
EYZ: vertical straightness error motion of Z (straightness error motion of Z in Y direction)
EZZ: positioning error
EAZ: pitch error motion of Z (tilt error motion around X)
EBZ: yaw error motion of Z (tilt error motion around Y)
ECZ: roll error motion

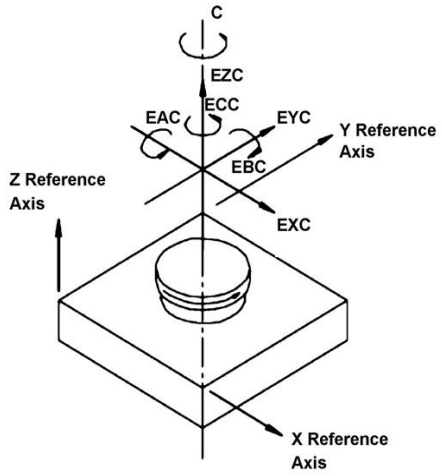

EXC: radial error motion of C in X direction
EYC: radial error motion of C in Y direction
EZC: axial error motion of C
EAC: tilt error motion around X of C
EBC: tilt error motion around Y of C
ECC: angular positioning error

Figure 2-3 Intra-axis errors of linear (Z-axis) and Rotary (C-axis) axes (Schwenke, Knapp et al. 2008)

2.2.3 Thermally induced errors

When machine tools are in operation, heat is generated by the moving elements and causes expansion to the different structural elements. The expansion creates geometric deviations of the tool location with respect to the workpiece. Bearing, gear and hydraulics, drives and clutches, pumps and motors, guide ways, cutting action and swarf, external heat source etc. are significant sources of heat causing thermal error.

2.2.4 Error induced by cutting force

During machining, force created by the cutting operation may propagate through different machine tool causing elastic deviations. The deformation in the machine tool's structure induced by cutting force causes dimensional and form errors in the machined part and tool wear affects the dimension of the machined part. The components of the machine tools under load considered as Elastically Linked System (ELS) in order to observe the individual deformation of any particular components (Archenti and Nicolescu 2013).

2.2.5 Error due to the machine load

Depending on the size, position and weight of the workpiece in the machine tool's working volume, the geometry of the machine tool can be altered (Schwenke, Knapp et al. 2008).

2.2.6 Fixturing errors

Location of the workpiece on the fixture and the flexibility of the fixture cause fixturing errors. Position of the fixturing elements, clamping sequence, clamping intensity, type of contact surfaces etc. can cause workpiece displacement (Ramesh, Mannan et al. 2000).

2.3 Inter- and intra-axis error calibration approaches

To calibrate five-axis machine tools, both direct and indirect approaches have been sought. Direct techniques required special instruments and precise setups along with specially trained personnel. The investigation process is sometimes arduous and time consuming which increases the production down time. Thus, indirect methods are becoming more popular for five-axis machine tool calibration. Since most of the five-axis machine tools are equipped with touch trigger probe, researchers are pursuing strategies to utilize the touch probe to gather necessary machine tool data for calibration.

2.3.1 Direct aproaches

Direct calibration involves the mechanical error measurement of a single axis without the involvement or influence of the other axes (Schwenke, Knapp et al. 2008). Straight edges, line scales, step gauges, squares, precision levels, slip gauge etc. are the most common calibration instruments for the errors associated with the prismatic axes and dial gauges and autocollimators can be used to measure the rotary axes errors. The following subsections will discuss the direct measuring techniques of linear axis positioning errors, such as straightness errors, angular errors and squareness errors, as well as the rotary axes errors.

2.3.1.1 Positioning errors measurement

Laser interferometer is the most widely used instrument to compute positioning errors. Gauge blocks, step gauges, line scales, calibrated scales or encoder systems can also be used. In interferometric techniques, linear positioning errors are converted into wavelength measurements. Figure 2-4 shows a typical laser interferometer technique for positional error measurements. The laser interferometer is aligned with the axis to measure the positioning error. The laser beam emitted from the leaser head (1) is split into two beams at the beam splitter (2). The beams are then reflected by the two retro reflectors (3) and recombined at the beam splitter before reaching the detector (Figure 2-4). The phase changes between these two beams provide the displacement of the axis in motion.

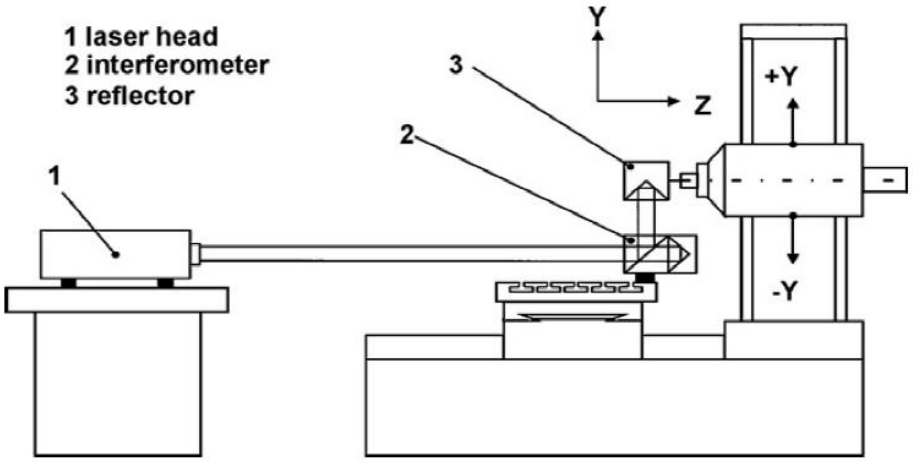

Figure 2-4 Laser Interferometer for positioning accuracy measurement (Schwenke, Knapp et al. 2008)

2.3.1.2 Straightness error measurement

Straightness errors are the lateral displacement along the axis motion. This is a motion error since the lateral displacement depends on the position of the corresponding axis. A straightness reference, such as a straightedge aligned with the average axis motion, and a dial indicator are typically used to measure the straightness error of an axis. As the axis moves, the dial indicates. The lateral displacement can also be measured using a capacitance or other proximity electronic

gauge. Alternately, a Wollaston prism and a roof reflector prism can be used with the laser interferometer to build a straightness interferometer (Figure 2-5). The prism splits the incoming laser beam into two separate beams at an angle. The beams are then reflected by the straightness reflector and recombined to generate an interference signal that allows to determine the lateral displacement (Schwenke, Knapp et al. 2008).

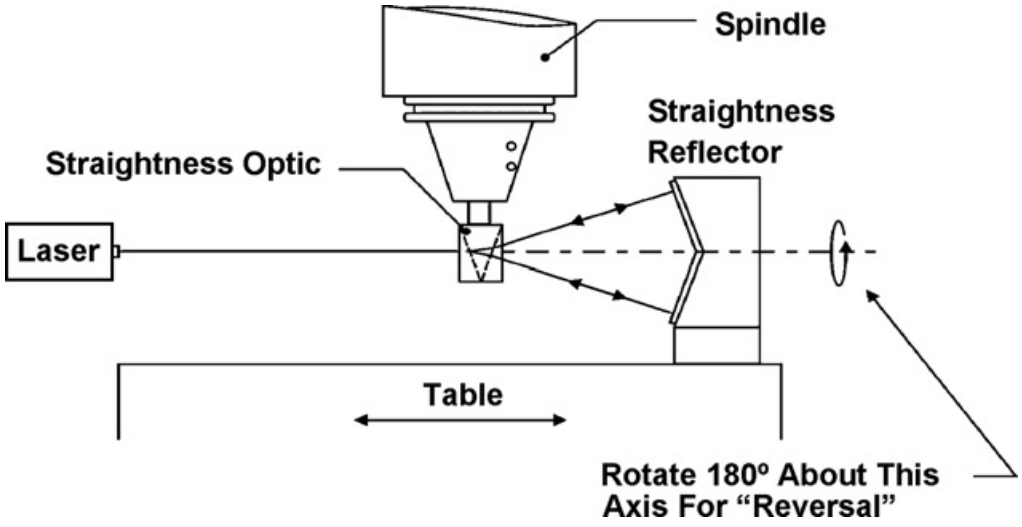

Figure 2-5 Straightness interferometer with a Wollaston prism (Schwenke, Knapp et al. 2008)

2.3.1.3 Angular error measurement

Angular errors can be measured by interferometry using an angular interferometer. In an angular interferometer, the source laser beam is split into two parallel beams both reflected by a separate retro reflector (Figure 2-6). The path variation of the beams results from the angular deviation of the linear axes. An autocollimator can also be used to measure the angular motion error. In an autocollimator, a light beam is aligned with a mirror attached to the machine tool`s moving axis (Schwenke, Knapp et al. 2008).

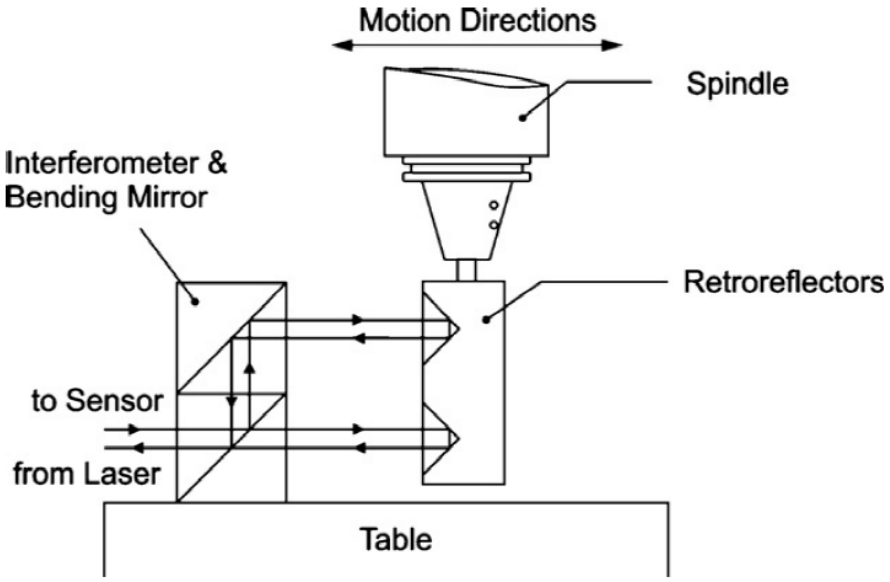

Figure 2-6 Angular Interferometer (Schwenke, Knapp et al. 2008)

2.3.1.4 Rotary axes error measurement

ISO 230-1 (ISO 2012) proposed a technique that involves dial gauge to measure the radial and the axial offsets of the rotary axes in a direct fashion. Capacitive or inductive sensors can also be used to measure these offsets. Two sensors are used to measure two radial error motions of the rotary axes by placing them along the respective axis directions. To measure the axial error motion, one sensor is placed in the center of the front surface of the rotary axes (Schwenke, Knapp et al. 2008).

2.3.2 Ballbar test

Ballbar is one of the most widely used device to have a quick snapshot of the machine tool's performance. Ball bar test provides graphical representation of the machine tool's behavior and allow the users to take corrective actions. In a ball bar test, one of the two precision magnetic sockets is attached to the machine tool table and the other to the machine spindle. A telescoping linear sensor with precision balls at each end is attached to the sockets. The distance between the two balls are precalibrated and known. Then a circular path is followed using the axis command of the machine tool where the ball connected to the spindle is considered as the center of the

circle and the other ball mounted on the machine table follows a circular path. The length of the ball bar measured as the radius of the circle. Ideally the circular path should form a perfect circle but due to the machine tools errors the table moves away from the programmed radius and create different pattern as shown in Figure 2-7 (Ballbar 1999-2009). These test patterns provide the necessary information about the eccentric behavior of the machine tools or the type of errors that the machine tool is suffering from. For example, if the circular test of a machine tool has a pattern like Figure 2-7 (top left) where there are inward or outward steps toward or from the center of the plot, it means that the machine is experiencing a jump in motion when the direction of motion is changing. This represents the backlash error of the machine tool. Negative backlash causes inward steps and positive backlash causes outward steps in the circular test. The backlash error can be due to the play in the guide ways or the drive system, the encoder hysteresis or a worn ball screw. Hence, the operator must check the machine backlash compensation, check if the machine is affected by the encoder hysteresis, remove the play in guide ways or drive system or check the possible wear in ball screw or guide ways.

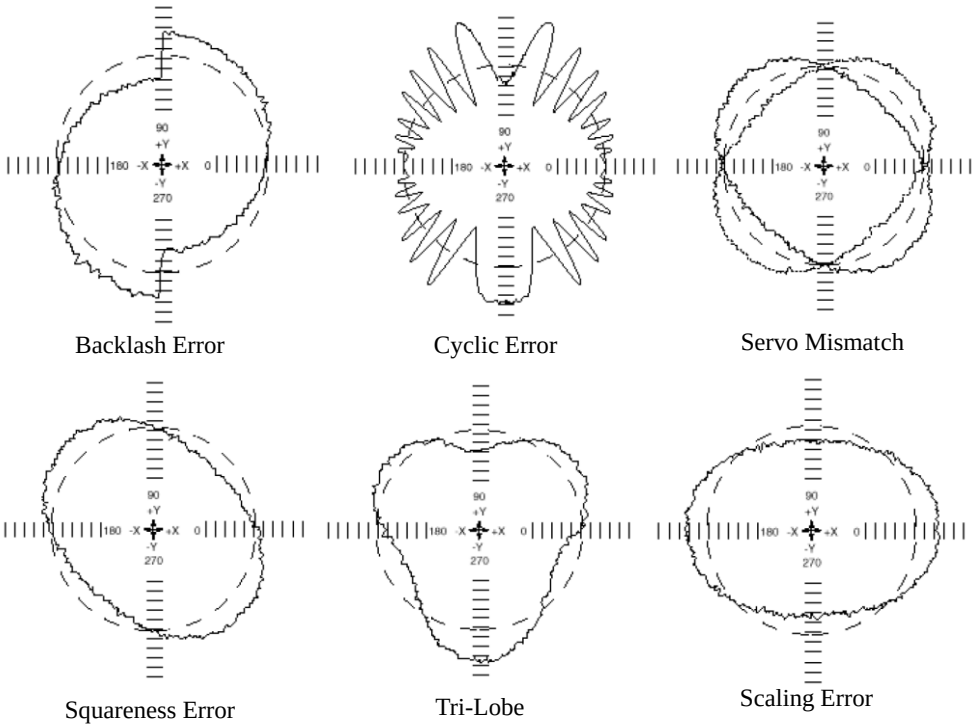

Figure 2-7 Machine behavior observed from a ball bar measurement (Ballbar 1999-2009)

Even though the ballbar test provides enormous information about the machine tool's eccentric behavior there are still geometric and motion error parameters remains uncalibrated for both rotary and linear axes which might significantly influence the accuracy of the machine tools.

2.3.3 Indirect approaches

In this section, existing indirect calibration approaches for five-axis machine tool will be discussed followed by the inaccuracies added by the measuring instruments and the uncertainties of the estimated parameters.

Schwenke et al. reviewed the indirect calibration techniques which involve partially or totally uncalibrated artefacts, ball bar and calibrated artefacts for the measurements for CNC machine tool. The authors suggested that the identification of the geometric errors through a proper error modeling, geometric data acquisition strategy and proper validation is required for this type of inspection. Considering the rigid body kinematics, these models can be based on the following hypotheses: for linear axes, six components errors and three location errors, and for rotary axes, six component errors and five location errors (Figure 2-2 and Figure 2-3) since these component and location errors cause the volumetric deviation in the machine tools (Schwenke, Knapp et al. 2008). Srivastava et al proposed a volumetric error model induced by the propagation of both scalar and position dependent geometric errors and time dependent thermal errors. The authors used small angle approximations considering the shape and joint transformations for inaccurate links and joints. The authors concluded that, the angular deviations are independent from the translational errors but the deviations of the tool point are dependent on rotational and translational errors. Authors also suggested that, CNC compensation for X-, Y- and Z- are possible based on simulated results (Srivastava, Veldhuis et al. 1995). Later on, Veldhuis and Elbestawi proposed a neural network model to compensate the errors induced by the thermal and axis motion change. Machine geometric data was obtained by ball bar measurements (Veldhuis and Elbestawi 1995).

Suk-Hwan et al. (Suh, Lee et al. 1998) proposed an error model based on homogeneous transformation matrix and compensation algorithm for rotary axes errors. A homogeneous transformation matrix carries the information of the rotational and translational deviation of the

machine tool axes. A polygon mirror with 12 faces at every 30° and two autocollimators (Figure 2-8) is used to measure the rotational error of the rotary table. For the translational errors, a master ball and three linear variable differential transformers (LVDTs) are used. The compensation algorithm modify the CL-data using the error model and the measured rotational and translational errors.

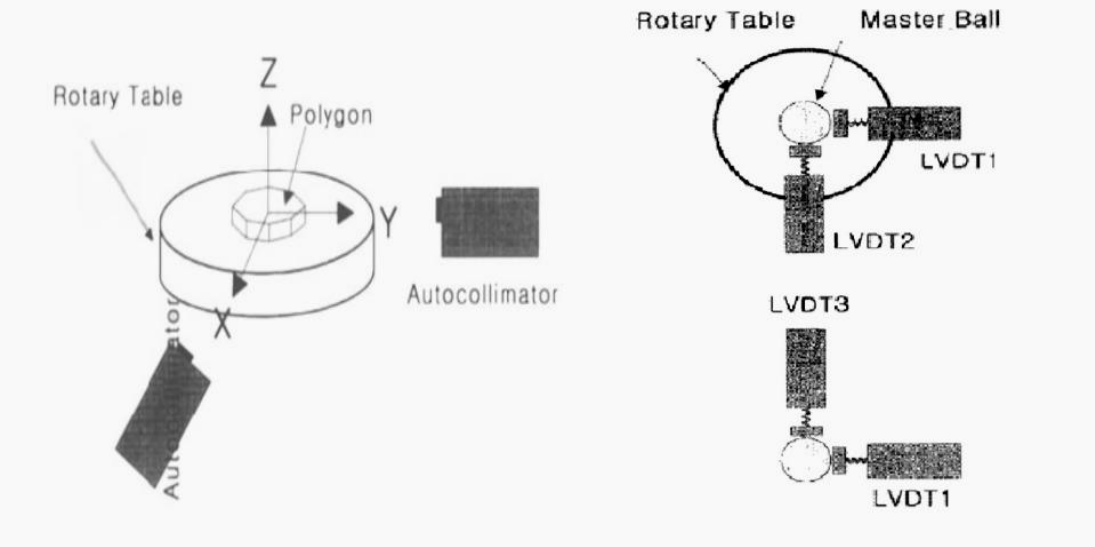

Figure 2-8 Polygon and autocollimator (left); Master ball and LVDTs (right) (Suh, Lee et al. 1998)

For the verification of error model and compensation algorithm, a ball table with 12 master balls of 18 mm diameter are manufactured and attached to the rotary table while the center of the rotary table considered as the origin of the ball table. A touch probe is then used to measure one surface point on each master ball at different rotary table indexations and the machine tool data is recorded to find the error components of the rotary table. Based on the rotational and translation errors, the surface point measurements are then analyzed to verify the error model and compensation algorithm. The authors claimed that, the precision of the rotary table can be improved by the developed algorithm but the misalignment of the ball table and the rotary axis is avoided which can be a greater sources of inaccuracy. Thus, a good error model includes the minimum number of machine error parameters which explains the maximum volumetric deviation. Abbaszadeh-Mir et al. developed a method based on the mathematical analysis of

singularities of the linear system to identify the minimum number of inter-axes error parameters to calibrate five-axis machine tools (Abbaszadeh-Mir, Mayer et al. 2002). The authors demonstrated the effectiveness of the method to identify the inter-axis error parameters accurately through numerical simulations. Forward kinematic model is used to calculate the position of the tool relative to the workpiece. Based on (Everett and Suryohadiprojo 1988), a machine model is constructed then the minimal set of inter-axis error parameters are selected. Simulated data is obtained from a telescoping magnetic ball-bar measurements used to support the parameter selection.

Mir et al. used Chebyshev polynomials to model inter- and intra-axis error parameters and compute the errors associated with the tool tip for a given command location. The authors proposed an approach to verify the machine tool's capability to produce a part within the desired tolerance while the influences of the inter- and intra-axis error parameters are considered. The effect of inter- and intra-axis errors on the tool path data is demonstrated for a curve and a surface profile. CAD/CAM system (e.g. CATIA) is used to generate the cutter location (CL) data for the tool path of the curve and surface profiles and a post-processor generates the machine axis commands based on its nominal inverse kinematics. The polynomial functions are then used to calculate the corresponding inter- and intra-axis errors. Forward kinematic error model is used to predict the tool path in the form of curve or surface profile (Mir, Mayer et al. 2002).

According to (Abbaszadeh-Mir, Mayer et al. 2002) eight parameters are required to define the geometry of five-axis machine tools in space. Thus, Tsutsumi et al. (Tsutsumi and Saito 2003) developed a method to estimate and compensate these eight inter-axis error parameters through exploiting the relative displacement between the tool and the workpiece measured by a telescoping ball bar system. The measurement involves only three axis motion including a rotary axis. Four measurements are required for the precise evaluation of the deviations and eccentricities of a circular arcs, afterwards, the authors proposed a calibration method for inter-axis parameters based on simultaneous control of four axes of five-axis machine centers with a tilting rotary table (Tsutsumi and Saito 2004). Two prismatic axes and both rotary axes are moved simultaneously. The first four of the eight inter-axis parameters are identified and computed from the observation equations while the observations are made using double ball bar.

The remaining four parameters are geometrically calculated. Zargarbashi et al. proposed a technique involving double ball bar measurements to estimate the intra-axis error parameters of the trunnion axes of five axis machine tools while only the trunnion axes moves for data acquisition. Five different ball bar configurations are obtained by a single set up and the ball bar positions remain unchanged in the work piece side (Figure 2-9) (Zargarbashi and Mayer 2006).

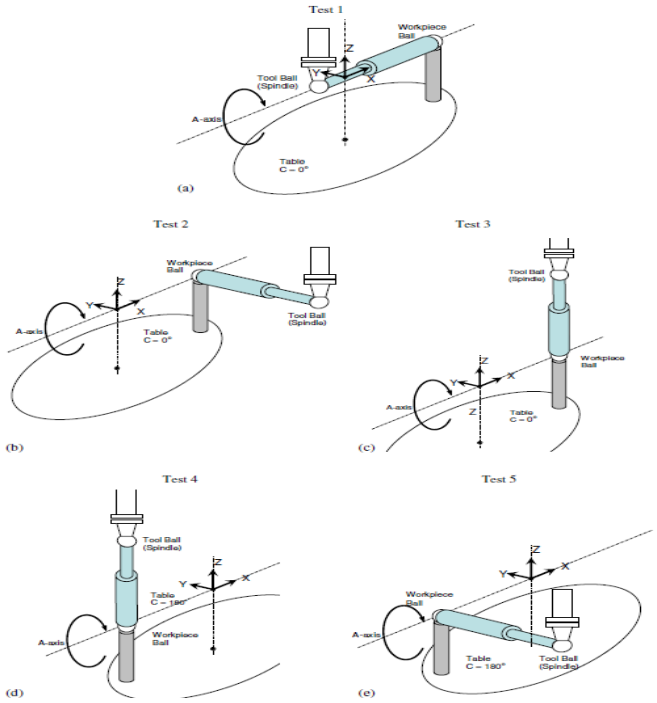

Figure 2-9 Ball bar configurations to estimate intra-axis errors of a trunnion axis (Zargarbashi and Mayer 2006)

In five-axis machine tools, rotary axes error parameters play an important role on the machining accuracy. Thus, Lei et al. proposed a method to measure intra-axis errors of the rotary axes using double ball bar measurements where three translational axes remains stationary and only the rotary axes are used to follow a particular circular path. The research concluded that, tracking speed of the double ball bar reflects the motion errors estimation quality. The servo mismatch of the two rotary axes was detected successfully (Lei and Hsu 2003). Later on, A National Aerospace Standard (NAS) proposed a scheme to test the machine's final performance by machining a cone frustum (NAS979 standard). The exact location of the cone frustum in the

machine's working envelop is not defined in the proposed method. Moreover, the influence of the machine errors on the geometric inaccuracy of the cone frustum is not covered. To understand this issue Uddin et al. proposed a simulator to analyze the effect of kinematic errors (inter-axis errors-relative location and orientation of the linear and rotary axes) on the machined cone frustum geometry. Kinematic model from (Tsutsumi and Saito 2004) was adapted and a similar error identification procedure is used. An error compensation model for the tool position and orientation is proposed to improve the machine tool's performance. Hong et al. demonstrated the influence of the error motions of the rotary axes on the geometric accuracy of the cone frustum. The authors analyzed the sensitivity of the circularity error of the cone frustum to the position dependent geometric error parameters of the rotary axes. The authors concluded that, angular positioning error of the rotary axis (C-axis) and the augmentation of the radial or the tilt error motions of the B-axis have critical influence on the circularity. On the other hand, the gravity-induced Z-direction deformation of the rotary axis and the radial or the tilt error motion of the C-axis have less influence on the circularity of the machined cone frustum (Hong, Ibaraki et al. 2011).

Hong et al. (Hong, Ibaraki et al. 2012) signified how the error motions of the rotary table change depending on the tilting axis by demonstrating some intuitive and graphical presentation of R-test measurements considering insignificant contribution of linear axis error motions and separation of the linear axes squareness errors. For the systematic geometric error correction and compensation, Khan and Chen (Khan and Chen 2011) proposed an efficient methodology capable of compensating the overall effect of intra- and inter-axis error parameters. To remove the effect of the machine errors from the tool path, recursive compensation methodology is used and NC codes are generated by the developed post processing software from the modified tool path which is directly fed to the machine controller. The cutter location (CL) data is obtained through CAD/CAM software and the tool path is generated. The machine tool's error information is used to generate a second cutter location data file. Later on, by defining the tool pose vector in the workpiece coordinate frame and the correction vector in the machine coordinate frame, the effect of machine tool's errors are removed and a new output code is obtained.

Zhu et al. proposed a new error identification model including six error components errors of the rotary axes. The proposed model integrates the geometric error model, error identification and compensation altogether into a software system where the geometric error data are the prerequisite and obtained from laser interferometer and ball-bar measurements. Using CAD/CAM system, the tool path is generated and converted into NC code. Later on, the NC code for machining operation is modified based on the geometric error data. Finally the actual tool tip position and orientation is modified to reach the desired position in an iterative manner (Shaowei, Guofu et al. 2012). Aside from all these approaches to estimate the inter- and intra-axis error parameters, some approaches gain higher popularity and some of them are already practiced in industry. In the following subsections, some well-known indirect calibration techniques will be discussed.

2.3.3.1 The 3D probe-ball

3D probe-ball is proposed for error modeling (Lei and Hsu 2002) and error estimation (Lei and Hsu 2002) of five-axis machine tools. A 3D probe is installed in the machine spindle and a base plate is installed on the machine table, a central ball is connected with the probe by an extension bar used to make contact with the base plate to create a close kinematic chain (Figure 2-10). The probe-ball device adapted the idea of the double ball bar and the three-dimensional measuring probe to measure the deviation of the relative position between the probe and the base plate. The deviation of the probe to the base plate is used in an error model which includes 59 machine tool errors as well as the linear positioning errors. Different test paths are defined (Figure 2-11) to make sure that all the machine tool axes move simultaneously to estimate the error parameters included in the model. The error model can also estimate the constant link errors of the rotary axis, main spindle and tool holder.

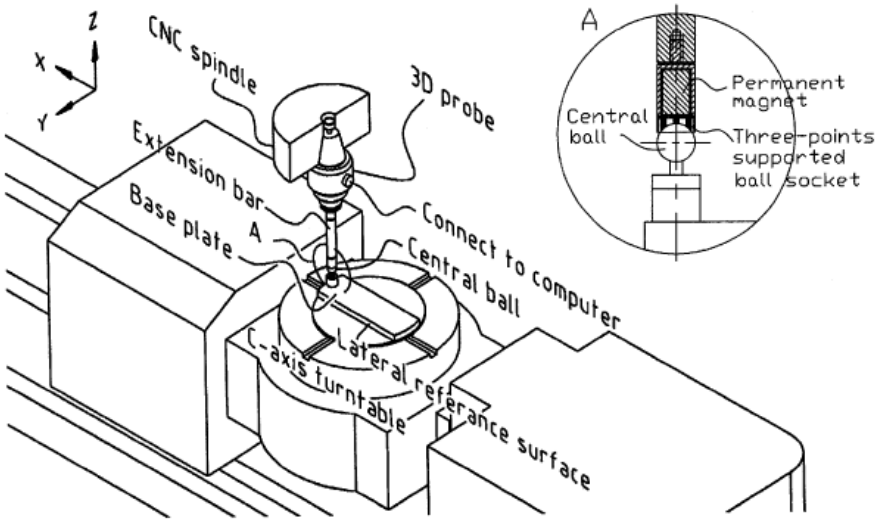

Figure 2-10 3D probe-ball for five-axis machine tool's accuracy test

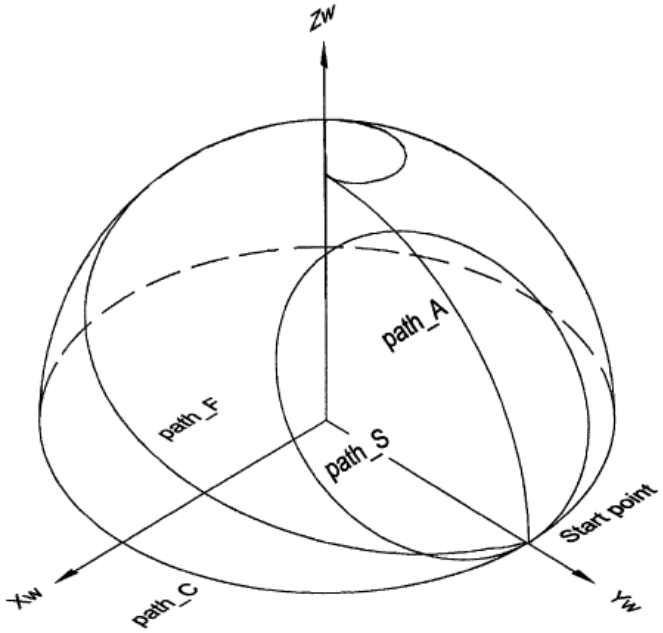

Figure 2-11 Proposed test paths for the 3D probe-ball device (Lei and Hsu 2002)

2.3.3.2 The R-test device

The R-rest device is developed by Weikert and Knapp to calibrate backlash, positioning, squareness and parallelism errors of the five-axis machine tools. In the proposed method, the

rotary axes are used in combination with the linear axes in order to achieve all the axes movements.

Figure 2-12 R-test device mounted on a five-axis machine tool (Weikert and Knapp 2004)

Three analogous incremental probes are mounted on the workpiece side to measure the 3D displacement deviations of a ceramic sphere of 28 mm diameter mounted on the tool holder (Figure 2-12). A circular path of 130 mm is measured both in clockwise and counter-clockwise directions while the machine tool's X-, Y- and C-axis move simultaneously. Z-axis displacement of 50 µm is used for both direction of motion and executed at 90° and at 630°. The method is in principle, similar to the 3D probe ball (Lei and Hsu 2002). The R-test device takes 20 minutes to evaluate the location of the rotary C- and A-axis and 42 geometric errors are measured for a parallel kinematic machine tool. Figure 2-12 shows the functional prototype of the device (Weikert and Knapp 2004).

2.3.3.3 Ball plate artefact

A measuring device was introduced by Bringmann et al. that allows to measure three dimensional deviations of X-, Y- and Z-axis to compute the relevant machine errors (Bringmann, Kung et al. 2005). The device is composed of a 2D ball plate and is used to create a pseudo 3D artefact. The

vertical position of the ball plate can be altered by using spacer which is kinematically coupled with the base plate. The ball plate can directly be used on the base plate (Figure 2-13).

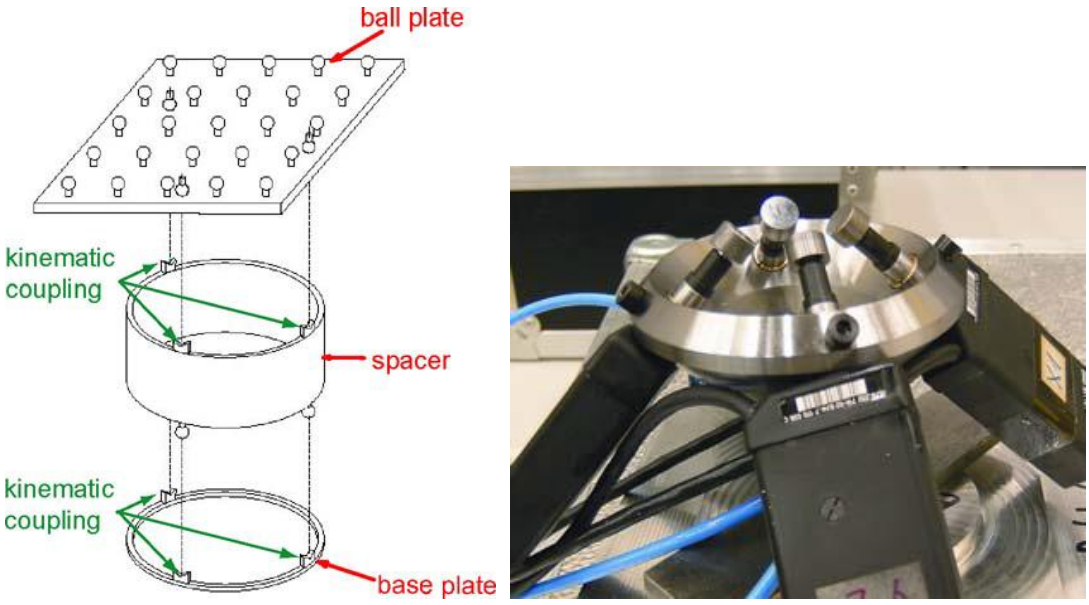

Figure 2-13 Ball plate artefact(left) and the measuring device (right) (Bringmann, Kung et al. 2005)

The ball plate consists of 6×6 array of aluminum sphere of 22 mm diameter. To measure the location of the spheres in the machine working volume, a measuring device composed of four one-dimensional analogous probes is used in a manner similar to the concept of the R-test device as described in (Weikert and Knapp 2004). The measuring device can compensate the direct 3D space error of three axis robots, machine tools and coordinate measuring machines without the involvement of any rotary axes. The measurement uncertainty is 5 µm in a working volume of $500 \times 500 \times 150$ mm^3.

2.3.3.4 Model based chase the ball

Model based calibration developed by Bringmann and Knapp required a single set up and the measurement method is similar to the 3D probe ball (Lei and Hsu 2002). A ceramic precision sphere mounted on the machine spindle represents the tool center position (TCP) (Figure 2-14) and its 3D deviations are measured. A calibration strategy is proposed. A suitable parameter set

is identified for the appropriate measuring poses. Mathematical stability of the model is assessed for the identified machine tool errors. The calibration quality is verified by a 3D circular test made with a double ball bar. Unidirectional mean diameter deviations for clockwise and counter clockwise direction are +106 µm/ 100 µm before calibration and -14 µm/ -19 µm after calibration. The Monte-Carlo method is used to simulate the calibration process, measurements and identification for 1000 error combinations. The tool center position deviations are calculated to verify the quality of the parameter set for 1000 runs. The average value found is 20 µm and for 95% it is below 32 µm (Bringmann and Knapp 2006).

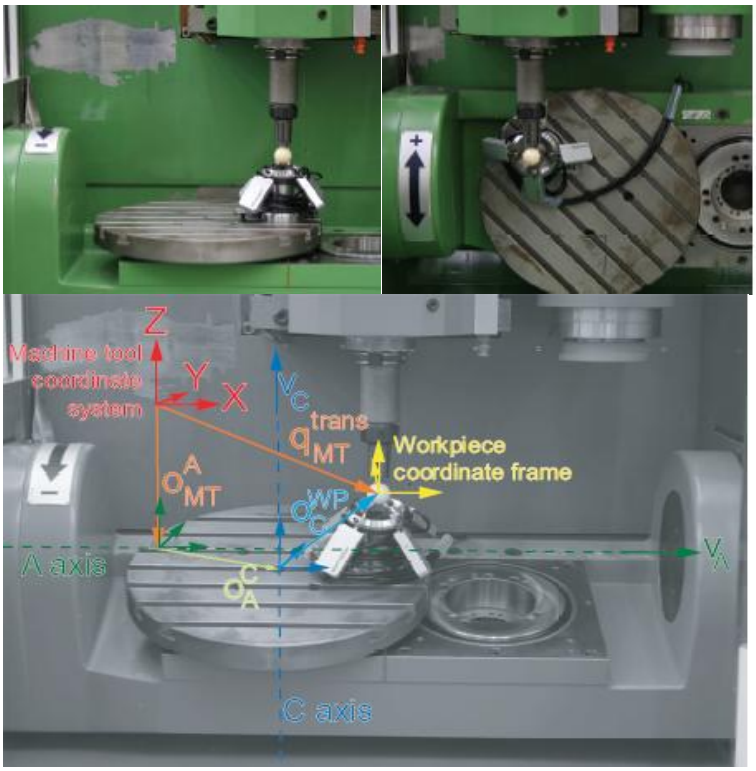

Figure 2-14 Model Based “Chase-the-Ball” technique (Bringmann and Knapp 2006)

2.3.3.5 The CapBall device

A non-contact measuring instrument called “CapBall” is proposed and used to measure machine tool’s volumetric error which is affected by the inter-axis errors (Zargarbashi and Mayer 2009). Figure 2-15 shows the “CapBall” instrument which consists of a sensing head equipped with

three capacitive sensors mounted on the tool holder and a precision ball of 19.05 mm diameter mounted on the machine table. The “CapBall” measures the relative position between the tool and the ball on the fly while all machine tool axes move simultaneously. A Jacobian matrix describing the sensitivity of the tool to workpiece position to the machine error parameters is used to extract the tool and workpiece setup errors as well as the inter-axis error parameters.

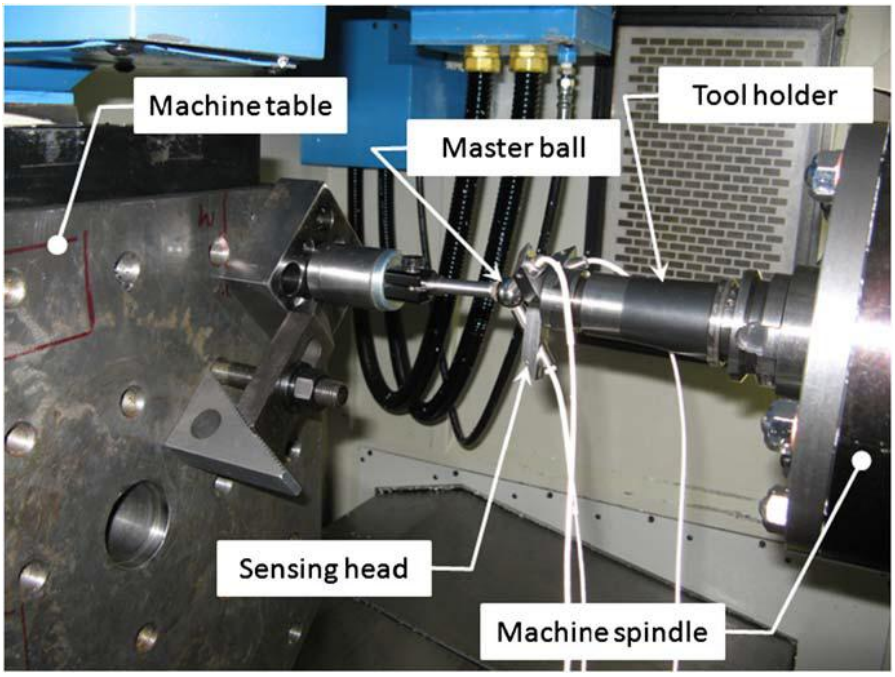

Figure 2-15 Functional prototype of the “CapBall” instrument (Zargarbashi and Mayer 2009)

The effect of the setup errors is removed from the estimated inter-axis parameters and volumetric error. Using the estimated inter-axis errors, volumetric errors are predicted for different axes combinations which are not used for the parameter estimation process. The estimated machine model can predict 52-84% of the measured volumetric error (Zargarbashi and Mayer 2009).

2.3.3.6 RUMBA & SAMBA

Erkan and Mayer proposed an uncalibrated 3D artefact to analyse the volumetric error of five-axis machine tools. A model based approach is proposed to estimate the artefact geometry without the effect of the isotropic scale gain errors. A point to point cluster analysis of the measured and predicted artefact is carried out to validate the artefact estimation quality. The

authors recommended that, simultaneous estimation of probe and artefact setup errors along with the machine link errors provide better picture of the machine tool's volumetric status (Erkan and Mayer 2010). Afterward, on-machine measurement of 3D Reconfigurable Uncalibrated Master Ball Artefact (RUMBA) was proposed to assess machine tool's volumetric distortion.

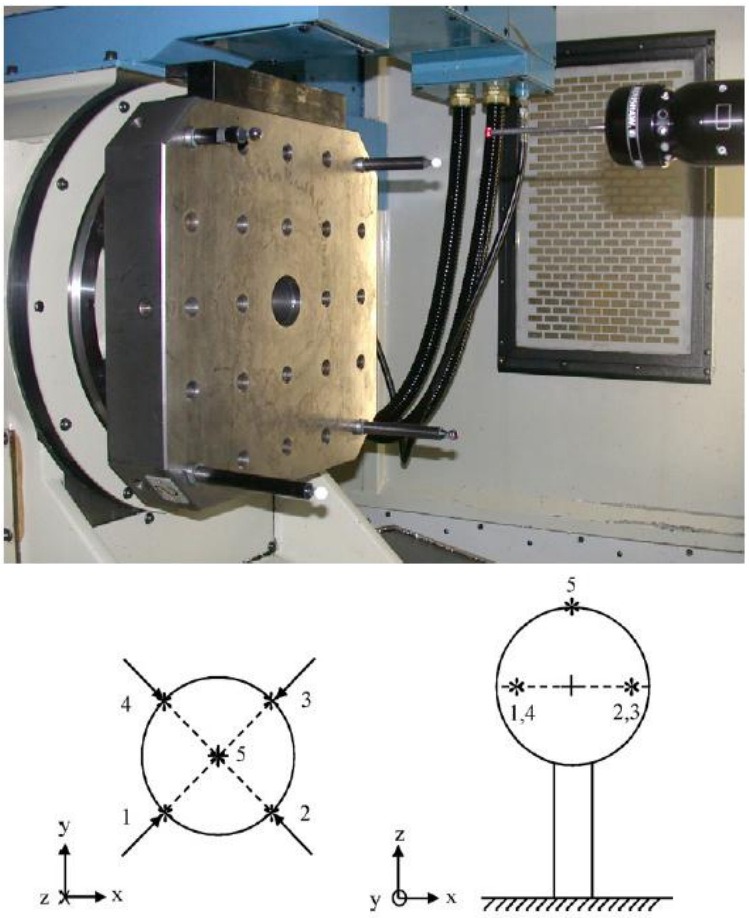

Figure 2-16 A 3D Reconfigurable Uncalibrated Master Ball Artefact (RUMBA) probing (top). Ball center measurement (bottom) (Erkan, Mayer et al. 2011)

The proposed mathematical model successfully identified the setup errors and was included in the machine model to improve volumetric distortion prediction. Figure 2-16 shows the artefact with four master balls connected with stems of different heights and the location of these master balls are reconfigurable. Combinations of all machine axes are used to measure the master balls. Four points are probed diagonally on the equator and one point on the accessible pole to obtain the

center coordinates of the ball. Homogeneous transformation matrices are used to calculate the stylus tip positions with respect to the master ball centers. The artefact geometry is validated by CMM measurement of the ball center using distance method (Erkan, Mayer et al. 2011).

Later on, Mayer (Mayer 2012) proposed a method where RUMBA is enriched by a scale bar artefact as a reference length called Scale And Master Ball Artefact (SAMBA) to estimate the inter-axis errors and the axis positioning errors. 24 master balls of 12.7 mm diameter mounted on carbon fiber tubes along with a scale bar of 304.6686 mm are measured at 11 B- and C-rotary axis combinations to gather the necessary machine tool data for the estimation process (Figure 2-17). Seven B- and C-axis combinations are used to estimate the parameters and another four combinations are used to predict machine's volumetric errors to assess the prediction capability of the proposed model. Author demonstrated that, the effectiveness of a thermally stable reference length measurement provides accurate picture of the positioning error of the linear axes and the importance of the data acquisition time vs. machine tool's thermal state change to the parameter estimation.

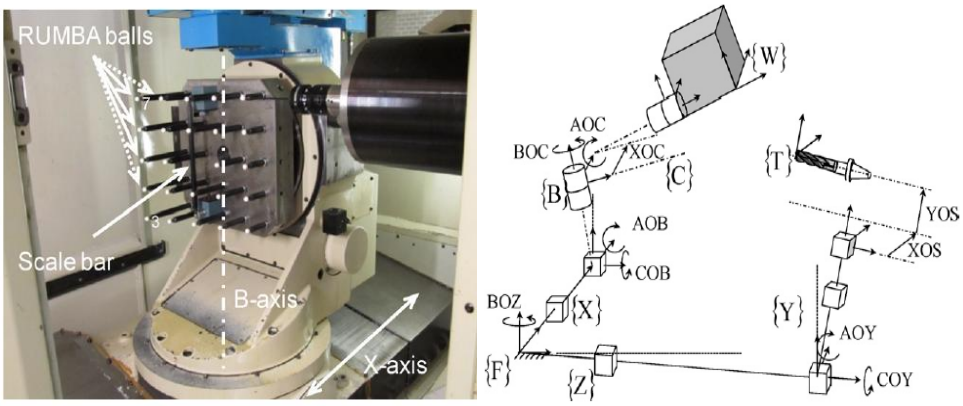

Figure 2-17 SAMBA probing on a WCBXbZYT machine tool (left) and the estimated inter-axis error parameters (right) (Mayer 2012)

2.3.3.7 Test piece measurement

Ibaraki et al. proposed a set of machining test patterns to identify the kinematic errors. The relationship between the kinematic errors and the finished work piece geometry is formulated for five-axis machine tools. A total of 11 straight side cutting patterns is proposed to estimate eight

kinematic errors associated with the rotary axes (tilting rotary table type machine tool) and three kinematic errors associated with the linear axes. The authors concluded that, the advantages of these machining patterns over ball bar measurement from the machine tool builder's point of view are that these tests are more comprehensible to the users, compatible to various size of the machine tools and simple setups does not required specially trained personnel (Ibaraki, Sawada et al. 2010).

The authors later proposed a calibration scheme (Ibaraki, Iritani et al. 2012) to estimate the location errors of the rotary axes that involves on-machine measurement of a test piece using a touch trigger probe.

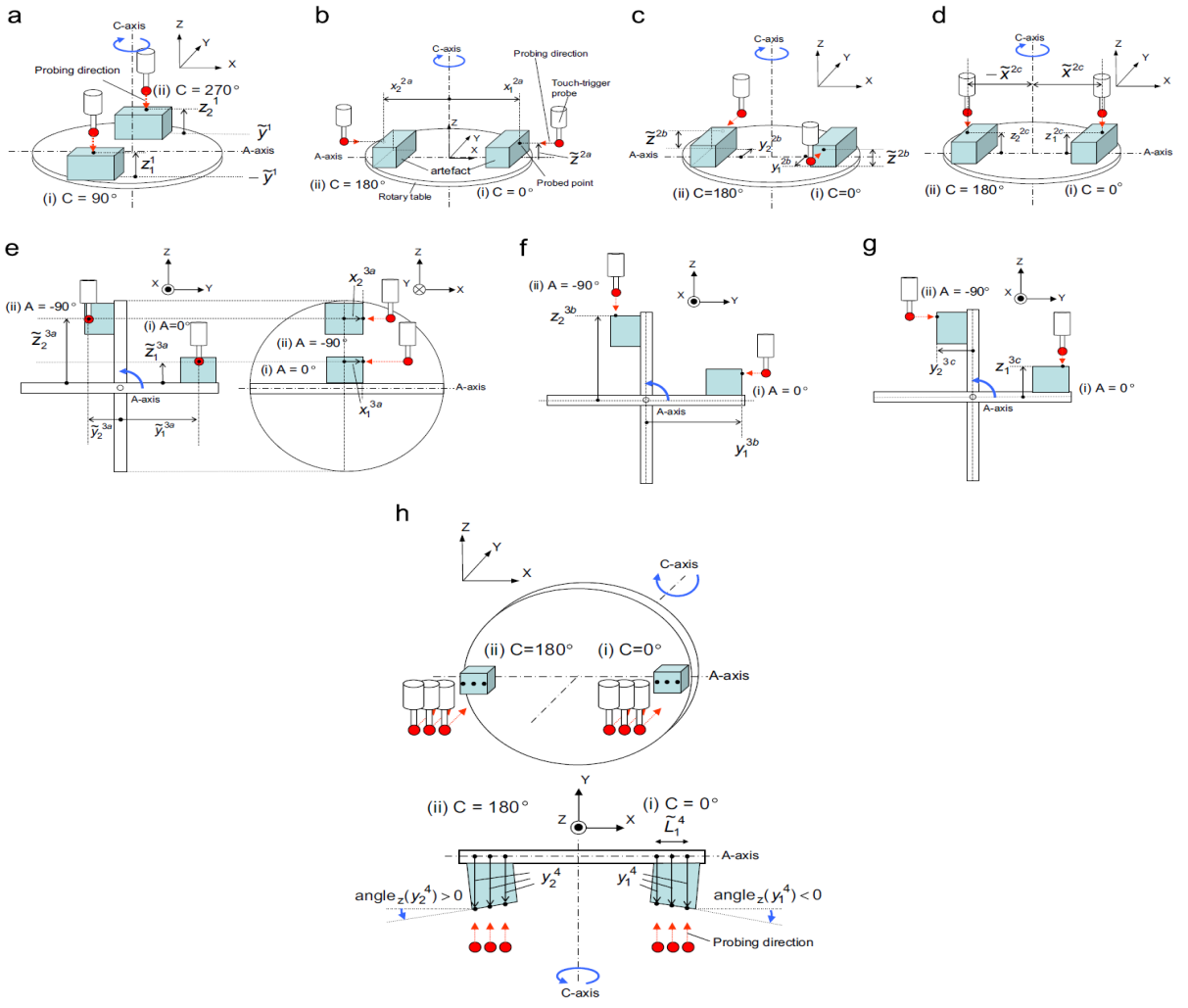

Figure 2-18 Test piece probing pattern (Ibaraki, Iritani et al. 2012)

A total of 154 points are probed at seven different (*A, C*) combinations with 28 points at each of the (*A=0, C=0*), (*A=0, C=90*), (*A=0, C=180*) and (*A=0, C=270*) combinations and 14 points at each of the (*A=-90, C=90*), (*A=-90, C=180*) and (*A=-90, C=270*) combinations. Figure 2-18 shows the probing procedure and Figure 2-19 shows the experimental setup.

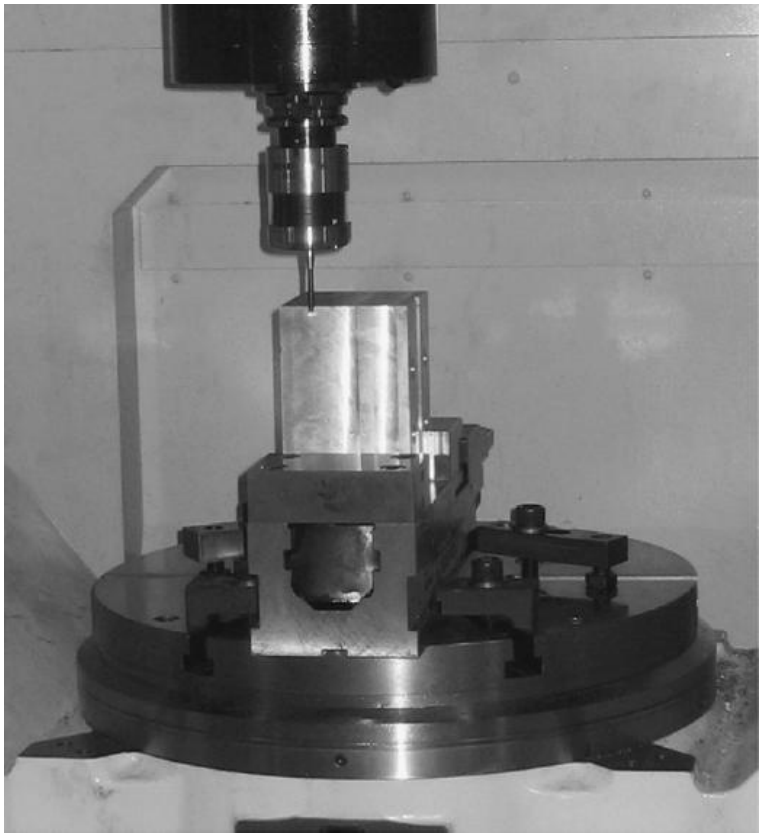

Figure 2-19 Experimental setup (Ibaraki, Iritani et al. 2012)

The authors considered the geometric errors of the linear axes are considerably smaller compared to the rotary and also the test piece setup errors hence these errors are neglected throughout the estimation process.

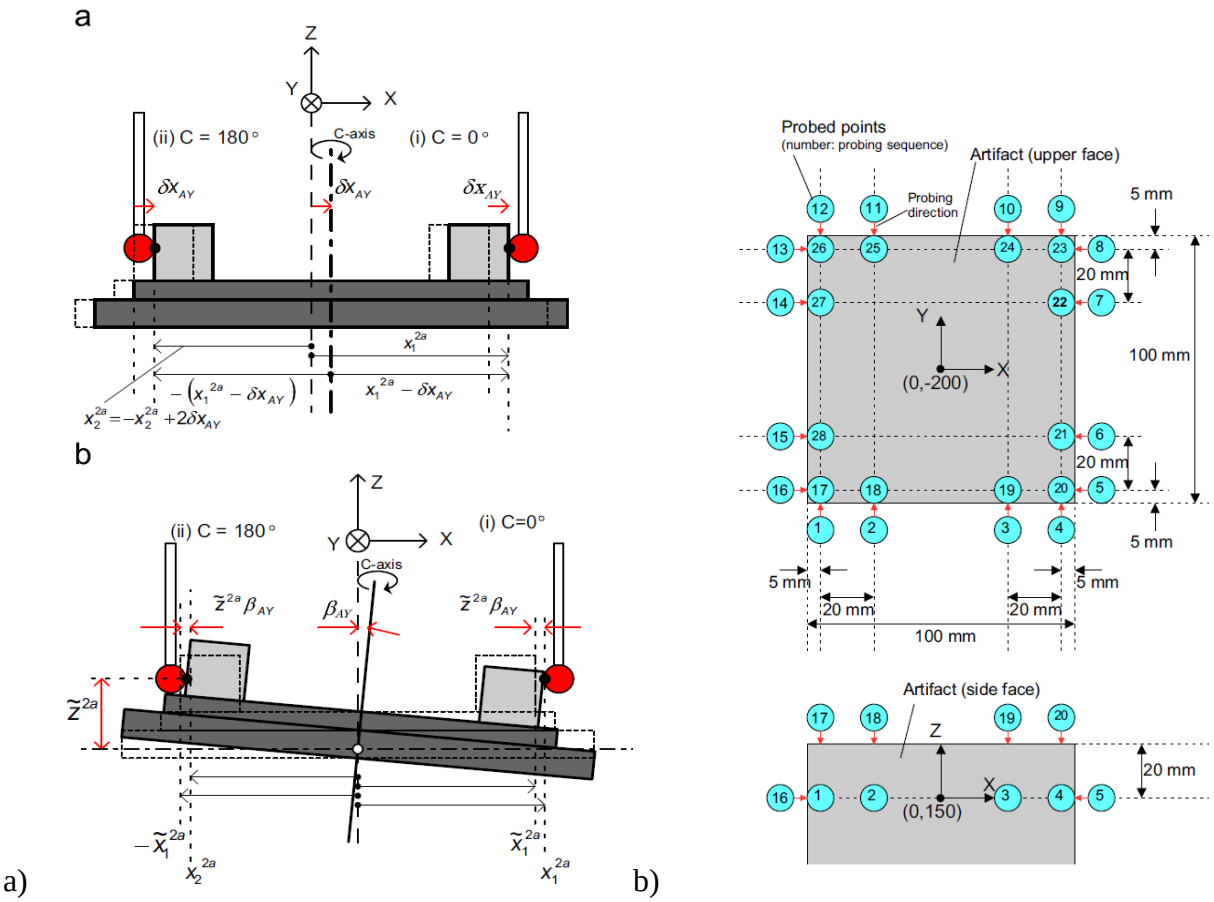

Figure 2-20 a) Influence of A-axis squareness to Z-axis and linear offset of C-axis in X-direction, b) position of the probing points (Ibaraki, Iritani et al. 2012)

Figure 2-20 shows the A-axis squareness to Z-axis and linear offset of C-axis in X-direction. To remove the effect of test piece setup errors, initial probing points (at *A=0, C=0*) are considered as the reference and the displacement of the measurement points relative to the reference points are calculated.

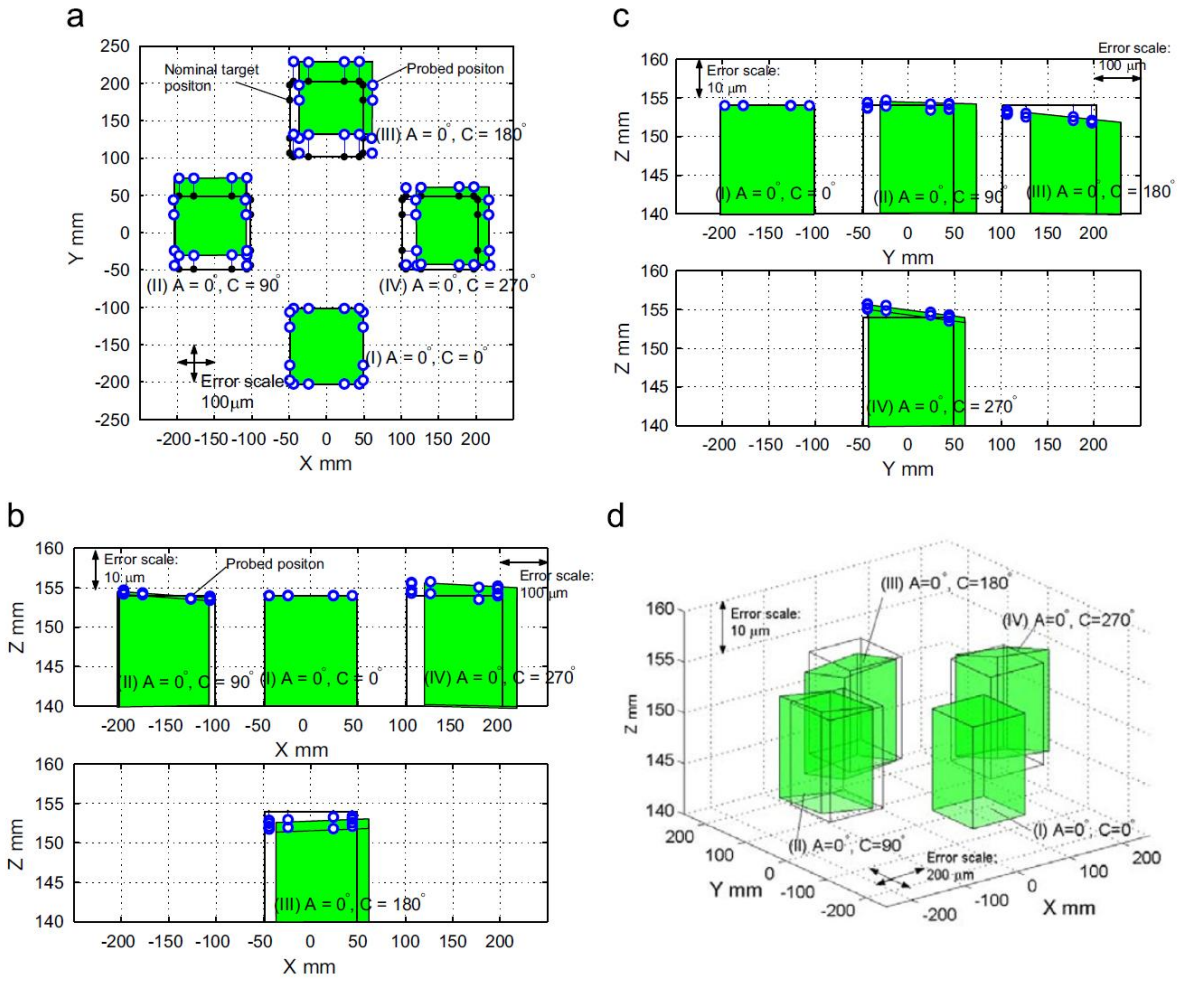

Figure 2-21 Projection of the probing points in a) XY, b) XZ and YZ plane. d) 3D view of the errors (Ibaraki, Iritani et al. 2012)

The location errors of the X- and Y-axis are identified through observing the measurements of the test piece in X-, Y- and Z- directions. Figure 2-21 a) shows the C-axis offsets in the X- and Y-direction and Figure 2-21 b) shows the squareness error between C-axis to Y-axis. Measurements were repeated for four times to check the repeatability and uncertainty of the parameters are also estimated.

2.3.3.8 The non-contact R-test device

Hong and Ibaraki proposed a non-contact optical R-test device (Hong and Ibaraki 2013) for five-axis machine tool calibration considering some potential drawbacks of the contact type R-test device such as: friction between the sphere surface and the probe, dynamics of the supporting springs etc. The authors found that, the measurement uncertainty in the dynamic test is about 6 µm for contact type R-test whereas the proposed non-contact type R-test device has only 1 µm. Instead of incremental probe, the method used laser displacement sensors to calculate the three dimensional displacement of a precision sphere. A new algorithm is also proposed for the non-contact laser displacement sensors. The sensors are chosen from the four different types of laser displacement sensors available in the market. The non-contact sensors have no physical contact with the precision sphere hence, the offset of the sphere center can introduce an error when compared to the conventional type R-test sensors (Figure 2-22).

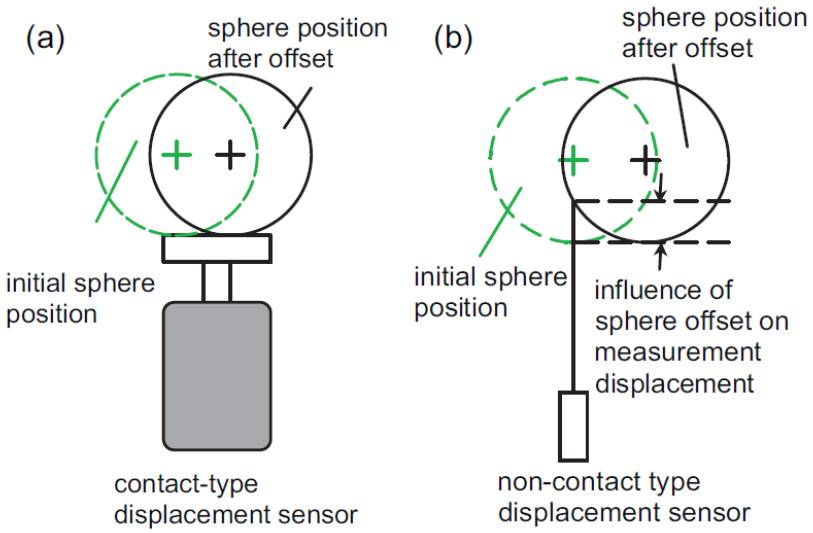

Figure 2-22 Effects of the sphere center offset on displacement sensors (Hong and Ibaraki 2013)

To calculate center offset of the sphere induced by the non-contact displacement sensors, orientation of the sensor's sensitive direction, V_i (i=1, 2, 3) and the intersection points of the sphere and the sensor at P_{i0} (i=1, 2, 3) are required. In the Figure 2-23, O_0 is the initial sphere

center with P_{i0} initial sensor's position and O_j is the j^{th} sphere position as the intersection moved to P_{ij} (i=1, 2, 3 & j=1……N) with a displacement of d_{ij} (i=1, 2, 3 & j=1……N).

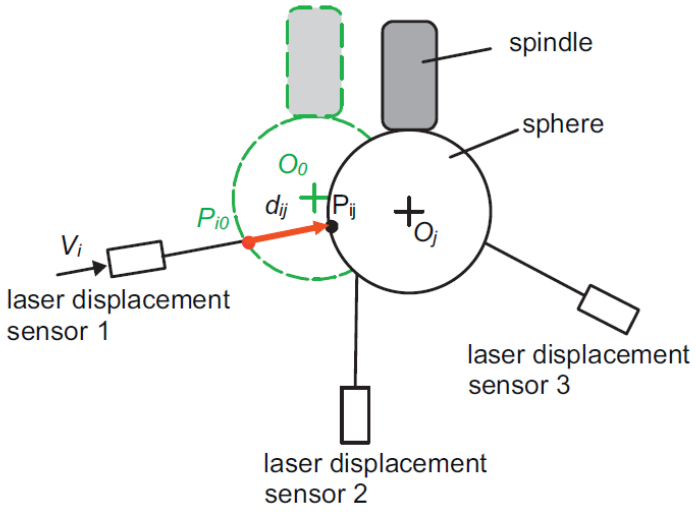

Figure 2-23 Sphere center offset correction for non-contact type laser displacement sensors (Hong and Ibaraki 2013)

The authors found good agreement between the contact and the non-contact type R-test device position profile in static measurements (Total 12 B- and C-axis orientations with7 B-axis and 12 C-axis). But for dynamic test, the sphere displacements relative to the sensors are decomposed into radial, tangential and axial directions. A double ball bar test is conducted to compare the contact and non-contact type R-test. Finally, the authors concluded that, for radial and axial trajectories, both contact and non-contact type R-test has good match with DBB test. But for tangential direction, non-contact R-test shows better results which may be due to the absence of friction between the sphere and the precision ball. The non-contact type R-rest also shows better repeatability than the contact type R-test.

2.3.4 Errors of touch probe in calibration

Touch trigger probe are used on CNC machine tools to perform simple on machine measurements primarily to locate the workpiece. Many indirect inspection techniques utilize this measuring device to measure artefacts in order to gather machine tool data to estimate error

parameters. But the inaccuracies of this measuring instrument can contribute to the parameter estimation. The probe approach direction, lobing, spring force, measuring speed, probe index angle etc., measurement environment (change in thermal status of the machine tool's working envelop), change in machine tool's status over time, surface of the artefact, machine tool's cooling system, cutting fluid etc. can contribute to the measurement inaccuracies (Cauchick-Miguel, King et al. 1996; Cauchick-Miguel and Kings 1998; Dobosz and Wozniak 2003; Dobosz and Wozniak 2005; Fesperman, Moylan et al. 2010; Jankowski and Wozniak 2016; Jankowski, Wozniak et al. 2014; Johnson, Qingping et al. 1998). Hence these factors draw attention to the metrologist.

The touch probe provides a binary signal as soon as they are in contact with the workpiece or any object. This signal is produced by opening and closing of electrical contacts inside the probe when the external mechanical contact occurred between the workpiece and probe stylus tip (Cauchick-Miguel and Kings 1998). The authors studied the factors that influence the probe performance through some experimental investigations. They measured a Rank Taylor Hobson standard hemisphere (Figure 2-24) for two dimensional probe lobing error assessment and a precision sphere (Figure 2-24) for three dimensional lobing error assessment. Result shows that, the probe pretravel (lobing) is the primary source of error and a function of length of stylus in particular. Aside from the stylus length, pretravel variation also depends on the measuring speed since the pretravel variation increases with the higher measuring speed. Probe index angle and spring pressure also contribute to the probe performance. Authors suggested that, the probe with smaller stylus length can be used to avoid pretravel and bending effect, and averaging the repeated measurements to improve probe repeatability.

a) 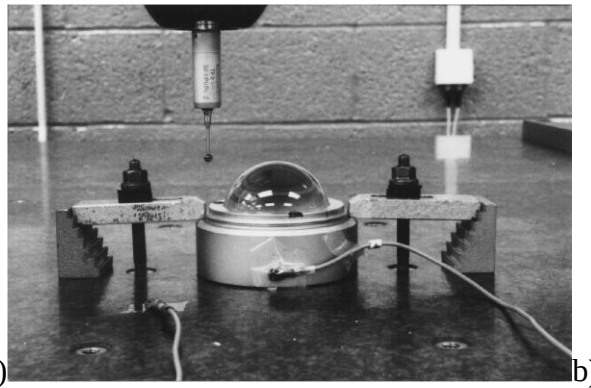 b) 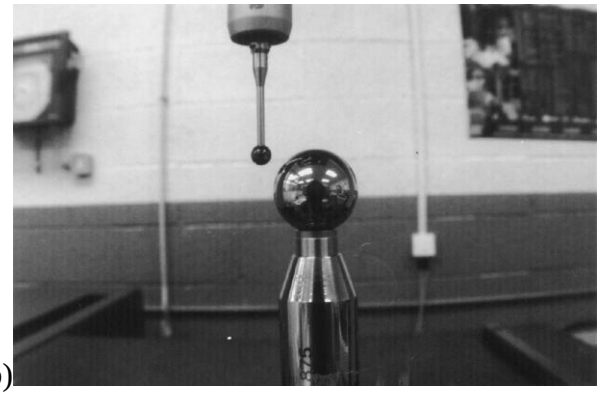

Figure 2-24 2-D and 3-D probe lobing assessment (Cauchick-Miguel and Kings 1998)

Wozniak and Dobosz proposed a new 3D model of the touch probe inaccuracy assessment (Wozniak and Dobosz 2003). The theoretical analysis has been carried out on one stage and two stage type probes (Figure 2-25). Since probe pretravel is considered as the most influential variable, the authors theoretically proved that, the pretravel is not only affected by the probing direction, but also the sum of a number of displacement components such as: switch pretravel (to break the electro-mechanical contact, the smallest distance that the stylus tip needs to make is called switch distance and the pretravel components of this switch distance is called switch pretravel), elastic deflections of the stylus and Hertz deflections of stylus ball and the part surface.

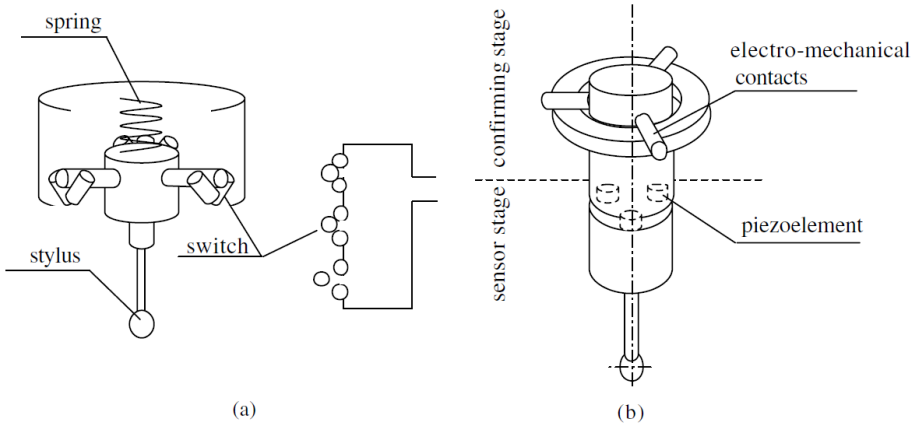

Figure 2-25 a) One stage type touch trigger probe, b) Two stage type touch trigger probe (Dobosz and Wozniak 2003)

The authors also observed that the accuracy of the probe is affected by the probe hysteresis that occurs when the stylus tip loses contact with the measuring surface and returns to a new neutral position before repeating the measurements. These can be categorized as: triggering point hysteresis, neutral position hysteresis and the hysteresis of the pretravel. For one stage probe, neutral position hysteresis is dominant while triggering point hysteresis is negligible. On the other hand, two stage probe has zero pretravel hysteresis and non-zero neutral position hysteresis. Later on, the authors verified the 3D model of the touch trigger probe inaccuracy experimentally using low force high resolution displacement transducer (Dobosz and Wozniak 2003). They also experimentally verified the influence of the probe operational parameters such as triggering force, rigidity and length of the stylus on the probe performance (Wozniak and Dobosz 2005) for one and two stage switching type touch trigger probe. The authors concluded that, for single stage switching type touch trigger probe, measuring force, stylus length as well as the rigidity of the stylus stem are dominant factors for pretravel variation. Pretravel instability along the perpendicular direction to the probing axis is dominant for one stage switching probe while the two stage switching probe has a circular character or insignificant probe pretravel instability. Also two stage switching probe has prevailing pretravel instability within the plane parallel to the probe axis.

For Coordinate Measuring Machines (CMMs) shorter cycle time is expected to perform different measurement tasks (i.e. faster CMM operation) hence the influence of the dynamic error in the CMM system is increased. Johnson et al. experimentally investigated the influence of dynamic error characteristics of a touch trigger probe for CMM. Authors identified that, probe longitude and latitude, approach distance, stylus tip diameter and stylus length, probe orientation, operating mode, scan pitch, pre-load spring force, probe type and the surface approach angle influence the probe performance. They conclude that preload spring force has a significant influence on dynamic error since higher spring forces cause larger probe dynamic errors. Optimum measuring speed for better dynamic performance is around 3-5 mm/sec and probe type also affects the dynamic error where TP7 shows better performance than TP2 (Johnson, Qingping et al. 1998). Fesperman et al. also investigated the probe performance in terms of repeatability, workpiece

location identification, 2D and 3D probing error to assess the performance of the machine tools (Fesperman, Moylan et al. 2010).

Dobosz and Wozniak developed a new method to test the touch trigger probe which involves measurement of different distances from a reference axis (most stable rotary axis). The touch trigger probe testing is done "off the CMM" since in the CMM calibration process is based on the summation of the stylus ball diameter and the average pretravel. The proposed method based on the rotation of a high resolution displacement transducer around a rotary axis while capturing the probe triggering points (Figure 2-26).

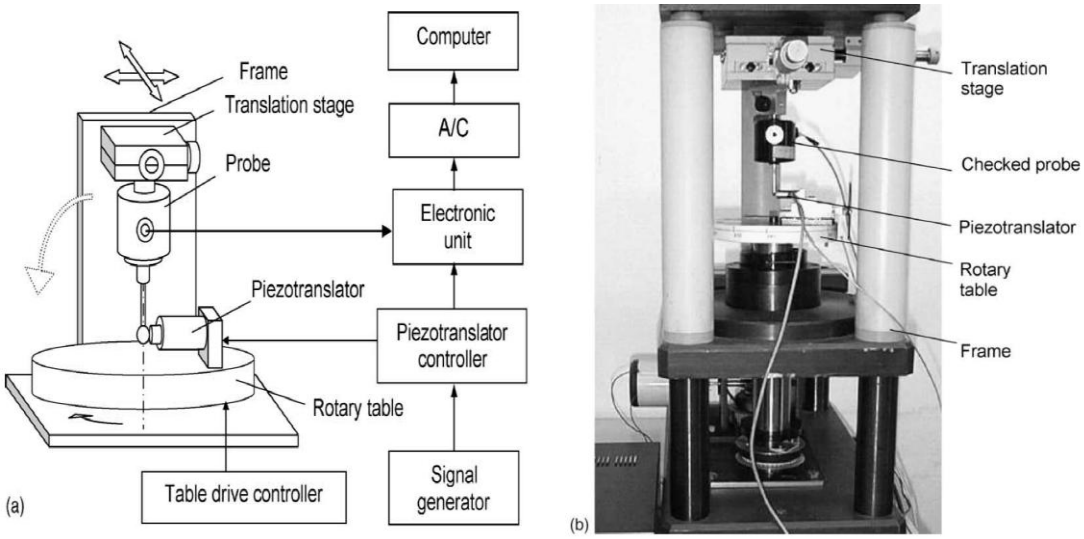

Figure 2-26 Touch trigger probe testing using reference axis: a) schematic and b) test set up (Dobosz and Wozniak 2005)

The method has been tested on both one stage (TP6) and two stage (TP200) switching type probes by Renishaw. Authors claimed that, the method possesses higher accuracy than other existing methods applied on CMM and can be easily performed with the help of a roundness measurement device which is commercially available (Dobosz and Wozniak 2005). The authors also investigated the influence of the measured object's stiffness, surface shape and roughness on touch trigger probe inaccuracy (Wozniak and Dobosz 2005) based on the rotary table axis as reference and "off the CMM". The authors experimentally showed that, measured object's

surface curvature has negligible influence on the probe accuracy while material stiffness and surface roughness has significant influence on the pretravel variation depending on the measuring force applied for probing.

Touch trigger probes are not only used to determine the work piece locations but also to gather machine geometric information for indirect inspection. ISO/DIS 230-10 provides standardized test procedures to evaluate the performance of contact type probing systems (ISO/DIS 230-10 : 2011). The standard describes relevant performance parameters, sources of uncertainty, factors influence the probing performance etc. and different test procedures to assess 2D- and 3D-probing error measurement. For 2D-probing test, 36 points on a 25 mm diameter reference ring is suggested to be measured along the circumference and the ranges of the measured radial distances are calculated. For 3D- probing error test, a reference sphere of 25 mm is suggested. Total 25 evenly distributed points over a hemisphere is recommended which are subjected to change up to 48 points for some applications. 3D-radial distances are calculated to estimate the 3D-probing error. In the past two decades, researchers and metrologists have been working on the modeling of CNC probe parameters and the potentially significant factors that might affects the probe performance.

Jankowski et al. developed a new method of machine tool's probe accuracy assessment based on the measurement of an inner hemispherical surface. The proposed method is applied to a precise TP200 strain gauge probe and OMP40-2 Renishaw probe in machine tools. For the TP200, triggering radius variation is 0.54 µm and the average unidirectional repeatability is 0.12 µm. For the OMP40-2 Renishaw probe, triggering radius variation value is 11.49 µm and average unidirectional repeatability is 0.34 µm (Jankowski, Wozniak et al. 2014). Figure 2-27 shows the characteristics of the both tested probes.

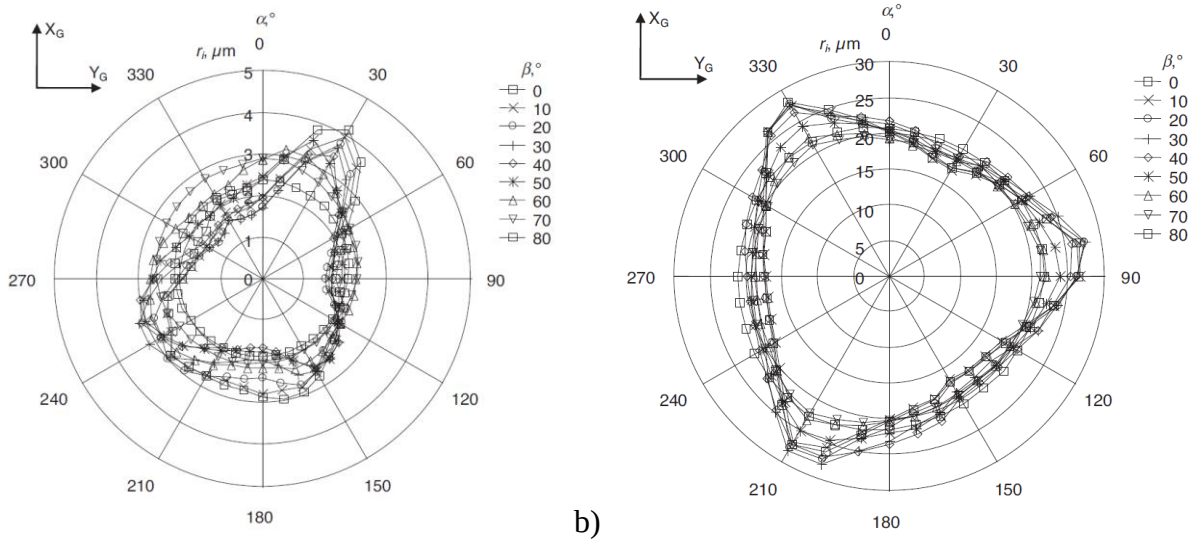

Figure 2-27 Characteristics of an average triggering radius: a) TP200 and b) OMP40-2 (Jankowski and Wozniak 2016)

Authors found that the uncertainty of the probe triggering radius variation is 0.31 µm in the laboratory and 0.35 µm on the machine tool.

All the above mentioned works clarify the fact that the touch trigger probe itself can be a significant source of measurement inaccuracy. Moreover, when used in CNC machine tools, the systematic errors of the probe become an additional source of the machine tool errors and expand the overall effect on the measurement inaccuracies. Recently Jankowski et al. develop a theoretical model to identify the probe errors of CNC machine tools (Jankowski and Wozniak 2016). Since the neutral position of the probe is unknown and only the triggering points are known, the model adapts the concept of triggering radius. The authors investigated that, the hertz's deflection (a pretravel components) is negligible and signal transmission delay depends on the measuring speed has significant impact on probe accuracy. Stylus deflection depends on the length of the stylus, radius of the transducer moving element, friction factor between stylus and artefact, stylus stiffness and measuring force has significant impact. The model was verified experimentally using m&h IRP32.00-MINI 1-point kinematic probe, Renishaw MP700 and RMP60 3-point kinematic probe. Triggering radius variation and average unidirectional repeatability is estimated and a very good conformity is observed between the theoretical and

experimental values (Jankowski and Wozniak 2016). Aside from these probe performance parameters, measuring environment, machine tool's cooling system, cutting fluid injection system, surface of the artefact/workpiece measured, thermal state change etc. influences the measurement accuracy. A very few research work has been found in the literature that deals with these process variables of CNC machine tools. Verma et al. investigated the performance of a machine tool under various operating conditions to estimate the effects of potentially significant variables. The authors concluded that, toll change and machine tool worm up cycle has significant influence on the measuring performance (Verma, Chatzivagiannis et al. 2014). Thus, the influence of these factors can be critical when calibration is done using indirect approaches.

2.3.5 Parameter uncertainty estimation

Once the parameters estimations is done still remains the question of the authenticity of the estimated values. Hence, proper validation is essential to support the estimation. Indirect estimation can be validated by comparing the estimated parameters with the directly measured values but for five-axis machine tools, estimation of the rotary axes parameters is difficult using direct techniques. Thus, parameters' uncertainty estimation is the most plausible way to assess the reliability of the estimated parameters. Direct measurement methods are also subjected to uncertainty which is required to be measured.

Since all the measurement instruments and methods are subjected to uncertainties, ISO/GUM (ISO 2008; ISO 2008; JCGM 102:2011) describes readily implemented, comprehending and generally accepted procedure to evaluate the uncertainties of the measurement data. Researchers incorporate those standardized procedures to estimate the uncertainties of the calibrated parameters. Measurement environment, measuring instruments, machine tool itself and non-estimated error parameters can contribute to the uncertainties of the estimated parameters.

Bringmann et al. verified that, non-estimated error parameters are more important uncertainty contributor than the measuring devices. The authors explained the interdependencies between these error parameters and proposed a method to estimate the overall test uncertainty for complex measurements. Figure 2-28 (a) shows the 3D-ball plate set-up of the proposed method and the ball center measurement technique is similar to the so called R-test. Figure 1-28 (b) shows the

interdependencies between the axes positioning error of the X- and Y-axis. The method can separate the single axis errors of the three linear axes while avoiding the interdependencies. Monte Carlo simulations are used to estimate the uncertainty of the estimated parameters even if they are distinguished explicitly. The authors concluded that, tilt, roll, run-outs or hysteresis not only affects the workpiece machining but also increase the uncertainties of the identification of the geometric errors.

a)

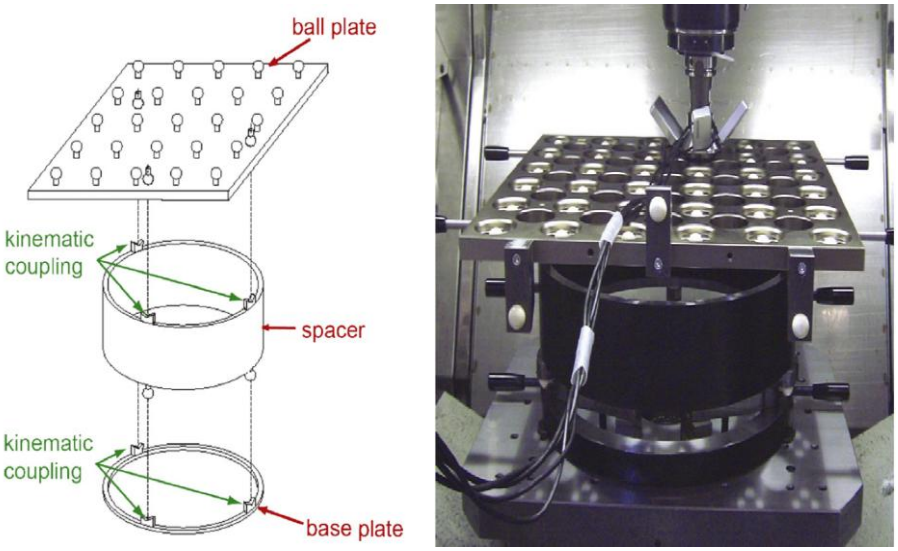

b)

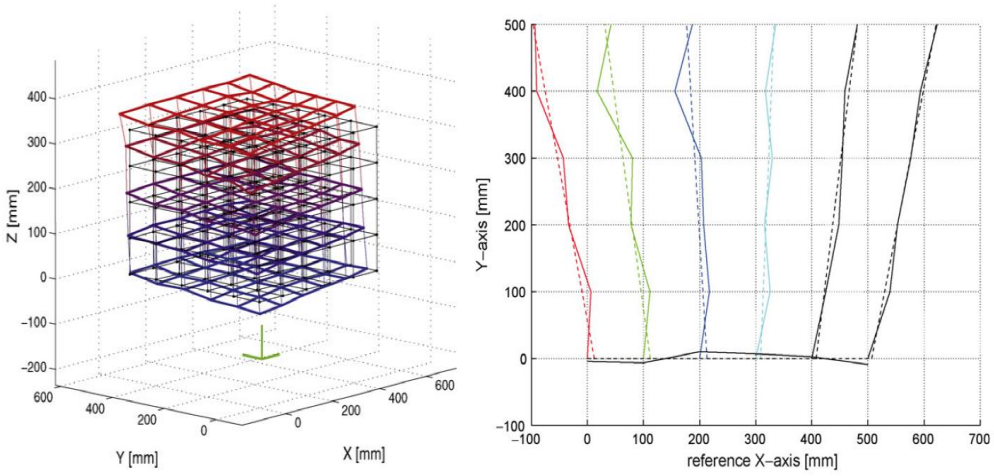

Figure 2-28 a) Set-up and application of 3D-ball plate for machining centers. b) Distorted workpiece obtained from 3D-ball plate measurements (left), change of squareness between Y- and X-axes (E_{C0Y}) at different measuring lines (12000x) (right)

Andolfatto et al. considered sensors output, machine tool's drift and frame transformation uncertainties in the model while estimating eight link error parameters (inter-axis error parameters) using a CapBall (a non-contact Cartesian measuring instrument) device. Multi-output Monte Carlo approach is implemented to estimate the uncertainties on the error parameters (Andolfatto, Mayer et al. 2011). Sladek and Gaska developed a CMM based virtual Monte Carlo Method (MCM) to evaluate the accuracy of the measurements online with the assumptions that, machine tools are equipped with CAA (computer aided correction) matrix, thermal compensation system, thermal influences measuring system (must have at least two temperature sensors), strict room environment for the machine where the machine can reaches to its best manufacturer accuracy etc. Cheng et al. proposed a Monte Carlo simulation method to explain how individual geometric errors can influence the machining accuracy. Considering multi-body system, a volumetric model is proposed to explain the coupling between the geometric errors and the machining accuracy. Machining accuracy reliability of the machine tool is considered as the ability of the machine tool and optimized basic machine geometric parameters as the reliability sensitivity. Using Monte Carlo method and geometric errors characteristics distribution, machining accuracy reliability is obtained for each test point. This is to determine the sensitivity of geometric error distribution to the machining accuracy reliability. The authors concluded that, the geometric errors have significant influence and can be manipulate to improve the machining accuracy reliability. (Cheng, Zhao et al. 2015).

2.4 Conclusion of the literature review

A good indirect calibration technique yields proper error modeling, fast and efficient measurement methods, extensive instrument calibration, proper validation through comparison of the estimated parameters and uncertainty estimation. Machine tools composed of both linear and rotary axes yield more geometric complexity and are difficult to calibrate efficiently with minimum calibration time. Moreover, brought in instruments increase production idle time and require expert personnel thus metrologist favor indirect approaches. Most of the indirect approaches use calibrated or uncalibrated artefact, instruments or ball bar measurements to obtain machine's geometric data. Since the method involves measurements hence, machine tool's

geometry, mode of operation, operating variables, thermal state of the machine tools, ambient conditions etc. are the potential sources of inaccuracy that affects the measuring performance and consequently the calibration quality. . Thus the conclusion of the abovementioned literature review can be stated as follows:

- Direct calibration techniques are very difficult to adapt to five-axis machine tools. Additionally, it requires precise setups and trained personnel.
- Calibration techniques require brought-in artefacts, instruments, double ball bars, laser interferometers etc. Therefore, artefact handling, installation, separate programming etc. requires additional time and personnel.
- Most of the research works are not considering the factors influencing the measuring accuracy aside from the touch probe. The measurement process variables can also contribute to the measuring inaccuracy therefore the estimation process.
- Geometric data acquisition is not an automated process hence production idle time increases due to the operation intervention and artefact/instrument setups.

CHAPTER 3 OVERALL THESIS STRUCTURE

According to the introduction and the objectives, the general structure of this thesis will be presented in this section to maintain the link between the objectives and the published articles. Five important phases of this research work namely: Calibratable model for inter- and intra-axis error by on-machine probing of an indigenous artefact, fast procedure to calibrate machine geometric model, propose schemes to validate the calibration, measuring instrument's accuracy investigation and evaluation of the calibration performance. The next chapters will be included journal articles establishing the accomplishments of the stated objectives concerning this thesis.

The succeeding chapter is entitled as, "Five axis machine tool volumetric error prediction through an indirect estimation of intra- and inter-axis error parameters by probing facets on a scale enriched uncalibrated indigenous artefact". The article is published in Precision Engineering Journal (Volume 40, Pages 94–105 in April 2015), describes the core achievements of this thesis. This article presents a method to measure facets on an existing machine tool table as an uncalibrated indigenous artefact to gather machine tool data and an error model to estimate 86 geometric error parameters (inter- and intra-axis). Four different parameter subsets are studied to observe the machine tool's volumetric error predictability of the subgroups. For validation, artefact geometry is estimated using calibrated model for each parameter subgroups and compare with the CMM measured artefact. Model's capability to predict the probe stylus position is also conducted. To do so, predicted probe stylus positions by estimated model are compared with the CMM measured artefact geometry.

The title of the chapter four is, "An uncalibrated cylindrical indigenous artefact for measuring inter-axis errors of a five-axis machine tool". The article is published in CIRP – Annals, Manufacturing Technology, Volume 64, Issue 1, 2015, Pages 487–490, describes the application of the proposed calibration technique to a machine tool integrated with indigenous cylindrical artefact as the source of facets. Different measurement strategies are studied to observe the effect of the facets distribution over the artefact. Machine tool's behavior throughout a day and between consecutive days are also investigated. For the validation purposes, parameter uncertainties are estimated using the covariance matrices obtained from the especially design measurement cycles

performed in consecutive days. Uncertainties pooled by cycles support the change in machine tool's behavior throughout a day and uncertainties pooled by day supports the machine's behavior between days.

In chapter five, a new method is proposed to evaluate the machine tool's measurement performance. The title of the chapter is "Performance of a five-axis machine tool as a coordinate measuring machine". The article is submitted to the Journal of Advanced Mechanical Design, Systems and Manufacturing, Japan Society of Mechanical Engineers (JSME) which is under review. Out of sphericity test of a precision ball measured in five-axis is proposed. Facets on the sphere are measured using all the five-axis movement of the machine tool. Measurement data is processed using the nominal and the compensated machine model. The compensated machine model includes the inter-axis parameters and the axis positioning errors. The estimation of these error parameters is done by on-machine probing of an uncalibrated indigenous artefact.

Chapter six and seven describes the two complimentary works related to this thesis. Chapter six entitled as "Measurement accuracy investigation of touch trigger probe with five axis machine tools" and submitted to the Archive of Mechanical Engineering which is under review. Factors that influence the measurement accuracy of the touch trigger probe (such as: artefact surface, measuring instruments, machine tool's status change over the time of operation, measuring environment etc.) is investigated in this article.

The title of the chapter seven is "Calibration performance investigation of an uncalibrated indigenous artefact probing for five-axis machine tool". The article is published in Journal of Machine Engineering, Vol. 16, No. 1, 2016. Chapter seven describes the repeatable performance of the proposed calibration method by on-machine probing of an indigenous artefact against some process variables such as: change is facet locations on the artefact, artefact dismount and remount cycle and the change is artefact measurement strategy by changing the number of rotary axes indexation combinations.

Finally, chapter eight titled as "general discussion", provides the outcomes of the thesis at different stages followed by conclusion and scope of future works in chapter nine. Chapter ten represents the list of publications accomplished throughout this research work.

CHAPTER 4 ARTICLE 1: FIVE AXIS MACHINE TOOL VOLUMETRIC ERROR PREDICTION THROUGH AN INDIRECT ESTIMATION OF INTRA- AND INTER-AXIS ERROR PARAMETERS BY PROBING FACETS ON A SCALE ENRICHED UNCALIBRATED INDIGENOUS ARTEFACT

Md Mizanur Rahman, J.R.R. Mayer

Mechanical Engineering Dept., Polytechnique Montréal, P.O. Box 6079, Station Downtown, H3C 3A7 Montréal (QC), Canada

Published in Precision Engineering, Volume 40, Pages 94–105, 2015

4.1 Abstract

The volumetric accuracy of five-axis machine tools is affected by intra-axis geometric errors (error motions) and inter-axis geometric errors (axes relative position and orientation errors). Self-probing of uncalibrated facets on the existing machine tool table is proposed to provide the necessary data for the self-calibration of the machine error parameters and of the artefact geometry using an indirect approach. A set of 86 non-confounded coefficients are selected from the ordinary cubic polynomials used to model both the intra- and inter-axis errors. A scale bar is added to provide the isotropic scale factor. The estimated model is then used to predict the actual tool to workpiece position. Experimental trials are conducted on a five-axis horizontal machining centre using its original unmodified machine table as an artefact. For validation purposes only, the estimated artefact geometry is compared to accurate coordinate measuring machine (CMM) measurements. A study of the volumetric error predictive capability of the model for selected subsets of estimated error coefficients is also conducted.

Keywords: Self-calibration; Five axis machine tool; Indigenous artefact; Geometric errors; Facet; Probing

4.2 Introduction

Five axis machine tools' ability to achieve both position and orientation control of the tool relative to the workpiece allows a reduction in the number of workpiece setups which increases productivity and, potentially, part quality. However, they are prone to numerous error sources, in part from the addition of two rotary axes, which also makes the calibration process more difficult. Volumetric errors between the tool and the workpiece are in part due to inter-axis geometric errors describing deviations in the position and orientation of successive axes average line of rotation or mean direction of translation in the machine kinematic chain and by intra-axis geometric error (also called error motions) parameters describing the deviations from perfect motion of each individual axis. The measurement of these errors is broadly conducted using direct and indirect approaches [1]. The direct methods to evaluate the geometric errors of a five-axis machine tool (e.g. laser interferometer, electronic level, autocollimator etc.) require precise setups, much time as well as specially trained personnel, thus there is relevance in seeking faster, simpler and less intrusive calibration procedures.

For five-axis machine tools in particular, indirect approaches are increasingly studied and used [2]. A so-called R-test device made of three analogous proximity sensors was used to conduct indirect geometric parameter estimation of a six axis parallel machine using discrete positions [3]. A similar device but using four sensors, the redundant forth sensor providing a data check, was later used to acquire discrete position readings to perform an indirect estimation of a five-axis machining centre axis alignments and relative linear scale gain errors [4]. A non-contact R-test with laser displacement sensors was recently developed to calibrate a five-axis machine [5]. A non-contact three capacitive sensor device was also studied to conduct quick on-the-fly data acquisition for indirect model estimation of axis alignments [6] and also to study the relative contribution of contouring errors, quasi-static geometric errors and dynamic geometric errors on a five-axis machine tool [7]. Volumetric errors on a five-axis machine tool involving the motion of two prismatic and one rotary axis were predicted using geometric and dynamic data. The geometric error parameters were estimated using an indirect on-the-fly approach [6] while the effect of servo errors for the linear axes is obtained from the machine controller encoder

feedback. This study combined the geometric error model with servo errors to predict the machine volumetric behavior [8].

Since most machines are now equipped with a touch trigger probe, it makes sense to investigate its use for machine performance evaluation and calibration as was done for coordinate measuring machines [9], [10]. The SAMBA (Scale And Master Balls Artetact) method was proposed to estimate axis position and orientation errors, linear axis positioning error gains and spindle axis offsets on a five-axis machine tools by probing a scale bar and up to 24 master balls mounted at the tip of rods with different lengths fixed at uncalibrated positions on the machine table [11]. In [12], uncalibrated test pieces were mounted on the machine table and measured with the machine probe to calibrate the location errors of rotary axes of a five-axis machine tool assuming negligible error contributions from the linear axes. The method does not allow separating the influence of errors from the linear axes. The technique was later extended to the measurement of error motions of rotary axes [13]. The work in [12] and [13] requires the geometric errors of linear axes to be negligible and use a test piece externally brought into the machine tool's working envelop.

This paper proposes to use on-machine probing of only nominally known small faces (facets) already present on the machine standard table, thus creating an uncalibrated indigenous artefact, to simultaneously estimate inter-axis (axes location errors) and intra-axis (error motions) errors as cubic polynomials. Errors pertaining to all five axes and the spindle axis are simultaneously estimated. Because each facet is considered as a distinct feature and requires a single measurement, the approach is called ''Touch ANd GO'' or TANGO since a facet is touched for probing and then the next facet is sought for the next probing operation. A reference length is added to evaluate volumetric performance and absolute positioning errors for all three linear axes. The paper begins with a presentation of the overall TANGO concept followed by the associated mathematical models and error parameters to be estimated. Then, the test strategy is described. Results of preliminary tests mainly to assess the probing robustness are then presented followed by tests of the TANGO procedure and model validation in terms of volumetric error prediction capability.

4.3 Concept of an Indigenous Artefact

It is proposed to exploit existing machine table features which can be reached by the machine touch probe to gather the necessary volumetric raw data for machine error parameters' estimation.

As shown in Figure 4-1, the machine table of the laboratory's Mitsui Seiki HU40T machining centre is an octagonal prism with nine nominally flat surfaces. Figure 4-2 shows the selection of 26 small surface areas to be probed, called facets, each defined by a nominal target point on the surface and its own local nominal unit normal vector which altogether define the indigenous artefact. Since the exact machine table dimensions and geometric deviations are not known and are not required throughout the machine estimation process, the indigenous artefact is deemed uncalibrated. The concept could, in principle, equally use a fixture mounted on the machine or a machined part if it provides access to a sufficient number of facets. The rich set of facets allows probing of a subset of facets at numerous B- and C-axis indexation combinations.

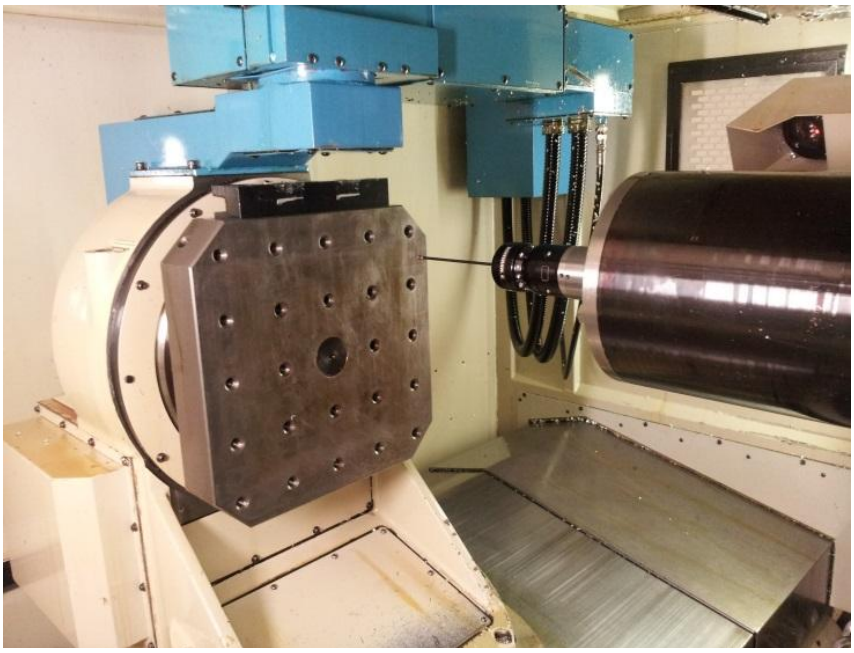

Figure 4-1 Machine table, of a WCBXFZYST five-axis machine tool, used as indigenous artefact for probing

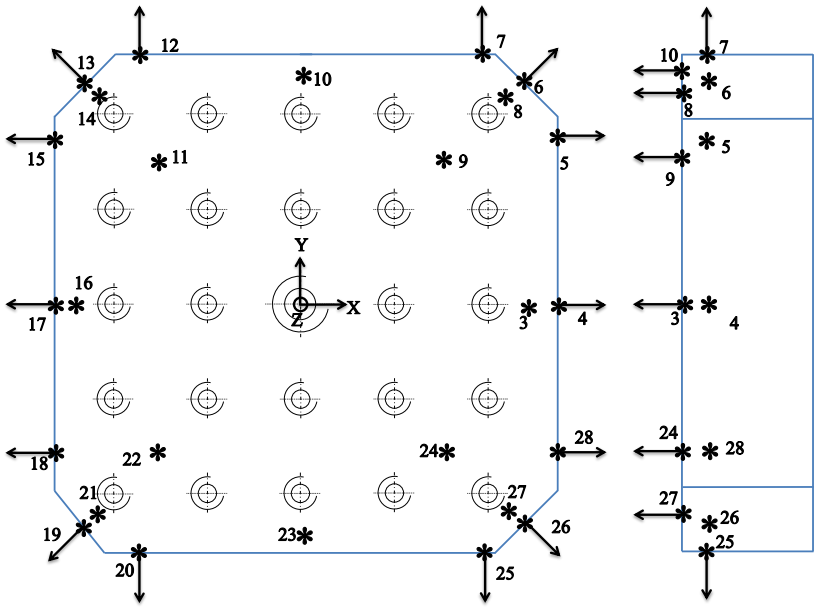

Figure 4-2 Selection of facets defined as nominal points' coordinates on the surface and their respective nominal local unit normal vector. Facets are numbered from 3 to 28; number 1 and 2 are kept for the identification of the two spheres of the scale bar

4.4 **Mathematical model**

Considering inter-axis error parameters, rotary and linear axes require four and two parameters respectively to locate them in space, which yields a total of 14 parameters for the five axes of the machine tool [14] This number is obtained from the known equation for a serial chain mechanism,

$$N = 4R + 2P \tag{4-1}$$

where, R is the number of rotary axes and P is the number of prismatic axes. However, removing consideration of the machine location in the universe, six parameters are removed leaving the usual eight inter-axis position and orientation errors of which seven are angular and one is translational. Using a parameter nomenclature based on [15] and [16] they are E_{AOB}, E_{COB}, E_{XOC}, E_{AOC}, E_{BOC}, E_{BOZ}, E_{AOY} and E_{COY}. For instance, E_{AOB} (squareness of B to Z) is the error in the orientation of axis B around the X-axis, an A rotation. Figure 4-3 depicts those parameters for a WCBXFZYST horizontal machining centre where W, F, S, T, C, B, X, Z, Y stand for the

workpiece, foundation, spindle, tool and C-, B-, X-, Z-, and Y-axis respectively. The eight parameters are defined as follows: the X-axis is first considered and has no alignment errors. Then the Z-axis has a squareness error to the X-axis, E_{B0Z}. Together they define the XZ plane. The Y-axis has potentially two out-of-squareness errors with respect to the XZ plane, one around X (E_{A0Y}) and one around Z (E_{C0Y}). The first rotary axis, B, has two out-of-squareness with respect to the XZ plane, E_{A0B} and E_{C0B}. The second rotary axis, C, has out-of-squarenesses relative to the B-axis and the X-axis as E_{A0C} and E_{B0C}. Because rotary axes have positions in space, they will in general not cross perfectly and so an X offset is defined for the C-axis with respect to the B-axis as E_{X0C}. These eight parameters locate the average lines of motion of the imperfect axes. The spindle, as a rotary axis, also requires up to four error parameters of which two are angular, E_{AOS} and E_{BOS}, and two translational, E_{XOS} and E_{YOS}. The tilt errors of the spindle cannot be estimated because the test will use a single probe stylus length. Each inter-axis error parameter is modelled as a real number or scalar.

Now considering intra-axis error parameters, prismatic and rotary axes undergo commanded linear and rotational displacements x, y, z, b, c and s (for the spindle axis indexation). Figure 4-4 illustrates the intra-axis error as three angular and three translation deviations from perfect motion for each individual axis [16]. Intra-axis errors are here modelled as ordinary polynomials of 3rd degree of the axis command [8], [17]. So as an example, for the straightness error motion of the X-axis in the Y-axis direction

$$E_{YX}(x) = E_{YX0}x^0 + E_{YX1}x^1 + E_{YX2}x^2 + E_{YX3}x^3. \quad (4\text{-}2)$$

The machine error parameters are listed in Table 4-1. The zero degree terms are not intra-axis errors since they do not change neither with the axis command position nor its direction of motion. They are position independent. However, they are used, as required, to model inter-axis errors [14]. Because the six intra-axis polynomials associated with each machine axis can produce both linear and angular offsets, they can represent the eight alignment errors. The coefficients corresponding to the ten retained inter-axis parameters E_{AOB}, E_{COB}, E_{XOC}, E_{AOC}, E_{BOC}, E_{BOZ}, E_{AOY} and E_{COY} are E_{AX0}, E_{CX0}, E_{XB0}, E_{AB0}, E_{BB0}, E_{XZ1}, E_{AZ0} and E_{CZ0} respectively. The spindle offsets E_{X0S} and E_{Y0S} are modelled using intra-axis coefficients E_{XY0} and E_{YY0}

respectively. This correspondence is apparent when one compares Figure 4-3 and Figure 4-4. Note how the error type, represented by the first letter of the subscript is the same for the inter- and corresponding intra-axis parameters. Note also that the corresponding intra-axis error applies to the preceding axis as compared to the inter-axis error. As an example consider E_{AOB} which is a tilt angle error of the B-axis around the X-axis (an A error) which is modelled as a constant (degree 0) error motion of the X-axis also around the X-axis, E_{AX0}. The only exception is E_{XZ1} where a straightness error is used to model an inter-axis angular error (E_{BOZ}). It is done so because there are no preceding axes in this case, the Z-axis being first in the tool branch. However, because of coupling between ordinary polynomial coefficients, in particular between zero degree and second degree terms, the selected zero degree terms will not numerically represent the corresponding inter-axis error parameters.

The degree one terms of a straightness error motion are generally not included since it induces a straight motion. Only one is kept, E_{XZ1}, since it can model the effect of the out-of-squareness of the Z-axis with respect to the X-axis, selected as primary axis. Thus, the inter-axis error parameters are embedded within the intra-axis error coefficients and so do not need to be estimated separately. The backlashes for linear and angular positioning of the X-, Y-, B- and C-axis are included but not for the Z-axis since all probing occurs with a negative Z approach and so its backlash cannot be observed. For positioning errors, a backlash term e.g. $E_{\mathrm{XXb}}\,\boldsymbol{dir}$, where $\boldsymbol{dir}$ is +1 or -1 for the direction of motion, is appended to the $E_{\mathrm{XX}}(x)$ polynomials,

$$E_{\mathrm{XX}}(x) = E_{\mathrm{XX0}}x^0 + E_{\mathrm{XX1}}x^1 + E_{\mathrm{XX2}}x^2 + E_{\mathrm{XX3}}x^3 + E_{XXb}\,dir. \qquad (4\text{-}3)$$

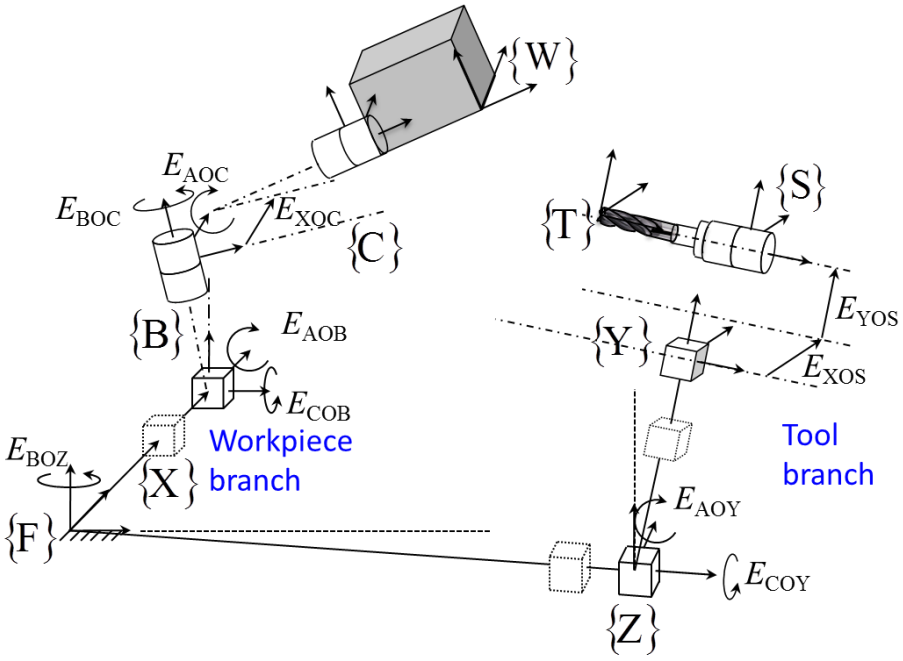

Figure 4-3 WCBXFZYST machine tool with inter-axis error parameters (adapted from [11])

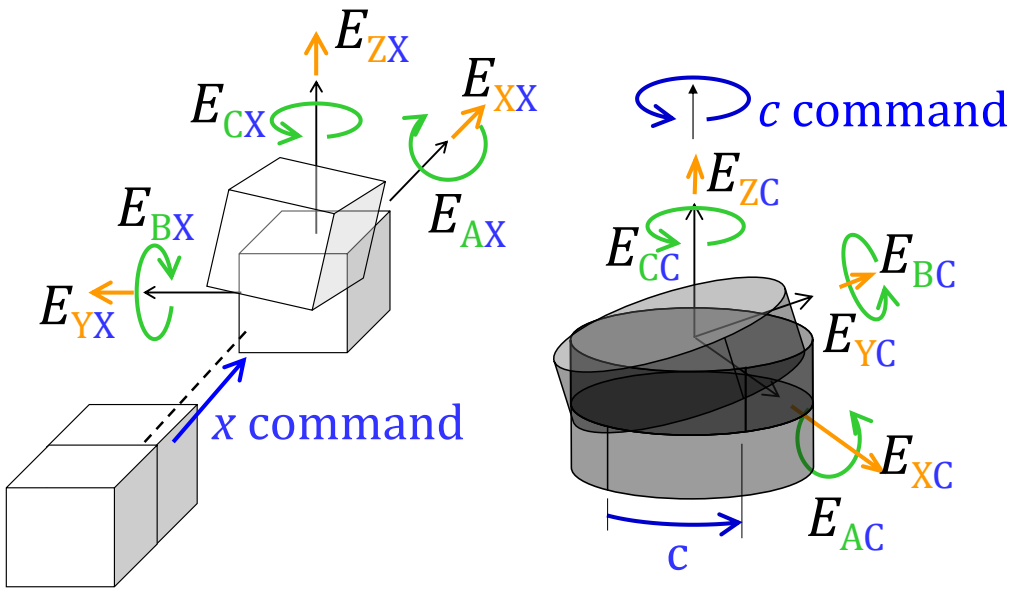

Figure 4-4 Linear and rotational displacements of axes with their intra-axis errors

The actual position and orientation of the tool with respect to the workpiece is calculated using a kinematic model. Each axis is modelled using three homogenous transformation matrices

representing the axis nominal position and orientation with respect to the previous axis in the chain, the nominal axis displacement and finally the intra-axis errors which embed the inter-axis errors. For example, the Z-axis is modelled as follows:

$$ {}^{\mathrm{F}}\boldsymbol{T}_{\mathrm{Z'}} = {}^{\mathrm{F}}\boldsymbol{T}_{\mathrm{Zo}}\,{}^{\mathrm{Zo}}\boldsymbol{T}_{\mathrm{Z}}\,{}^{\mathrm{Z}}\boldsymbol{T}_{\mathrm{Z'}} \tag{4-4} $$

where,

$$ {}^{\mathrm{F}}\boldsymbol{T}_{\mathrm{Zo}} = \mathbf{I} \tag{4-5} $$

is the HTM of the nominal axis location;

$$ {}^{\mathrm{Zo}}\boldsymbol{T}_{\mathrm{Z}} = \begin{bmatrix} 1 & 0 & 0 & 0 \\ 0 & 1 & 0 & 0 \\ 0 & 0 & 1 & z \\ 0 & 0 & 0 & 1 \end{bmatrix} \tag{4-6} $$

is the HTM of the nominal axis motion and finally,

$$ {}^{\mathrm{Z}}\boldsymbol{T}_{\mathrm{Z'}} = \begin{bmatrix} \left[\boldsymbol{R}(\hat{\mathrm{k}}_{\mathrm{Z}}, E_{\mathrm{CZ}})\,\boldsymbol{R}(\hat{\mathrm{j}}_{\mathrm{Z}}, E_{\mathrm{BZ}})\,\boldsymbol{R}(\hat{\mathrm{i}}_{\mathrm{Z}}, E_{\mathrm{AZ}})\right]_{3\times 3} & \begin{matrix} E_{\mathrm{XZ}} \\ E_{\mathrm{YZ}} \\ E_{\mathrm{ZZ}} \end{matrix} \\ \begin{matrix} 0 & 0 & 0 \end{matrix} & 1 \end{bmatrix} \tag{4-7} $$

is the HTM for intra-axis errors with embedded inter-axis errors where for example, $\boldsymbol{R}(\hat{\mathrm{j}}_{\mathrm{Z}}, E_{\mathrm{BZ}})$ represents a rotation by an angle E_{BZ} around the Y-axis of the Z-axis reference frame and E_{XZ}, E_{YZ} and E_{ZZ} are the linear error motions of the linear Z-axis along the X-, Y- and Z-axis directions. In this case they are the two straightness error motions and the linear positioning error motion.

For each facet probing, the distance between the stylus tip centre and the target facet is equal to the effective stylus tip radius. This provides the necessary constraint to drive the optimization

process to estimate all unknown variables which are estimated using a local linearization of the kinematic model in the form of a set of linear equations

$$\delta d = \boldsymbol{J}\delta E \tag{4-8}$$

with δd the facets to stylus tip signed predicted distances calculated with the nominal model, δE the unknown machine tool error coefficients, artefact facet position offset errors and the stylus tip setup errors, and $\boldsymbol{J}$ the Jacobian matrix establishing the sensitivity of the facet to stylus tip distances to small changes in the unknowns. An iterative Gauss-Newton process is used. The algorithm is similar to that presented in [14]. The initial error coefficients are set to 0. The estimated model is used with exact homogenous transformations matrices to produce the predicted observations. In this case the stylus tip should just touch the facet surface. The discrepancy between the predicted and actual observations are fed to the linear Jacobian based Equation 8 to produce adjustments to the error parameters. These adjustments are cumulated until the last calculated adjustment is smaller than a threshold, usually set to about 10^{-12}.

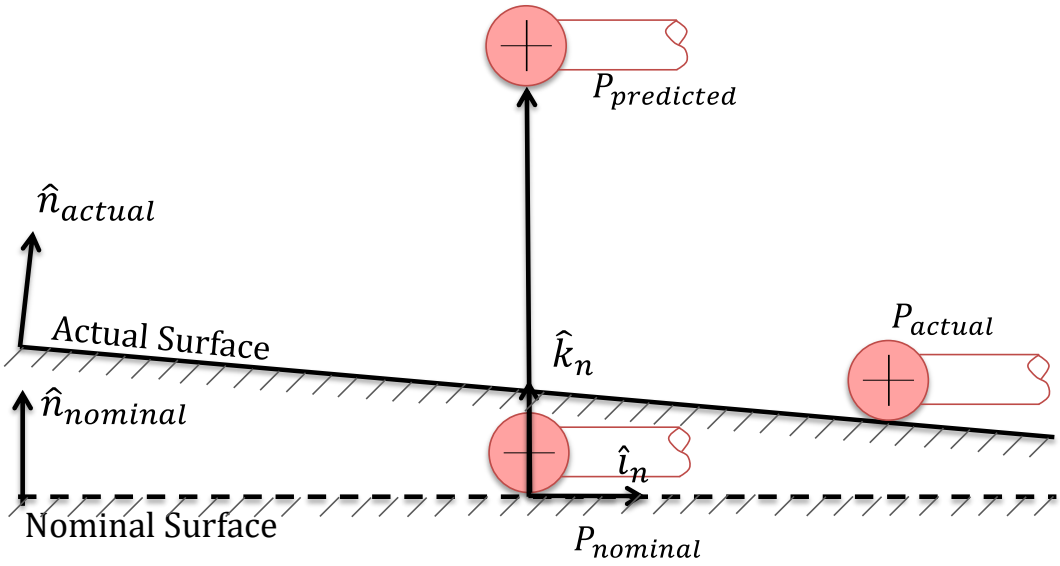

Figure 4-5 Facet probing. The red circle is the probe stylus tip

Figure 4-5 illustrates the facet probing. $P_{nominal}$ is the programmed stylus tip position where contact is expected. Due to the combined effect of setup and machine errors P_{actual} is the actual

tip position when contact occurs. Finally, $P_{predicted}$ is the model prediction using the recorded axis readings when contact occurred.

In order to evaluate the relative usefulness of sub-groups of error coefficients, four error parameter coefficients estimation subsets were studied:

Subset S1- setup error parameters only (stylus tip centre and facets position errors). No machine tool error coefficients are estimated. As much as possible of the observations are explained by adjusting these setup errors. What is left, the residuals, are attributed to the machine tool. Subset S1 only contains:

-stylus tip centre position error relative to the spindle axis frame E_{Xt}, E_{Yt} and E_{Zt};

-translational error of facet i normal to facet i, E_{Zfi}.

Subset S2-parameters included in subset S1 plus the linear axis linear positioning error gains [11]. Thus, subset S2 also contains:

-linear axes positioning error gains E_{XX1}, E_{YY1} and E_{ZZ1}.

Subset S3-parameters included in subset S2 plus the inter-axis error parameters and backlashes. Thus, subset S3 also contains the inter-axis error parameters [11]:

-eight axis alignments errors E_{AOB}, E_{COB}, E_{XOC}, E_{AOC}, E_{BOC}, E_{BOZ}, E_{AOY}, E_{COY} which are modelled as intra-axis errors polynomial coefficients [14] E_{AX0}, E_{CX0}, E_{XB0}, E_{AB0}, E_{BB0}, E_{XZ1}, E_{AZ0}, E_{CZ0}.

-the spindle offsets E_{XOS}, E_{YOS} which are modelled as intra-axis errors polynomial coefficients E_{XY0} and E_{YY0}.

S4-parameters included in subset S3 plus identifiable intra-axis parameters. Thus, subset S4 also contains additional axis positioning errors:

-additional axis positioning errors (E_{XX2}, E_{XX3}), (E_{YY2}, E_{YY3}), (E_{ZZ2}, E_{ZZ3}), (E_{BB1}, E_{BB2}, E_{BB3}), (E_{CC1}, E_{CC2}, E_{CC3});

-other intra-axis errors' coefficients:

E_{YX2}, E_{YX3}, E_{ZX2}, E_{ZX3}, E_{AX1}, E_{AX2}, E_{AX3}, E_{BX1}, E_{BX2}, E_{BX3}, E_{CX1}, E_{CX2}, E_{CX3}, E_{XB1}, E_{XB2}, E_{XB3}, E_{YB1}, E_{YB2}, E_{YB3}, E_{ZB1}, E_{ZB2}, E_{ZB3}, E_{AB1}, E_{AB2}, E_{AB3}, E_{CB1}, E_{CB2}, E_{CB3}, E_{XC1}, E_{XC2}, E_{XC3} E_{YC1}, E_{YC2}, E_{YC3}, E_{ZC1}, E_{ZC2}, E_{ZC3}, E_{AC1}, E_{AC2}, E_{AC3} E_{BC1}, E_{BC2}, E_{BC3}, E_{XZ2}, E_{XZ3}, E_{YZ2}, E_{YZ3}, E_{AZ1}, E_{AZ2}, E_{AZ3}, E_{CZ1}, E_{CZ2}, E_{CZ3}, E_{XY2}, E_{XY3}, E_{ZY2}, E_{ZY3}

-observable backlash errors for rotary and linear axes E_{XXb}, E_{YYb}, E_{BBb} and E_{CCb}.

Table 4-1 All potential polynomial coefficients of intra-axis errors parameters of the WCBXFYZT machine tool. Subset S1 contains none of those parameters. Subset S2 includes coefficients in red bold. Subset S3 also includes coefficients in purple underlined and subset S4 also includes coefficients in blue bold underlined

C						B					
E_{XC}	E_{YC}	E_{ZC}	E_{AC}	E_{BC}	E_{CC}	E_{XB}	E_{YB}	E_{ZB}	E_{AB}	E_{BB}	E_{CB}
E_{XC0}	E_{YC0}	E_{ZC0}	E_{AC0}	E_{BC0}	E_{CC0}	E_{XB0}	E_{YB0}	E_{ZB0}	E_{AB0}	E_{BB0}	E_{CB0}
E_{XC1}	E_{YC1}	E_{ZC1}	E_{AC1}	E_{BC1}	E_{CC1}	E_{XB1}	E_{YB1}	E_{ZB1}	E_{AB1}	E_{BB1}	E_{CB1}
E_{XC2}	E_{YC2}	E_{ZC2}	E_{AC2}	E_{BC2}	E_{CC2}	E_{XB2}	E_{YB2}	E_{ZB2}	E_{AB2}	E_{BB2}	E_{CB2}
E_{XC3}	E_{YC3}	E_{ZC3}	E_{AC3}	E_{BC3}	E_{CC3}	E_{XB3}	E_{YB3}	E_{ZB3}	E_{AB3}	E_{BB3}	E_{CB3}
					E_{CCb}					E_{BBb}	
X						Y					
E_{XX}	E_{YX}	E_{ZX}	E_{AX}	E_{BX}	E_{CX}	E_{XY}	E_{YY}	E_{ZY}	E_{AY}	E_{BY}	E_{CY}
E_{XX0}	E_{YX0}	E_{ZX0}	E_{AX0}	E_{BX0}	E_{CX0}	E_{XY0}	E_{YY0}	E_{ZY0}	E_{AY0}	E_{BY0}	E_{CY0}
E_{XX1}	E_{YX1}	E_{ZX1}	E_{AX1}	E_{BX1}	E_{CX1}	E_{XY1}	E_{YY1}	E_{ZY1}	E_{AY1}	E_{BY1}	E_{CY1}
E_{XX2}	E_{YX2}	E_{ZX2}	E_{AX2}	E_{BX2}	E_{CX2}	E_{XY2}	E_{YY2}	E_{ZY2}	E_{AY2}	E_{BY2}	E_{CY2}
E_{XX3}	E_{YX3}	E_{ZX3}	E_{AX3}	E_{BX3}	E_{CX3}	E_{XY3}	E_{YY3}	E_{ZY3}	E_{AY3}	E_{BY3}	E_{CY3}
E_{XXb}							E_{YYb}				
Z											
E_{XZ}	E_{YZ}	E_{ZZ}	E_{AZ}	E_{BZ}	E_{CZ}						
E_{XZ0}	E_{YZ0}	E_{ZZ0}	E_{AZ0}	E_{BZ0}	E_{CZ0}						
E_{XZ1}	E_{YZ1}	E_{ZZ1}	E_{AZ1}	E_{BZ1}	E_{CZ1}						
E_{XZ2}	E_{YZ2}	E_{ZZ2}	E_{AZ2}	E_{BZ2}	E_{CZ2}						
E_{XZ3}	E_{YZ3}	E_{ZZ3}	E_{AZ3}	E_{BZ3}	E_{CZ3}						
		E_{ZZb}									

4.5 **Probing strategy**

Up to 26 facets are probed at 28 different B-, C- and S-axis indexation combination triplets using a machine touch trigger probe model MP700 from Renishaw with a 100 mm stylus length. The table has overall dimensions of 400×400 mm (Figure 4-2). The B- and C-axis can rotate from

+90° to -90° and +360° to -360° respectively. The B-axis is indexed at 0°, +15°, +45°, +60°, +90°, +75°, +30°, -30°, -60°, -90°, -75°, -45°, and -15°. The C-axis is indexed at +90°, +180°, +270°, +225°, +45°, 0°, -45°, -135°, -180°, -270°, -180°, and -90°. Positive and negative axis motions are used for the B- and C-axis in order to observe any backlash. The X- Y- and Z-axis are programmed to accomplish the facet probing. Negative and positive probing approach directions will occur for the X- and Y-axis but for the Z-axis only negative probing approach direction will occur.

Table 4-2 Facets probing strategy. Facet numbers are followed according to Figure 4-2. Numbers 1 and 2 (Red and bold) refer to the sphere of the scale bar measured only once

Rotary axes indexations			Accessible facets ID
A(C1)	B	C	
0	+30	-90	3 5 8 9 10 11 14 16 19 20 21 22 23 24 25 26 27 28
0	+60	-180	10 11 12 13 14 15 16 17 18 19 20 21 22 23
0	+90	-270	5 6 7 8 10 12 13 14 15
0	+75	-225	10 12 13 14 15 16 17 18 21
0	+45	-135	10 11 13 14 15 16 17 18 21 22 23
0	+15	-45	3 5 8 9 10 11 14 16 19 20 21 22 23 24 25 26 27 28
0	0	0	3 5 6 7 8 9 10 11 12 13 14 15 16 17 18 19 20 21 22 23 24 25 26 27 28
0	-15	+45	3 8 9 10 11 14 15 16 17 18 19 20 21 22 23 24 25 26 27 28
0	-45	+135	3 5 6 8 9 10 21 22 23 24 25 26 27 28
0	-60	+180	3 5 6 7 8 9 10 23 24 25 26 27 28
0	-90	+270	5 6 7 8 10 12 13 14 15
0	-75	+225	3 5 6 7 8 26 27 28
0	-30	+90	3 9 11 15 16 17 18 19 20 21 22 23 24 25 26 27 28
0	0	+270	3 4 5 6 7 8 9 10 11 12 13 14 15 16 17 18 19 20 21 22 23 24 25 26 27 28
0	0	+180	3 4 5 6 7 8 9 10 11 12 13 14 15 16 17 18 19 20 21 22 23 24 25 26 27 28
0	0	+90	3 4 5 6 7 8 9 10 11 12 13 14 15 16 17 18 19 20 21 22 23 24 25 26 27 28
0	0	0	**1 2** 3 4 5 6 7 8 9 10 11 12 13 14 15 16 17 18 19 20 21 22 23 24 25 26 27 28
0	0	-90	3 4 5 6 7 8 9 10 11 12 13 14 15 16 17 18 19 20 21 22 23 24 25 26 27 28
0	0	-180	3 4 5 6 7 8 9 10 11 12 13 14 15 16 17 18 19 20 21 22 23 24 25 26 27 28
0	0	-270	3 4 5 6 7 8 9 10 11 12 13 14 15 16 17 18 19 20 21 22 23 24 25 26 27 28
0	0	0	5 7
+90	0	0	5 7
+180	0	0	5 7
+270	0	0	5 7
0	0	0	12 15
+90	0	0	12 15
+180	0	0	12 15
+270	0	0	12 15

The number of facets probed at each B- and C-axis combination depends on the accessibility of the probe to those facets. For instance, at B=+90° or -90° numerous facets are not accessible although extra indexations of the C-axis could improve access to more facets. The length of the probe stylus also affects accessibility.

The spindle is indexed at 0°, +90°, +180° and +270° to allow estimation of the stylus tip offsets from the spindle axis and so avoid their being confounded with the spindle position error parameters. Finally the scale bar is measured. The purpose of using a reference length, in the form of a scale bar, is to determine the ability of the machine to produce motions correct with respect to the international meter. Without the bar only the relative scale errors (scale mismatches) E_{YY1}-E_{XX1} and E_{ZZ1}-E_{XX1} are visible. The bar allows all three scale gain errors E_{XX1}, E_{YY1} and E_{ZZ1} to be included [11]. It is not required for the inter-axis errors. The two balls of the scale bar, which are separated by a calibrated distance, are probed once. The orientation of the bar is not thought to be critical but it was measured when aligned with the X-axis. Table 4-2 shows the probing strategy for facet probing at different rotary axes indexations.

In the conducted experiments the bar was always included in order to have CMM verifiable estimates of the artefact geometry since the bar provides a link to the international meter. The bar is simply fixed, as in [11], on the machine table i.e. the indigenous artefact. Total test time for the 383 facet probing is 2H41M (2 hours and 41 minutes).

4.6 **Results of preliminary tests**

Because the artefact is the machine table, tests were conducted to assess its suitability as a reference artefact. The main concern here is the quality of the surface in terms of surface finish, possible damage and the likely presence of machining liquids and how this could affect the probing results. Facets were oriented relative to the machine linear axes and a single surface point is probed repeatedly 300 times using a normal approach direction for a test duration of 1H45M with the full retraction of the probe along the Z-axis by approximately 300 mm after each probing. In order to observe non repeatability while excluding the effect of drift the pooled standard deviation is evaluated with a sample window of 25 measurements over 300

measurements. The standard deviations along the X, Y and Z directions were of 0.63, 0.59 and 0.63 µm respectively. Two dimensional (2D) probing is assessed using an inclined facet with its normal in the X-Y plane making a 45 degree angle with the X-axis, which yielded a measurement standard deviation along the facet normal of 0.64 µm. A three dimensional (3D) probing requiring synchronised X, Y and Z motion yielded a standard deviations of 0.46 µm.

Surface wetness effect on probing was also evaluated for Z- and 3D-direction probing. The surface was cleaned, probed one hundred times, then wetted with cutting fluid and probed again one hundred times. This cycle was repeated three times for a total test time of 1H53M. The result shown in Figure 4-6 exhibits a drift in the first half of the test which was started with a cold machine.

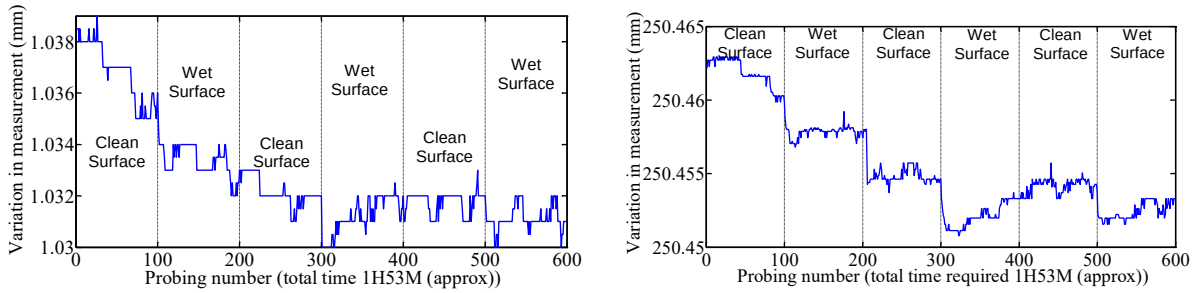

Figure 4-6 Wetness effect on probing in Z-axis (left) and 3D-direction (right). Each probing takes approximately 11.3 seconds

The effect of wetting the surface on probing is analysed for last 300 repeated measurements when the drift seems to stop. The drift contributes approximately 12 µm during the first hour of the test. Cutting fluid was sprayed to wet the surface just before the 301st probing. As a result, for probing 301 to 400 the surface was wet; the surface was cleaned just before the 401st probing and so was clean for probing 401 to 500; from 501 to 600, the surface was wet again. Standard deviations of these three states are 0.69, 0.44 and 0.46 µm with means of 1.03122, 1.03175 and 1.03113 mm respectively for the Z-axis for a range of the means of 0.62 µm. Similarly, the standard deviations for 3D-directional probing are 0.79, 0.49 and 0.58 µm and the respective means are 250.45214, 250.45415 and 250.45244 mm for a range of the means of 2.01 µm, all in the direction normal to the surface. The effect of wetness appears to be quite small.

The effect of surface irregularities and probing direction on probing was also analysed. This is important because each facet will be probed for multiple rotary axes indexations and the many error sources will inevitably mean that the facet will be probed at slightly different places within a small region.

Separate grids of n=25 points on facets 2x2 mm were probed repeatedly using normal approaches, one grid for each of k=5 different directions (the machine's X-, Y- and Z-axes, and in 2D and in 3D directions). Each grid was measured m=25 times for a duration of approximately 1H45M. These measurements are simultaneously influenced by the unknown drift as discussed before, surface irregularities and probing repeatability. So, for each direction, the total variability over the grid surface due to these factors is calculated by computing the standard deviation for all the measurements for that direction k (k=1, 2, 3, 4 and 5 for X-, Y-, Z-, 2D- and 3D-direction respectively),

$$s_{T,k} = \sqrt{\frac{\sum_{i=1}^{n}\sum_{j=1}^{m}(P_{i,j,k}-\hat{P}_k)^2}{(n\times m)-1}}; \tag{4-9}$$

with

$$\hat{P}_k = \frac{\sum_{i=1}^{n}\sum_{j=1}^{m}P_{i,j,k}}{n\times m}; \tag{4-10}$$

where i=1, 2, …, n (n=25) represent the facet's grid point identifier and j=1,2, …, m (m=25) represents the cycle identifier. Results are given in Table 4-3. The ranges of $(P_{i,j,k}-\hat{P}_k)^2$ for each directions are also provided.

The effects of the surface and the drift are removed to analyse the effect of repeatability by calculating the pooled standard deviation for each grid point i, and direction k, $s^2_{\text{pooled},i,k}$ with a sample window of 5 measurements over the m=25 measurement cycles for each respective directions k. Then, the maximum value $s^2_{\text{pooled},k}$ of the pooled standard deviations is shown in Table 4-3. Again, if i represent the facet's grid point identifier and j the cycle identifier then the pooled variance $s^2_{\text{pooled},i,k}$ can be estimated by the weighted mean of the variances $s^2_{i,k,l}$,

$$s^2_{i,k,l} = \sum_{j=(l-1)r_l+1}^{lr_l}\frac{(p_{i,j,k}-\hat{p}_{i,k,l})^2}{r_l-1}; \tag{4-11}$$

$$s^2_{\text{pooled},i,k} = \frac{\sum_{l=1}^{m/5}(r_l-1)s^2_{i,k,l}}{\sum_{l=1}^{m/5}(r_l-1)}; \quad (4\text{-}12)$$

where, l is the population window identifier for each grid point, r_l is the sample size of the population window.

Then the effect of the surface itself should be revealed by removing the effect of repeatability and drift by calculating the mean of each grid point $\hat{P}_{i,k}$ over all *m* cycles for a particular direction *k*,

$$\widehat{P}_{i,k} = \frac{1}{m}\sum_{j=1}^{m} P_{i,j,k}. \quad (4\text{-}13)$$

The standard deviation of the *n* =25 grid point's means is then calculated for each respective direction.

$$s_k^2 = \sum_{i=1}^{n} \frac{(\hat{P}_{i,k}-\hat{T}_k)^2}{n-1}; \quad (4\text{-}14)$$

$$\text{where, } \hat{T}_k = \frac{1}{n}\sum_{i=1}^{n} \hat{P}_{i,k}; \quad (4\text{-}15).$$

In another test, a particular facet with *n*=25 grid points was measured once for each of the five directions and this cycle was repeated *m*=19 times over a period of 7H30M approximately. The purpose of this test is to analyse the effect of the drift during a TANGO test. To do so, the means of each of the *n* grid points for each direction is calculated over all cycles and the range of means was observed. The means of *n* grid points of *m* cycles is calculated by using the following formula

$$\widehat{P}_{j,k} = \frac{1}{n}\sum_{i=1}^{n} P_{i,j,k}. \quad (4\text{-}16)$$

The range and standard deviations of the mean of each grid cycle for a specific direction is given in Table 4-3. This propagation of means for each grid cycle measurement contains the effect of the drift over a time period of 7H30M.

Table 4-3 Variability of probing due to non-repeatability, surface irregularities, drift and direction of probing

	Total variability on grid measurements				
	X	Y	Z	2D	3D
Standard deviation (μm): $s_{T,k}$	1.28	1.11	0.64	2.52	2.14
Measurement Range (μm)	7.50	6.00	4.5	12.73	10.89
	Effect measurement repeatability (surface and drift effect is removed)				
	X	Y	Z	2D	3D
Maximum of the pooled standard deviation: $S_{pooled,k}$ for the *n* grid points over *m* cycle	0.68	0.65	0.63	0.72	0.60
	Effect of Surface (repeatability and drift effects are				
	X	Y	Z	2D	3D
Standard deviation for *n* point's means over *m* cycle (μm): S_k	0.89	0.95	0.30	2.25	2.09
Range of the *n* point's means over *m* cycle (μm)	4.26	3.84	1.52	8.82	8.52
	Effect of drift (surface and repeatability effects are				
	X	Y	Z	2D	3D
Standard deviation for *n* (=25) grid point's means over *m* (=19) cycle on the same grid surface for all directions (μm): S_k	1.6 (5.05*)	2.47	1.7	2.17	1.18
Measurement range of *n* (=25) grid point's means over m (=19) cycle on the same grid surface for all directions (μm)	4.84 (22.92*)	8.3	7.86	6.51	5.48

**A large variation between first and second cycle of X-axis grid measurements was observed. Thus, the range calculation for X-axis omits the first cycle measurement.*

The results tend to show that drift over time and surface irregularities are important factors.

Because the TANGO method uses individual probing measurements any lobing in the probe response directly affects the input data for the machine estimation. Manufacturer's specification of the probe fitted with a 100 mm stylus is a 2D pretravel variation of 0.35 µm and a 3D variation from a true sphere of 1.75 µm [18].

4.7 **Results for TANGO**

Table 4-4 gives the estimated values for the four different error parameter subsets using TANGO. Similar color codes as defined for Table 4-1 are used to distinguish the different parameter subsets. It is noticeable that the parameter values change when additional parameters are estimated.

Table 4-4 Estimated parameters for the four subsets

Subset 1	Subset 2		Subset 3		Subset 4					
	Name	Estimated value	Name	Estimated value	Name	Estimated value	Name	Estimated value	Name	Estimated value
-	E_{XX1}	-1.35E-05	E_{AX0}	-9.31E-06	E_{XC1}	-5.98E-05	E_{AB0}	2.58E-04	E_{CX2}	-2.63E-11
	E_{YY1}	3.25E-05	E_{CX0}	-1.09E-05	E_{XC2}	1.08E-04	E_{AB1}	-3.84E-04	E_{CX3}	-2.96E-12
	E_{ZZ1}	-4.46E-05	E_{XB0}	-1.08E-01	E_{XC3}	1.06E-05	E_{AB2}	-1.05E-04	E_{XY0}	-2.52E-01
			E_{AB0}	-7.83E-06	E_{YC1}	7.05E-04	E_{AB3}	4.30E-05	E_{XY2}	-5.21E-08
			E_{BB0}	2.10E-05	E_{YC2}	3.55E-07	E_{BB0}	1.99E-05	E_{XY3}	3.31E-10
			E_{XZ1}	7.36E-05	E_{YC3}	-5.00E-05	E_{BB1}	-9.47E-05	E_{YY1}	-5.31E-05
			E_{AZ0}	-4.34E-06	E_{ZC1}	-2.98E-04	E_{BB2}	-1.72E-05	E_{YY0}	1.32E-02
			E_{CZ0}	1.60E-05	E_{ZC2}	-8.70E-06	E_{BB3}	4.81E-05	E_{YY2}	-1.74E-07
			E_{XY0}	-1.34E-01	E_{ZC3}	8.66E-06	E_{BBb}	5.51E-06	E_{YY3}	3.07E-10
			E_{YY0}	2.86E-02	E_{AC1}	1.03E-06	E_{CB1}	2.71E-04	E_{YYb}	-4.93E-03
			E_{XXb}	6.95E-03	E_{AC2}	-1.17E-07	E_{CB2}	-1.57E-04	E_{ZY2}	1.47E-08
			E_{YYb}	-9.29E-04	E_{AC3}	-5.93E-08	E_{CB3}	-3.24E-05	E_{ZY3}	1.55E-11
			E_{BBb}	5.55E-06	E_{BC1}	-7.94E-07	E_{XX1}	-3.67E-06	E_{XZ1}	-4.38E-05
			E_{CCb}	-4.73E-05	E_{BC2}	-2.14E-08	E_{XX2}	4.89E-08	E_{XZ2}	2.26E-07
			E_{XX1}	-8.64E-06	E_{BC3}	4.44E-08	E_{XX3}	-1.88E-10	E_{XZ3}	-3.00E-10
			E_{YY1}	-1.79E-05	E_{CC1}	1.05E-05	E_{XXb}	6.08E-03	E_{YZ2}	5.06E-07
			E_{ZZ1}	-2.58E-05	E_{CC2}	6.85E-07	E_{YX2}	3.24E-08	E_{YZ3}	-1.06E-09
					E_{CC3}	-8.13E-07	E_{YX3}	-1.57E-09	E_{ZZ1}	-4.44E-05
					E_{CCb}	-3.61E-05	E_{ZX2}	3.34E-08	E_{ZZ2}	-6.26E-08
					E_{XB0}	-2.51E-01	E_{ZX3}	8.81E-11	E_{ZZ3}	7.21E-11
					E_{XB1}	-9.40E-02	E_{AX1}	-2.76E-08	E_{AZ0}	5.85E-05
					E_{XB2}	5.57E-02	E_{AX0}	-2.58E-04	E_{AZ1}	-1.97E-08
					E_{XB3}	1.17E-02	E_{AX2}	-1.02E-10	E_{AZ2}	-1.05E-09
					E_{YB1}	-5.71E-03	E_{AX3}	9.40E-13	E_{AZ3}	2.08E-12
					E_{YB2}	1.15E-03	E_{BX1}	-2.08E-08	E_{CZ0}	-4.04E-04
					E_{YB3}	1.32E-03	E_{BX2}	-2.16E-10	E_{CZ1}	3.52E-06
					E_{ZB1}	-1.46E-01	E_{BX3}	4.49E-13	E_{CZ2}	-1.06E-08
					E_{ZB2}	-4.21E-02	E_{CX0}	-4.47E-04	E_{CZ3}	1.07E-11
					E_{ZB3}	1.95E-02	E_{CX1}	1.33E-07		

Table 4-5 contains results when estimating subset S3 using the uncalibrated indigenous artefact only (TANGO) and then with the addition of the scale bar, a fixed length double ball bar 304.6686 mm long (scale enriched TANGO). It can be observed that the BC axes offset in X, E_{XOC}, and the spindle offset in X axis, E_{XOS}, have the largest values. This is consistent with machine operator's practice of setting the CNC spindle offset parameters such that the spindle is aligned with the C-axis at x=y=b=0. Without the scale bar data only scale mismatches (anisotropic scale) are estimated, i.e. E_{YY1}-E_{XX1} and E_{ZZ1}-E_{XX1} [4], [11]. All other parameters show negligible change.

Table 4-5 Estimated parameters (subset S3) using the TANGO (Touch ANd GO) method; all machine position compensation tables are set to 0

Estimated parameter [parameter equivalence]	Pure TANGO	Scale enriched TANGO
E_{AX0} (µrad) [E_{AOB}]	- 9.31	-9.31
E_{CX0} (µrad) [E_{COB}]	-10.92	-10.92
E_{XB0} (µm) [E_{XOC}]	-108.07	-108.06
E_{AB0}(µrad) [E_{AOC}]	-7.83	-7.83
E_{BB0}(µrad) [E_{BOC}]	21.00	21.00
E_{XZ1}(µrad) [E_{BOZ}]	73.60	73.60
E_{AZ0}(µrad) [E_{AOY}]	-4.34	-4.34
E_{CX0}(µrad) [E_{COY}]	16.03	16.03
E_{XY0} (µm) [E_{XOS}]	-134.24	-134.24
E_{YY0} (µm) [E_{YOS}]	28.60	28.60
E_{XX1}(µm/m)	n/a	-8.64
E_{YY1}-E_{XX1} or E_{YY1} (µm/m)	-9.24	-17.88
E_{ZZ1}-E_{XX1} or E_{ZZ1} (µm/m)	-17.15	-25.79
X-axis backlash E_{XXb} (µm)	6.95	6.95
Y-axis backlash E_{YYb} (µm)	-0.93	-0.93
B-axis backlash E_{BBb} (µrad)	5.88	5.88
C-axis backlash E_{CCb} (µrad)	-47.27	-47.27

4.8 **Results analysis**

The validity of the specific values for each parameter is not verified in this paper. To do so requires the estimation of uncertainties in the context of a multi-input multi-output process considering correlations amongst inputs and outputs. However, the estimated results will be studied in four different ways. First the capability of the estimated models to explain the volumetric deviation will be analysed. Then the accuracy of the estimated artefact geometry will

be compared to direct measurements of the artefact using a CMM. Finally, the accuracy of the volumetric tool position prediction will be assessed in two different ways.

The ability of the estimated models to explain the probing observations is evaluated by analysing the unexplained volumetric deviation between the stylus tip and the facet. Since during actual probing, contact occurred, a rich and well estimated machine model and artefact geometry should yield null unexplained deviations. Table 4-6 gives the maximum and mean unexplained volumetric error norms for the four different subsets. The general trend, as expected, is that as more parameters are estimated the ability of the model to explain the observations increases. The estimation of inter-axis errors on this machine yields a significant reduction in the unexplained volumetric behaviour of the machine. Intra-axis errors estimation yields a further halving of the same. For each subset, the respective estimated artefact is used. All observations are used both for the estimation and the verification i.e. no data set is kept aside for validation only.

Table 4-6 Unexplained volumetric error norms for different estimated parameter subsets

	Subset S1	Subset S2	Subset S3	Subset S4
Maximum volumetric error norm (μm)	145.63	139.51	22.31	10.69
Mean volumetric error norm (μm)	25.93	25.85	2.87	1.38

The improvement in the model's ability to explain the observations is illustrated in Figure 4-7 which shows the unexplained distance (residual) between the stylus tip and the facets.

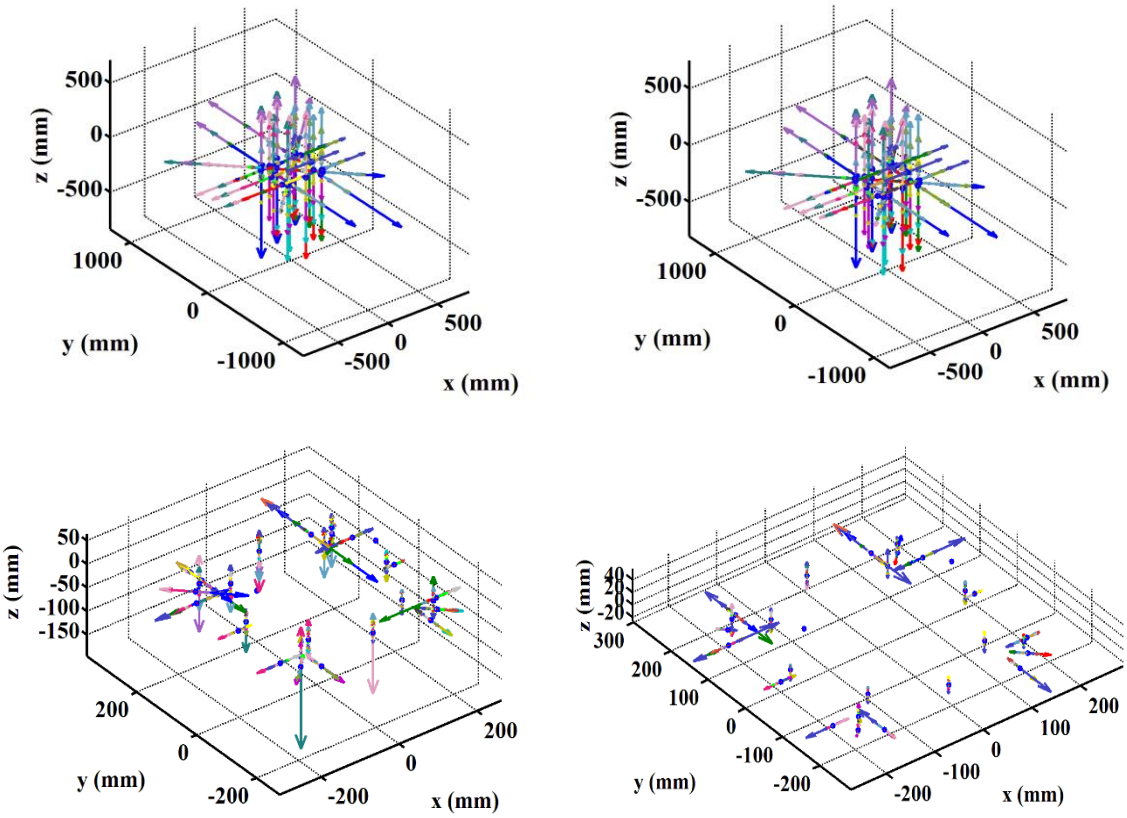

Figure 4-7 Unexplained volumetric residual vectors magnified 10000x. Each arrow color corresponds to a (b, c, s) indexation triplet. Top left: using subset S1 (stylus tip centre and facets errors only). Top Right: using subset S2 (Subset S1 plus the linear axis linear positioning errors). Bottom left: using subset S3 (subset S2 plus the inter-axis error parameters and backlashes). Bottom Right: using subset S4 (all identifiable inter- and intra-axis errors coefficients). All residuals are projected in the artefact frame

Because TANGO is an indirect self-calibration approach, the artefact geometry is also estimated. For the second validation way, it is worthwhile to assess the accuracy of the estimated artefact by comparing it with actual CMM metrology results obtained on a Legex 910 coordinate measuring machine. This is done for all four subset estimation cases. First let us mention that the artefact dimension differences from nominal dimensions (used as initial guess for the TANGO estimation) are in a range of 197.25 µm. The residual distances between TANGO estimation and CMM measurements of the facets for the four different subsets are shown in Figure 4-8. The

range of the residuals distances are 13.61, 14.40, 14.85 and 15.34 µm and the standard deviations are 3.82, 3.79, 3.72 and 3.72 µm respectively (Table 4-7).

Table 4-7 Comparison of the TANGO estimated artefact geometry with the CMM metrology of the facets; maximum, mean and standard deviations for the four different estimation subsets

Measures/criteria	Subset S1 No parameters included	Subset S2 Only scale included	Subset S3 Scale, link, backlash included	Subset S4 All 86 parameters included
Maximum (µm)	4.42	9.56	2.68	3.43
Mean (µm)	-1.55	1.03	-2.96	-3.01
Standard deviation (µm)	3.82	3.79	3.72	3.72
Range (µm)	13.61	14.40	14.85	15.34

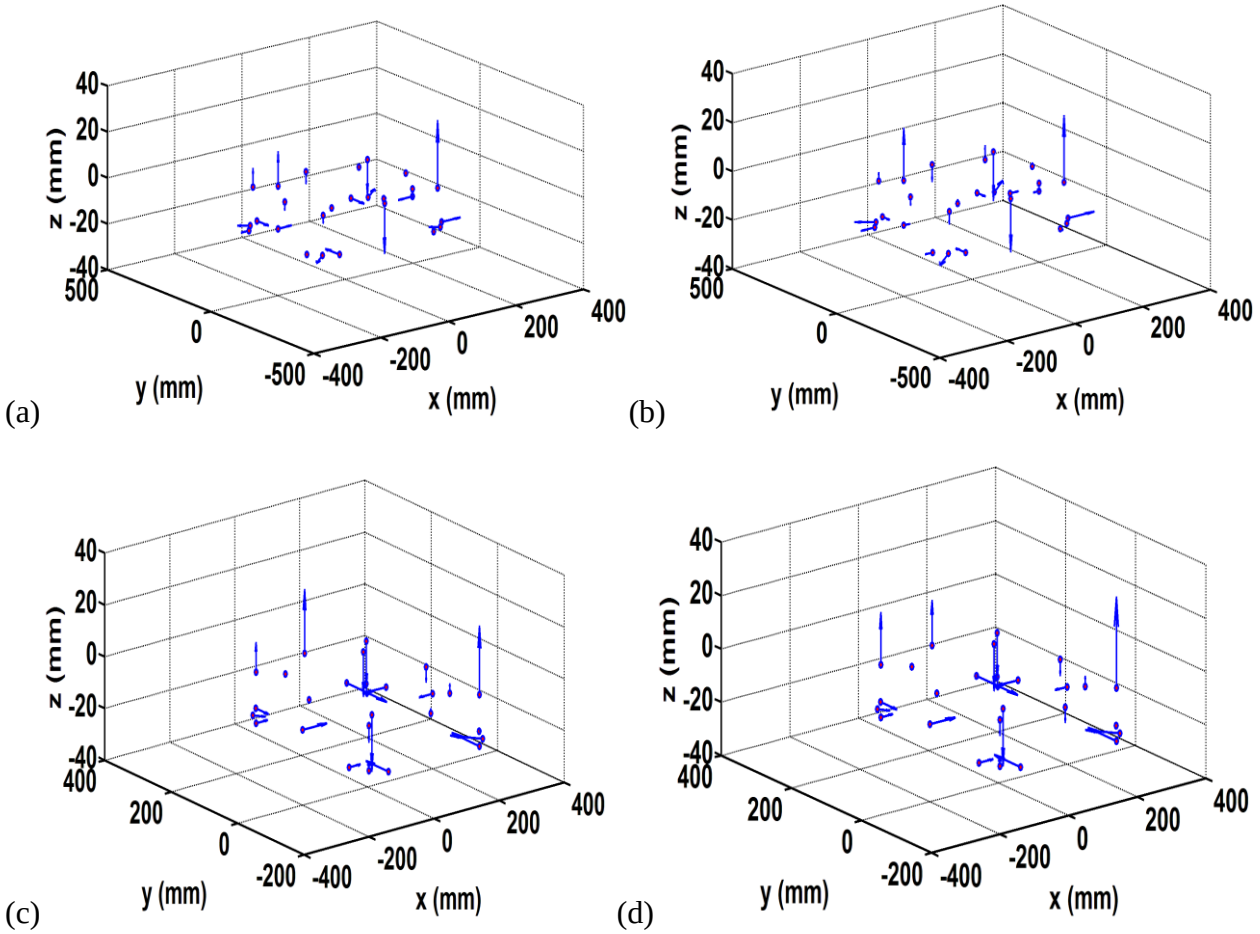

Figure 4-8 Residuals between TANGO estimation and CMM measurement of the artefact (10000x). a) Subset S1, b) Subset S2, c) Subset S3 and d) Subset S4

Unexpectedly it seems that no further improvement results from the increase in the number of machine estimated parameters. It suggests that there is a very little coupling between the machine and the artefact error parameters. However, the comparison with the CMM data includes a best fit so there may still be an overall shift, as a group, of the artefact estimated geometry which would not show here.

The volumetric position prediction capability of the estimated machine model is now conducted using the CMM measurements of the artefact, not the estimated ones. Firstly, the probe stylus tip positions relative to the last workpiece branch axis frame, the C frame (the artefact is rigidly attached to this frame) are predicted using the axis commands obtained for each facet probing and the estimated machine model. The predicted stylus tip positions are compared with the CMM

measured artefact through a least square fit. This is done to analyse the volumetric predictive capability of the estimated model as measured by the residuals between the predicted stylus tip positions for each facets using the TANGO model and the CMM measurement of the facets on the indigenous artefact. The standard deviations of the residuals for the S1, S2, S3 and S4 estimated parameter subsets are 34.69, 34.59, 5.53 and 4.28 µm respectively. The residuals of this comparison are listed in Table 4-8. The residuals are shown in Figure 4-9. Results show that the ability of the model to predict the facets position is improved significantly with the addition of more machine error parameters. The largest improvement is obtained for inter-axis errors (subset S3). The maximum error is further improved with the estimation of intra-axis errors. For this analysis all A-, B- and C- axis indexations triplets' data is used both for the estimation.

Table 4-8 Volumetric position prediction capability, all data used for estimation and for validation: maximum, minimum, mean and standard deviation of the residuals distances for the four different subsets

	Subset S1	Subset S2	Subset S3	Subset S4
Predicted probe tip position vs. CMM measure of the facets				
Maximum (µm)	139.50	135.53	19.03	6.92
Minimum (µm)	-112.50	-116.47	-28.46	-21.74
Mean (µm)	-0.12	0.99	-2.86	-2.91
Std deviation (µm)	34.69	34.59	5.53	4.28

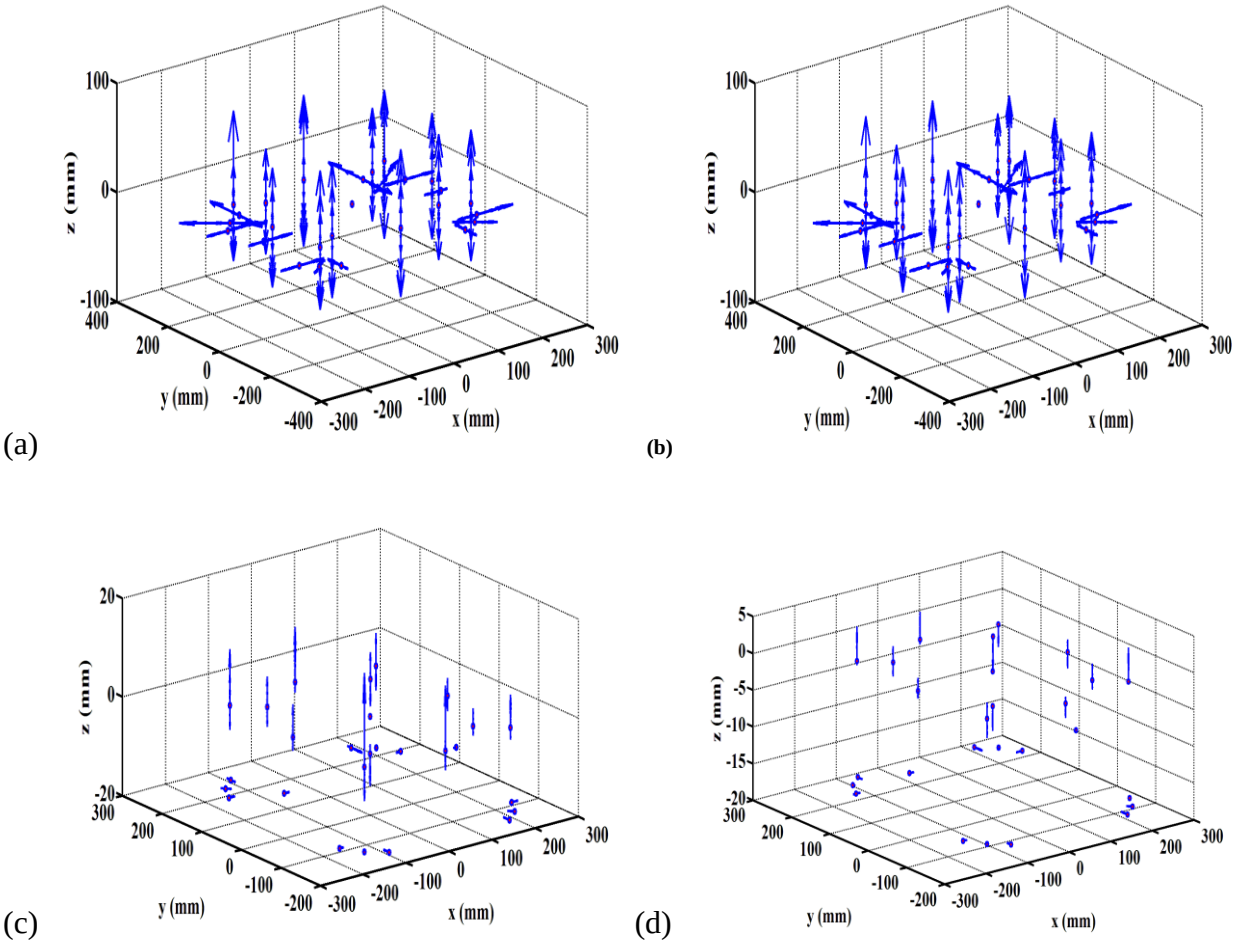

Figure 4-9 Volumetric position prediction capability, all data used for estimation and for validation: residual distances (1000x) between predicted probe stylus tip position in C frame and CMM measured artefact

For the last validation, out of a total 28 ABC indexation triplets used for facet probing, 23 sets are used to estimate the machine model and the remaining 5 sets are kept for validation purposes. These 5 sets are used to predict the probe stylus tip position in the last workpiece branch axis (rigidly connected to the artefact) as previously and compared with the CMM measured artefact geometry. The purpose of this test is also to evaluate the volumetric error prediction of TANGO method where a number of ABC indexation triplets used for facet probing is utilized only to predict the stylus tip positions for each facet and not for the estimation process. Figure 4-10

shows the residual distances for each facet and the maximum, minimum, mean and standard deviations of the residual distances are given in Table 4-9.

Table 4-9 Volumetric position prediction capability, five indexation data used for validation only: maximum, minimum, mean and standard deviation of the residuals between predicted stylus tip in C frame using 5 ABC indexations vs. CMM measurements of the artefact

	Subset 01	Subset 02	Subset 03	Subset 04
Predicted stylus tip on C frame vs. CMM				
Maximum residual distance (µm)	80.27	77.99	22.40	16.25
Minimum residual distance (µm)	-86.07	-89.18	-18.86	-13.99
Mean residual distance (µm)	-3.61	-2.47	-0.65	1.18
Standard deviation of residual distances (µm)	29.93	29.89	5.57	4.80

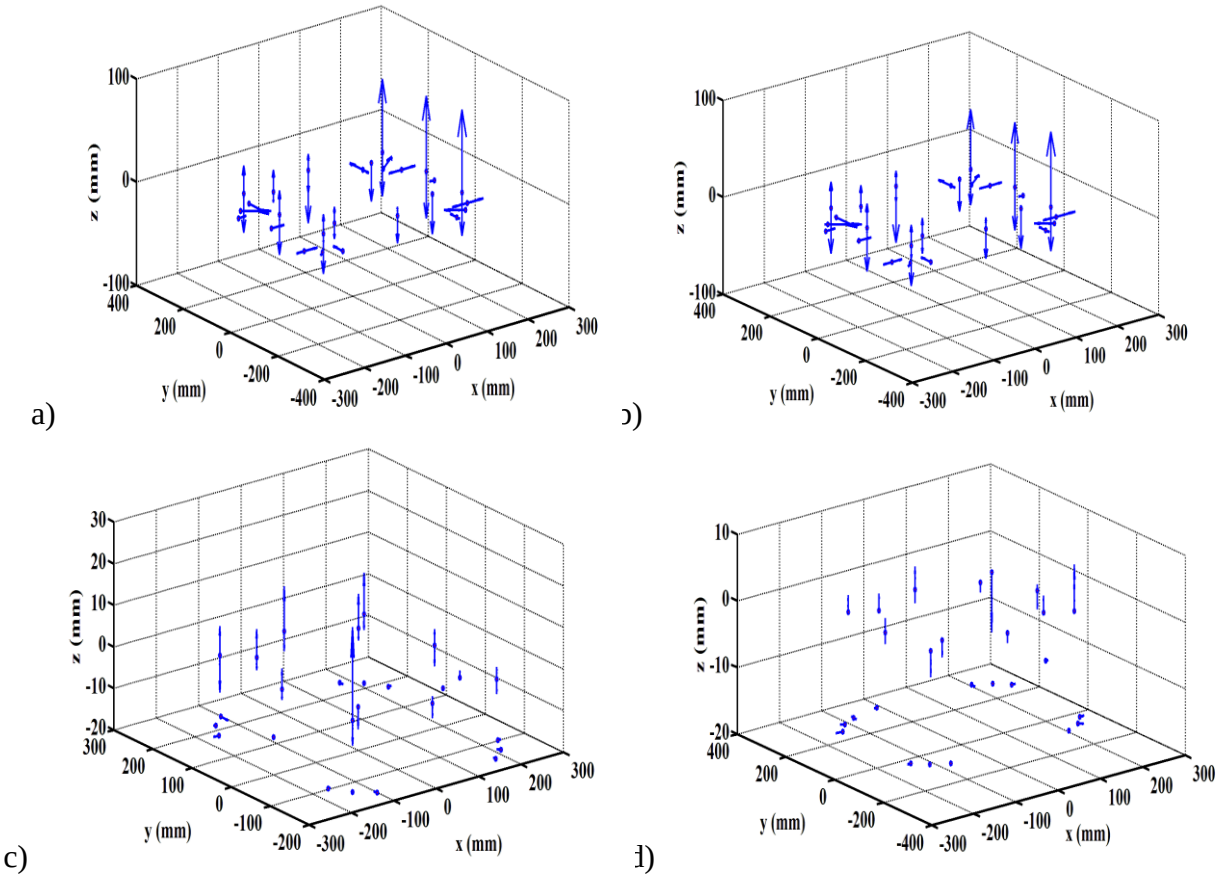

Figure 4-10 Volumetric position prediction capability, five indexation data used for validation only: residual distances (1000x) between TANGO predicted facets using a subgroup of probing information vs. CMM measured artefact. a) Subset S1, b) Subset S2, c) Subset S3 and d) Subset S4

Table 4-9 shows that, for the validation group of probing data (5 ABC indexation triplets), the standard deviation of the residuals between the TANGO prediction and CMM measurement of the facets reduced from 29.93 µm to 4.80 µm. The prediction gradually improves as additional parameters are estimated with subset S3 (inter-axis errors) being the most effective.

4.9 **Conclusion**

A scale enriched uncalibrated indigenous artefact consisting of selected facets on the machine tool standard table is probed to simultaneously estimate machine and artefact error parameters.

The TANGO method does not required any externally introduced artefact within the machine tool's working envelop except for an optional scale bar to provide absolute, as opposed to relative, scale factors. Nominally known small faces (facets) already present on the machine standard table, thus forming the uncalibrated indigenous artefact, are probed. The raw probing data was processed for four machine error parameter subsets, from none up to 86 inter-axis (axis location) and intra-axis (error motions) errors modelled as ordinary polynomials of 3rd degree, including axis position backlash except for the Z-axis. The estimated model is evaluated in four different ways. First the capability of the model to explain the volumetric observations was quantified by the unexplained maximum and mean volumetric residual vectors' norms which were reduced from 145.63 down to 10.69 and 25.93 down to 1.38 µm respectively as machine model parameters were gradually added for the four parameter subsets estimated. Secondly, the artefact geometry is validated by comparing the TANGO estimation of the artefact with CMM metrology data. The standard deviations for the four parameter subsets are 3.82, 3.79, 3.72 and 3.72 µm respectively. Thirdly, model volumetric prediction capability was tested by comparing the calculated tool tip position in the last workpiece branch frame (rigidly connected to the indigenous artefact frame) with the CMM metrology data of the artefact. As more model polynomial coefficients are estimated substantial improvements are obtained. The standard deviations of the prediction residuals are 34.69, 34.59, 5.53 and 4.28 µm for the four subsets, S1 to S4 respectively. The model volumetric prediction capability is also assessed by taking the probing measurements of 23 rotary axes combinations for machine model estimation and then using the remaining five for validation of the volumetric prediction of the tool tip position. The prediction is compared with the CMM artefact data and the residuals obtained have standard deviations of 29.93, 29.89, 5.57 and 4.80 µm for the four parameter subsets S1, S2, S3 and S4 respectively. The effects of facet wetness and unidirectional probe repeatability are around 1 µm standard deviation. On the other hand, the surface irregularity can reached 2.1 µm as standard deviation. Machine drift is significant and account for a maximum range of 8.3 µm over a period of 7H30M. In this work, the numerical validity of the estimated parameters is not claimed. Work is now underway to provide uncertainty estimates which are essential to assess the validity of the specific values obtained for the error parameters. This requires considering the multi-input multi-

output nature of the process including the correlations amongst the many inputs and outputs variables.

4.10 Acknowledgements

This research work is funded by the National Science and Enginering Reasearch Council of Canada (NSERC), The Consortium for Research and Innovation in Aerospace in Quebec (CRIAQ), Pratt & Whitney Canada, Meloche Group and SONACA Montreal. The authors are very grateful for the experimental support of Guy Gironne, Vincent Mayer and François Ménard.

4.11 References

[1] Schwenke, H., Knapp, W., Haitjema, H., Weckenmann, A., Schmitt, R., and Delbressine, F., "Geometric error measurement and compensation of machines—An update" , CIRP Annals - Manufacturing Technology (2008), 57(2), pp. 660-675.

[2] S. Ibaraki, W. Knapp, “Indirect Measurement of Volumetric Accuracy for Three-Axis and Five-Axis Machine Tools: A Review”, International Journal of Automation Technology (2012), Vol.6, No.2.

[3] S. Weikert and W. Knapp, "R-test, a new device for accuracy measurements on five axis machine tools," CIRP Annals - Manufacturing Technology (2004), vol. 53, pp. 429-432.

[4] B. Bringmann and W. Knapp, "Model-based 'Chase-the-Ball' calibration of a 5-axes machining center," CIRP Annals - Manufacturing Technology (2006), vol. 55, pp. 531-534.

[5] Hong, Cefu, Ibaraki, Soichi, “Non-contact R-test with laser displacement sensors for error calibration of five-axis machine tools”. Precision Engineering (2013), 37(1), pp. 159-171.

[6] S.H.H. Zargarbashi, J.R.R. Mayer, “Single setup estimation of a five-axis machine tool eight link errors by programmed end point constraint and on the fly measurement with Capball sensor”, International Journal of Machine Tools & Manufacture, 49 (2009), 759–766.

[7] Andolfatto, L., Mayer, J.R.R., Lavernhe, S. 2011, Adaptive Monte Carlo applied to uncertainty estimation in five axis machine tool link errors identification with thermal disturbance, International Journal of Machine Tools and Manufacture, 51 (2011), 618–627.

[8] Mohamed Slamani, Rene Mayer, Marek Balazinski,Seyedhossein H. H. Zargarbashi, Serafettin Engin, Claire Lartigue, “Dynamic and geometric error assessment of an XYC axis subset on five-axis high-speed machine tools using programmed end point constraint measurements”. International Journal of Advanced Manufacturing Technology (2010), 50(9-12), pp. 1063-1073.

[9] Kruth, J. P., Vanherck, P., and De Jonge, L., "Self-calibration method and software error correction for three-dimensional coordinate measuring machines using artefact measurements," Measurement: Journal of the International Measurement Confederation (1994), 14(2), pp. 157-167.

[10] Hocken, R., Simpson, J. A., Borchardt, B., Lazar, J., Reeve, C., and Stein, P., "Three dimensional metrology," Annals of the CIRP (1977), 26, pp. 403-408.

[11] Mayer, J. R. R., "Five-axis machine tool calibration by probing a scale enriched reconfigurable uncalibrated master balls artefact," CIRP Annals - Manufacturing Technology (2012), 61(1), pp. 515-518.

[12] Ibaraki, S., Iritani, T., and Matsushita, T., "Calibration of location errors of rotary axes on five-axis machine tools by on-the-machine measurement using a touch-trigger probe," International Journal of Machine Tools and Manufacture (2012), 58, pp. 44-53.

[13] Ibaraki, S., Iritani, T., and Matsushita, T., "Error map construction for rotary axes on five-axis machine tools by on-the-machine measurement using a touch-trigger probe," International Journal of Machine Tools and Manufacture (2013), 68, pp. 21-29.

[14] Mir, Y. A., Mayer, J. R. R., and Fortin, C., "Tool path error prediction of a five-axis machine tool with geometric errors," Proceedings of the Institution of Mechanical Engineers, Part B: Journal of Engineering Manufacture (2002), 216(5), pp. 697-712.

[15] Schultschik, R., "The components of the volumetric accuracy," Annals of the CIRP (1977), 25(1), pp. 223-228.

[16] ISO, "Test Code for Machine Tools-Part 1: Geometric accuracy of machines operating under no-load or quasi-static conditions," (2012) 230-1.

[17] Donmez, M. A., Blomquist, D. S., Hocken, R. J., Liu, C. R., and Barash, M. M., "General methodology for machine tool accuracy enhancement by error compensation," Precision Engineering (1986), 8(4), pp. 187-196.

[18] Machine tool probes and software (2014, June 09). Component setting and inspection probes-MP700 high accuracy touch probe. Retrieved from http://www.renishaw.ca/en/mp700-high-accuracy-touch-probe--6104

CHAPTER 5 ARTICLE 2: AN UNCALIBRATED CYLINDRICAL INDIGENOUS ARTEFACT FOR MEASURING INTER-AXIS ERRORS OF A FIVE-AXIS MACHINE TOOL

J.R.R. Mayer (2), Md. Mizanur Rahman, Anna Los

Mechanical Engineering Dept., Polytechnique Montréal, P.O. Box 6079, Station Downtown, H3C 3A7 Montréal (QC), Canada

Published in CIRP Annals Manufacturing Technology, Volume 64, Issue 1, 2015, Pages 487–490

5.1 Abstract

Ever simpler means of monitoring the geometry of five-axis machine tools are required to support automated production lines. This paper investigates the automated probing of the indigenous uncalibrated cylindrical machine table of a five-axis machine tool for estimating its inter-axis error parameters, i.e. the position and orientation errors of its axes. The uncertainties on the estimated errors are calculated from pooled covariance considering the correlation amongst input probing results as obtained from a specially designed series of repeated five daily cycles to distinguish between machine and measurement process variability.

Keywords: Calibration, Uncertainty, Probing

5.2 Introduction

In a five-axis machine tool, the additional two rotary axes add versatility to machine parts by eliminating numerous setups but the machine is also prone to additional errors. Geometric inaccuracies such as inter-axis errors (location and position errors of axis average line) [1] affect the volumetric accuracy. Direct and indirect approaches have been proposed to estimate such errors. Direct approaches require trained personnel and precise setups which is time consuming and entail operator involvement. Indirect approaches, generally easier to implement, demand more complex data processing increasing concerns over the uncertainty of the estimated errors [2].

A method based on mathematical analysis of singularities of linear system was proposed to determine the essential set of eight inter-axis errors of a five-axis machine tool [3]. In [4], an error model is developed where machine tool's inter-axis errors are estimated on the basis of a number of double ball bar test patterns and then used to calculate the 3D tool to the workpiece volumetric errors for the trajectories used when machining a cone frustum. The measurement of the coordinates of a single ball using a multi-sensor head in [5] yielded the inter-axis errors and linear axis relative positioning error motions. In [6], probing a scale and master-ball artefact (SAMBA) was proposed to estimates the inter-axis error parameters along with scale gains and spindle offsets by measuring 24 master-balls mounted at the tip of rods of different length and a scale bar attached to the machine table. In [7], probing of flat surfaces on an uncalibrated test piece was used to estimate the inter-axes errors of rotary axes of a five-axis machine tool. Facets were also probed in [8] but this time directly on the existing uncalibrated standard prismatic shape machine table thus constituting an indigenous uncalibrated artefact. The gathered data was used to estimate both inter- and intra-axis errors modelled as polynomials.

It was shown in [9] that the machine tool itself, measuring devices, measurement environment and even the operating personnel can contribute to the uncertainties of the measurement results while testing the machine tool accuracy. As the machine tool's errors have interdependencies among each other [10], covariances should be considered. An approach was proposed to identify these interdependencies by measuring a 3D-ball plate.

This paper presents a scheme where the eight inter-axis and two anisotropic scale gains (E_{YY1}-E_{XX1} and E_{ZZ1}-E_{XX1}) error parameters are estimated by touch probing nominally flat or curved facets of an existing cylindrical machine table as an indigenous artefact. First the artefact and machine model are described. Then, the mathematical model is presented followed by details of the artefact probing strategies and the patterns of measurement cycles used to build the input covariance matrices. Estimated errors and associated uncertainties are then presented and discussed followed by a conclusion.

5.3 The artefact

The indigenous uncalibrated artefact consists of a selection of nominally flat or curved facets on the standard ϕ500 mm cylindrical machine table shown in Figure 5-1.

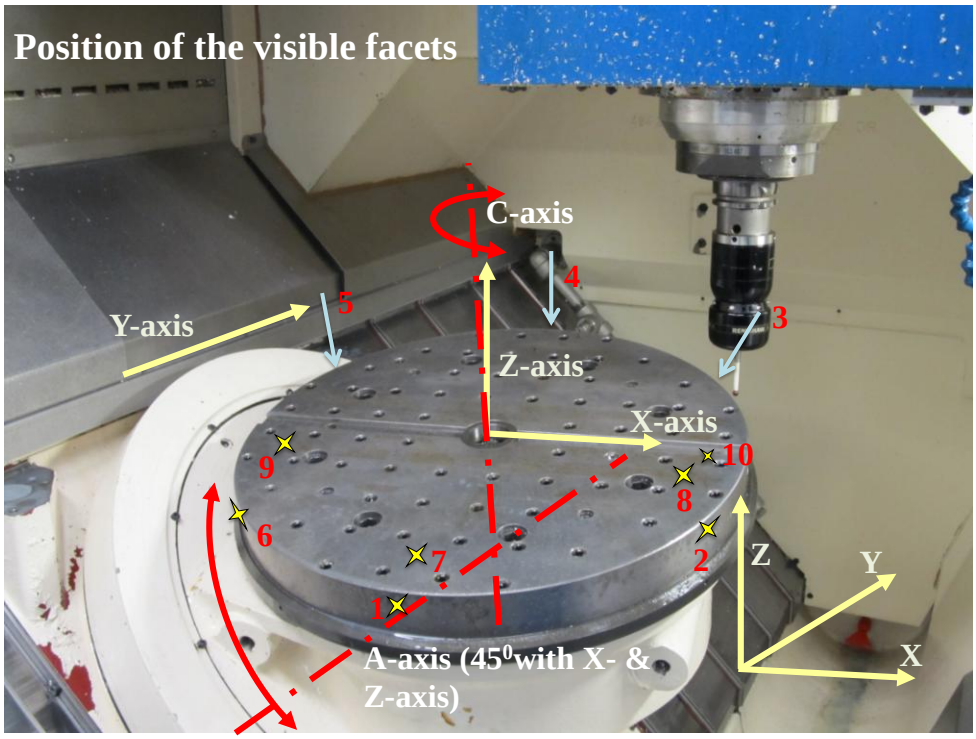

Figure 5-1 Indigenous artefact probing on the wCAYbXZ(C1)t machine tool. A-axis is shown slightly rotated. Facets are shown for Strategy S1

Each facet is defined by a target point and its local surface normal. Numerical simulation of the measurement and error estimation process for different measurement strategies indicated that when facets are only on the cylindrical surface at a single section in z, poor numerical conditioning results. Further simulations supported either adding up to three facets on the top flat surface or adding a second section of facets on the cylindrical surface in z. As a result, two different measurement strategies are experimentally studied. Figure 5-2 shows Strategy S1 with a total of ten facets among which six (facets 1 to 6) are on the nominally cylindrical portion of the table 10 mm from the nominally flat top surface of the table, three (7 to 9) are on the top surface of the table and one (facet 10) is on one side of the slot.

Figure 5-3 shows Strategy S2 with eight facets. Facets 1, 3, 5 and 7 are 30 mm from the top surface of the table whereas facets 2, 4, 6 and 8 are 10 mm from the top. Figure 5-1 shows the artefact probing on a Huron Graffenstaden HU40-KX8 five machining centre equipped with a MP700 Renishaw touch trigger probe.

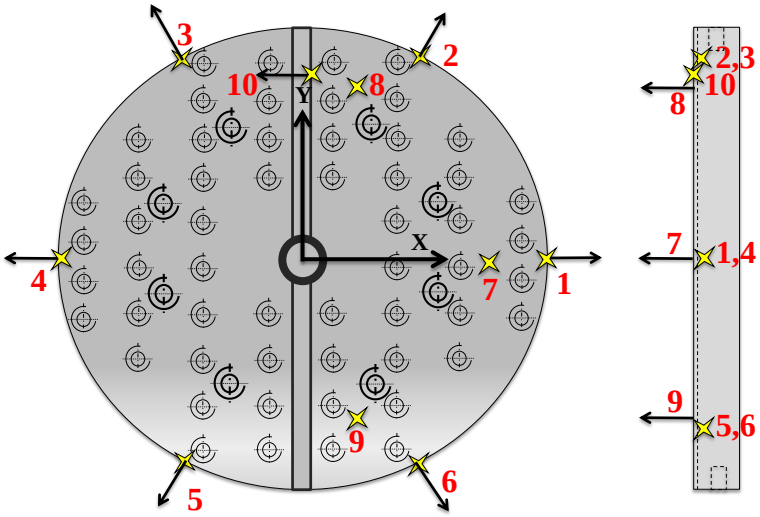

Figure 5-2 Indigenous artefact with the nominal target points and their local nominal normal for Strategy S1

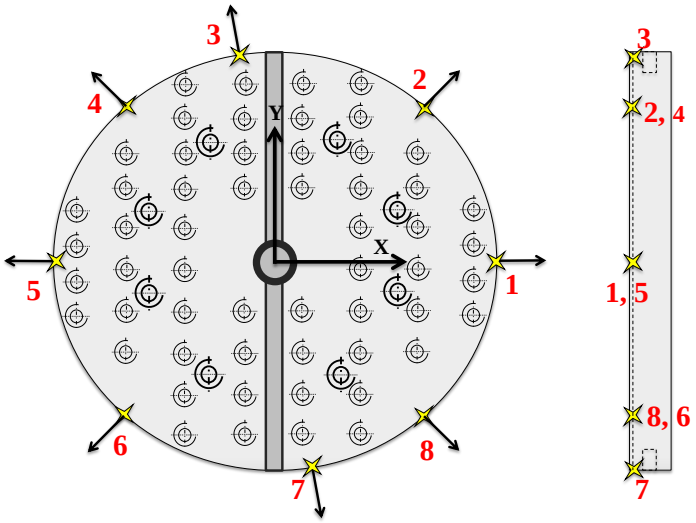

Figure 5-3 Indigenous artefact with the nominal target points and their local nominal normal for Strategy S2

5.4 **Mathematical model**

For the machine model the Y-axis and X-axis are chosen as the primary and secondary axes respectively [1]. The reference frame of the machine tool has its y-axis oriented with the machine Y-axis and then its z-axis normal to the plane containing the machine X- and Y-axis. Its origin is on the A-axis where a line segment (of length $|E_{\mathrm{Y0C}}|$) parallel to the Y-axis and passing through the C-axis intersects the A-axis. The nominal A-axis is tilted around Y by 45° relative to the X-axis. The spindle position and orientation errors are not considered. Table 5-1 lists the eight machine inter-axis errors.

Table 5-1 Inter-axis error (symbols as per ISO 230-1:2012(E) [1])

Symbol	Description
E_{Y0C}	Y-offset of C-axis
E_{A0C}	Squareness error of C- to Y-axis
E_{B0C}	Squareness error of C- to X-axis
E_{B0A}	Orientation error of A-axis about Y-axis
E_{C0A}	Squareness error of A- to Y-axis
E_{C0X}	Squareness error of X- to Y-axis
E_{A0Z}	Squareness error of Z- to Y-axis
E_{B0Z}	Squareness error of Z- to X-axis
E_{YY}-E_{XX}	Relative Y- to X-axis positioning error gain
E_{ZZ}-E_{XX}	Relative Z- to X-axis positioning error gain

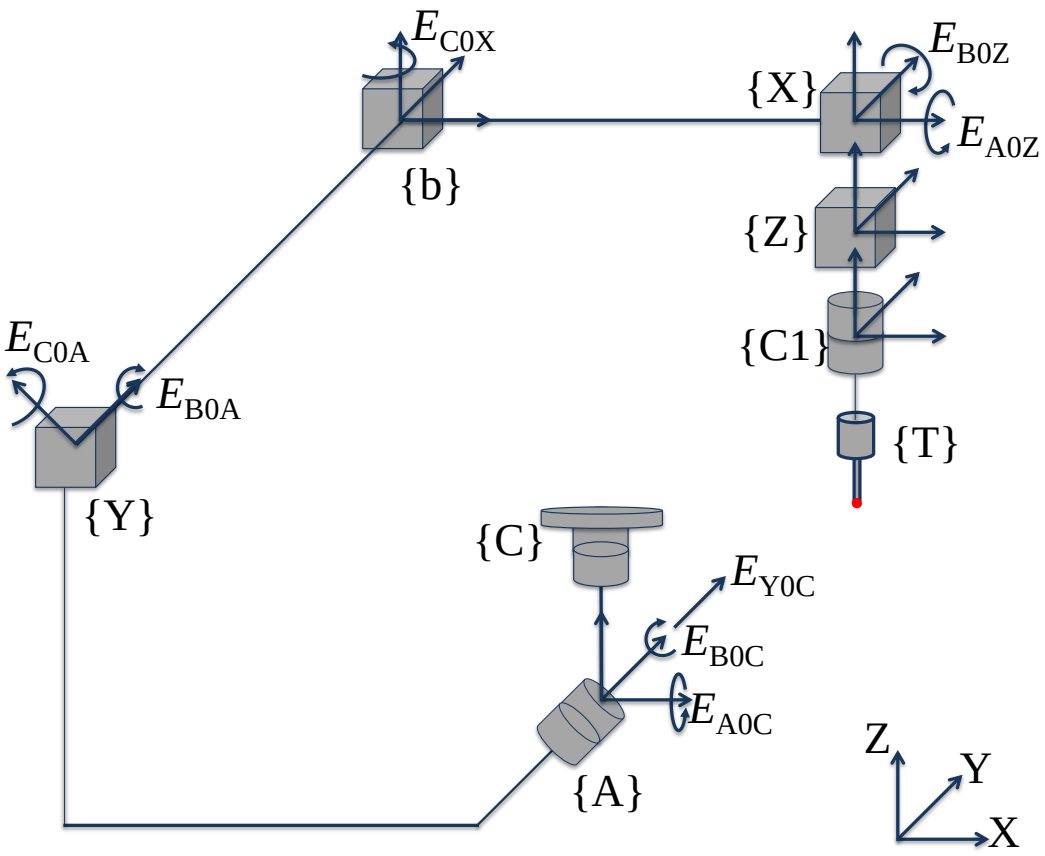

Figure 5-4 Kinematic model of the wCAYbXZ(C1)t machine tool with inter-axis errors

The error estimation is obtained via a Gauss-Newton procedure alternating between the solution of a set of linear equations defining the influence of small changes in the inter- and intra-axis errors on the position of the stylus tip with respect to the facets,

$$\delta \boldsymbol{d} = \boldsymbol{J}\delta \boldsymbol{E} \tag{5-1}$$

where $\delta \boldsymbol{d}$ is the change in distance between the stylus tip and the facet due to the machine errors array $\delta \boldsymbol{E}$. $\boldsymbol{J}$ is the Jacobian matrix built from error propagation matrices developed using geometric principles and small angular error approximations [3]. All inter-axis errors are modelled using scalar values acting at the locations shown in Figure 5-4. Previous work by the authors used error motion polynomial coefficients. For example, E_{C0X} is here modelled as a pure angular rotation whereas it would otherwise have been modelled as the linear term of the out-of-straightness E_{YX1} [8]. $\delta \boldsymbol{E}$ is then used to update the error array $\boldsymbol{E}$ and the new mistouch distance

is recalculated using the following erroneous kinematic chain from the facet to the stylus tip passing through the workpiece and tool branches using homogenous transformation matrices (HTMs)

$$
\begin{aligned}
{}^{\text{facet}'}\boldsymbol{T}_{\text{tip}'} &= {}^{\text{facet}'}\boldsymbol{T}_{\text{b}}\,{}^{\text{b}}\boldsymbol{T}_{\text{tip}'} = \left({}^{\text{b}}\boldsymbol{T}_{\text{facet}'}\right)^{-1}{}^{\text{b}}\boldsymbol{T}_{\text{tip}'} \\
&= \left({}^{\text{b}}\boldsymbol{T}_{\text{Y}'}\,{}^{\text{Y}'}\boldsymbol{T}_{\text{A}'}\,{}^{\text{A}'}\boldsymbol{T}_{\text{C}'}\,{}^{\text{C}'}\boldsymbol{T}_{\text{facet}'}\right)^{-1}{}^{\text{b}}\boldsymbol{T}_{\text{X}'}\,{}^{\text{X}'}\boldsymbol{T}_{\text{Z}'}\,{}^{\text{Z}'}\boldsymbol{T}_{\text{tip}'}
\end{aligned}
\tag{5-2}
$$

where each axis can have both inter- and intra-axis (for the scale gain) errors. For example, the X-axis has four HTMs describing the nominal axis location, inter-axis errors, nominal motion and its intra-axis errors:

$$
\begin{aligned}
{}^{\text{b}'}\boldsymbol{T}_{\text{X}'} &= {}^{\text{b}'}\boldsymbol{T}_{\text{X0}}\,{}^{\text{X0}}\boldsymbol{T}_{\text{X0}'}\,{}^{\text{X0}'}\boldsymbol{T}_{\text{X}}\,{}^{\text{X}}\boldsymbol{T}_{\text{X}'} \\
&= I\begin{bmatrix} & & & 0 \\ & R\left(\vec{k}_{\text{X0}}, E_{\text{C0X}}\right) & & 0 \\ & & & 0 \\ 0_{1\times3} & & & 1 \end{bmatrix}\begin{bmatrix} & & & x \\ & I_{3\times3} & & 0 \\ & & & 0 \\ 0_{1\times3} & & & 1 \end{bmatrix}\begin{bmatrix} & & E_{\text{XX}}\times x \\ & I_{3\times3} & 0 \\ & & 0 \\ 0_{1\times3} & & 1 \end{bmatrix}
\end{aligned}
\tag{5-3}
$$

5.5 Parameter estimation and results analysis

For Strategy S1, 156 facet probings were taken for a total of 23 A- and C-axis combinations. For Strategy S2, 118 points were probed. Figure 5-5 shows the 23 A- and C-axis combinations used for the artefact probing for both strategies. Test times are 0H45M and 0H30M for S1 and S2 respectively. Linear relationship between A and C is avoided as recommended in [11].

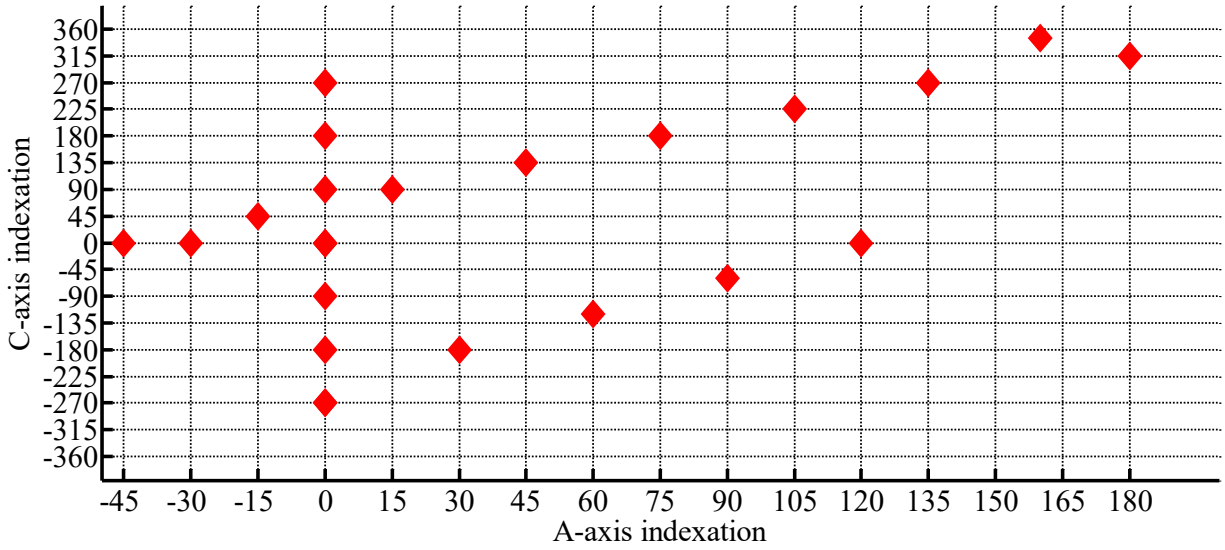

Figure 5-5 A- and C-axis indexation combinations (Strategies S1 and S2)

Two test procedures were conducted. For procedure A, six cycles of Strategy S1 were conducted in sequence during a day from a morning machine cold start. This was repeated for five days. The entire procedure was repeated for Strategy S2 but over three days. For procedure B, both strategies were conducted alternately four times in one day again from a morning machine cold start.

Table 5-2 Mean and range of the estimated errors for Procedure B (Strategies S1 and S2 alternating four times in a single day); data is processed per Strategy or combined with the points on the top surface of the machine table (S1+S2) or without those points (S1+S2-Points on the table)

		Estimated Parameters [µm, µrad or µm/m]										
Data set		E_{Y0C}	E_{A0C}	E_{B0C}	E_{B0A}	E_{C0A}	E_{C0X}	E_{A0Z}	E_{B0Z}	E_{YY}-E_{XX}	E_{ZZ}-E_{XX}	Range sum
S1+S2	Mean	2.0	16.3	-19.3	34.9	28.9	7.2	-3.6	-49.4	33.1	-16.4	
S1		1.9	16.3	-15.4	29.7	31.1	8.2	-3.1	-38.6	34.6	-10.5	
S2		4.7	72.8	-3.5	19.2	62.1	6.7	-4.6	-53.4	31.8	-21.9	
(S1–Pts on table)+S2		5.5	87.5	10.3	4.8	1.1	7.1	-4.5	-52.2	33.5	-25.8	
S1+S2	Range	1.5	35.9	9.9	23.6	36.4	4.9	4.1	23.2	4.7	14.3	158.5
S1		2.6	40.1	25.2	37.7	40.7	7.9	15.2	19.9	5.3	13.7	208.3
S2		3.4	61.3	19.4	19.6	97.5	3.3	3.2	24.4	4.1	22.9	259.1
(S1–Pts on table)+S2		2.9	68.3	104.8	77.6	78.2	4.3	8.5	37.8	5.9	37.6	425.9

Table 5-2 shows the results when processing the data using four different data sets. The results are presented in the order from smallest to largest mean range values. When the data set includes points on the top of the machine table (set S1+S2 and set S1), the sum of the ranges is lower although half of the range values are larger. Also the means departs significantly when those top points are not used. Those points greatly influence the rotary axes parameters. This supports the geometric fact that the points on the top surface provide strong constraints on the orientation of the table unlike the points on the shallow cylindrical feature (in set S2).

Procedure A is used to observe the variation of the estimated errors throughout a day and also between days. Table 5-3, Figure 5-6 and Figure 5-7 shows the mean and range (day wise and cycle wise) of the error values. Variation between the days is represented by the range of the mean estimated errors of all cycles for each day. The maximum and minimum observed variations for S1 are 10.7 (for E_{B0Z}) and 0.5 µm (for E_{Y0C}) respectively. The change of errors in a

day (between cycles) is represented by the range of the mean estimated errors for each cycle over 5 days. The maximum and minimum error variations during the day are 44.3 µm and 2.7 µm for E_{C0A} and E_{Y0C} respectively (Table 5-3).

It is observed that the overall means are mostly close except for E_{B0C}. Also noticeable is the much larger range of the error values during the day (between cycles) even though no machining or strenuous motion cycles were performed. This is important from the machine user point of view. Although not shown, the variation between cycles visible in Figure 5-7 (S1) was not apparent for the results of Strategy S2; this supports the usefulness of the top surface points.

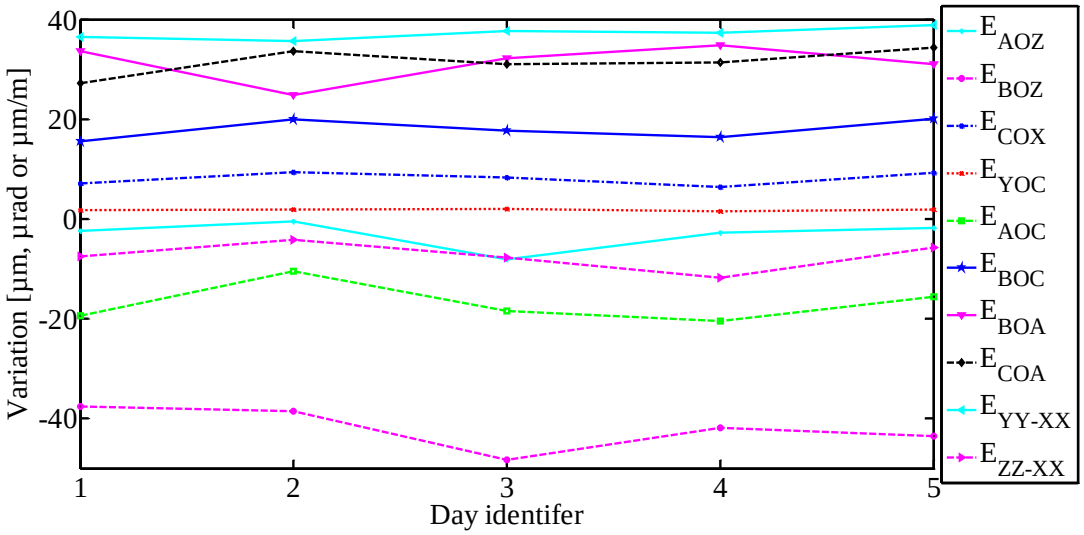

Figure 5-6 Variation of the estimated errors between days (Strategy S1)

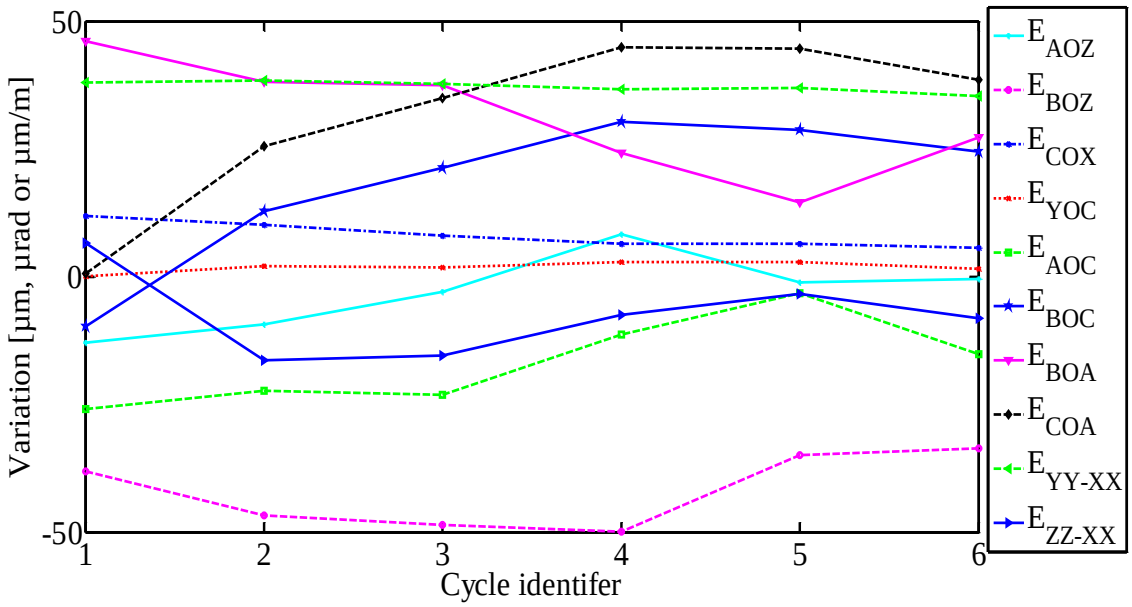

Figure 5-7 Variation of the estimated errors between cycles (Strategy S1)

Table 5-3 Variation of inter-axis and relative scale errors between the days and the cycles for Procedure A

Estimated Inter-axis parameters [μm, μrad or μm/m]	Strategy S1			Strategy S2		
	Overall mean	Range of day mean	Range of cycle mean	Overall mean	Range of day mean	Range of cycle mean
E_{Y0C}	1.8	0.5	2.8	4.0	0.1	2.6
E_{A0C}	-16.8	9.9	22.6	-4.7	2.7	40.6
E_{B0C}	17.9	4.5	40.1	60.9	3.6	52.6
E_{B0A}	31.3	9.9	31.5	31.1	6.9	29.3
E_{C0A}	31.5	7.2	44.3	47.9	6.1	44.3
E_{C0X}	8.1	3.1	6.2	8.4	0.3	7.7
E_{A0Z}	-3.1	7.6	21.3	2.3	4.6	22.7
E_{B0Z}	-41.9	10.7	16.3	-53.1	0.6	28.4
E_{YY}-E_{XX}	37.2	3.2	3.1	32.8	2.0	5.8
E_{ZZ}-E_{XX}	-7.4	7.6	22.7	-21.2	6.2	13.1

5.6 **Parameter's uncertainty analysis**

The estimation process has a multi-input (probing results) multi-output (machine errors) model so the output's uncertainties require estimating their covariance and the coverage factor k_q=2.6 for the chosen confidence level p=0.95 [12]. The uncertainties are estimated through the (generalized) GUM Uncertainty Framework (GUF) validated using Monte Carlo method (MCM) with M=10 000 trials. The Probability Density Functions (PDFs) and the covariance matrix of the input quantities are obtained through procedure A. Observations suggested that the machine errors (the measurands) changed through the day, so, two covariance matrices were calculated from the repeated measurements. Pooling by cycles removes the effect of daily machine change but preserves the measurement process variability so that all 30 measurements can be used. Pooling by days removes the change of the machine between days but preserves both the daily machine variation and the measurement process variability.

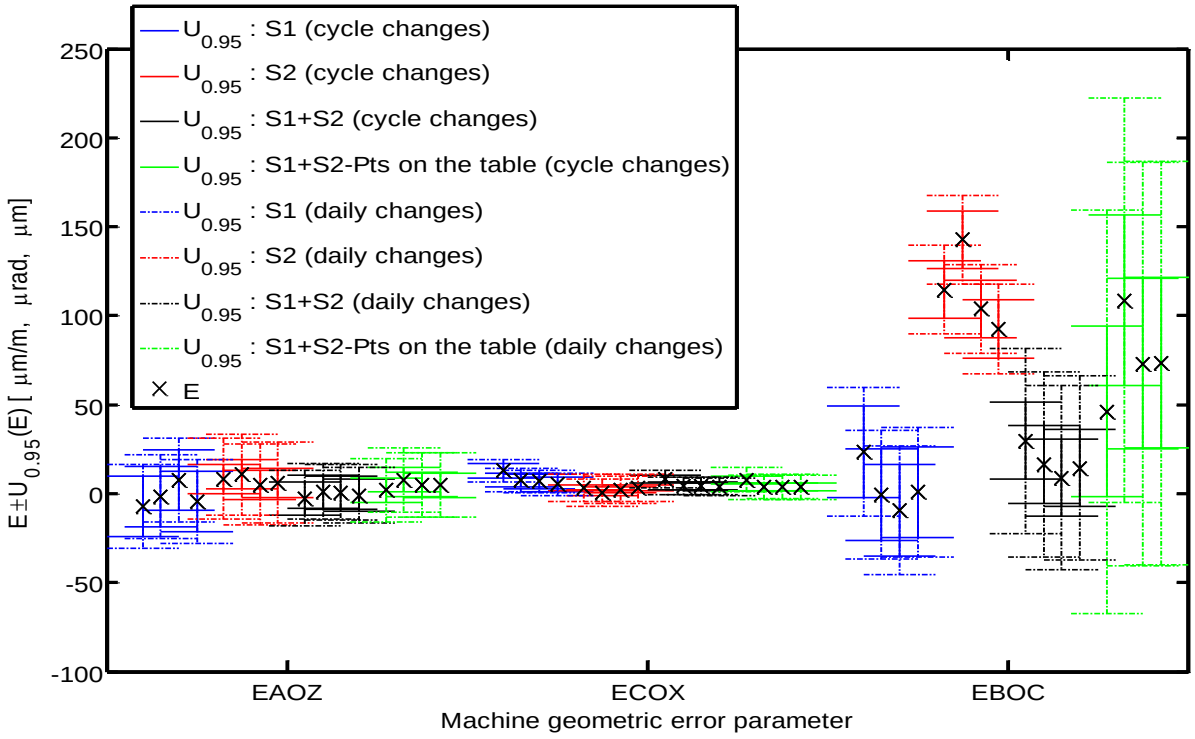

Figure 5-8 Calibration results for the four cycles of procedure B and four data sets with the pooled by cycles and pooled by days uncertainties

Figure 5-8 shows estimation results for three machine errors for Procedure B. The pooled by cycles uncertainty represents where the true value may lie at the time of measurement. The pooled by days provides the region where the machine error may be if the measurement had been taken at some other time that day. The uncertainties pooled by cycles are smaller than those pooled by days. The least variation between the cycles and the strategies can be observed for E_{COX}. Its uncertainties are also small. When the uncertainties pooled by days are considered the uncertainty regions overlap for E_{COX}, as well as for E_{AOZ}. This means that the measurand E_{C0X} and E_{AOZ} are not varying significantly between data sets and that the uncertainty values are realistic. The estimated E_{B0C} varies significantly, both between days and between cycles. There is no common uncertainty region considering the uncertainties pooled by cycles or by days when all four strategies are considered. However, within a particular data set uncertainty bands overlap. For E_{BOC} the uncertainties estimated for S1, S2 and S1+S2 are significantly smaller than for (S1-Pts on the table) + S2. A bias is observed between sets. So, the choice of measured facets affects the uncertainty and the error values.

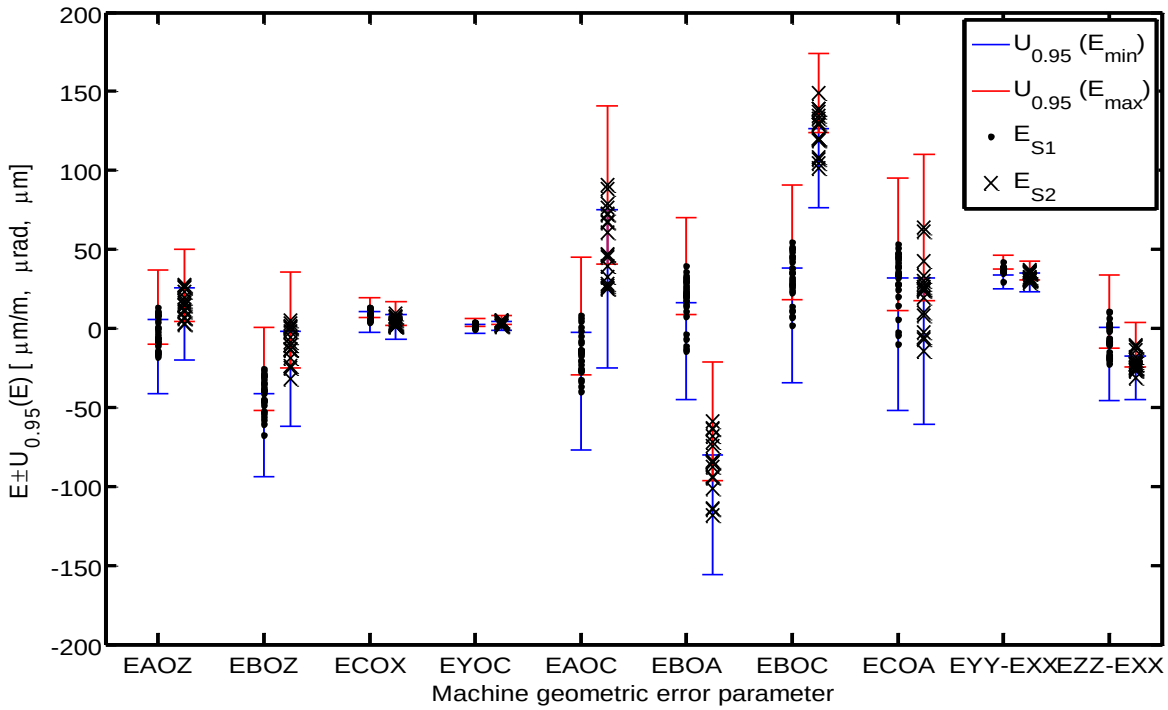

Figure 5-9 Results for repeated measurement of strategies S1 and S2 with the uncertainty including daily changes attached only to extreme values

Figure 5-9 shows the 30 (S1) and 18 (S2) repeated measurement results with the uncertainty including daily changes (pooled by days) shown only for the minimum and maximum value for each parameter, separately for each strategy. Almost all of the parameters have overlapping uncertainty bounds (except for EYY-EXX for S1) between the measurements and the strategies. Thus, the daily measurand changes can be explained by the uncertainty pooled by days. For all of the parameters the uncertainties have comparable values between S1 and S2.

5.7 **Conclusion**

The uncalibrated indigenous machine table, a cylindrical artefact with nominally flat and cylindrical facets, was probed to estimate eight inter-axis and two intra-axis errors (E_{YY}-E_{XX} and E_{ZZ}-E_{XX}) of a five-axis machine tool. Simulations indicated that facets on a cylindrical section cannot alone estimate the machine errors. Hence, two probing strategies, one with facets on the top flat surface and another with facets on two cylindrical sections were tested. The ranges of the estimated errors generally increase when those top points were removed. The mean error values were also affected by the strategy.

Repeating the measurement strategy during a day from a cold start and again over successive days allowed discriminating between variations due to the machine changing throughout the day and the measurement process itself. The largest changes between days were around 10 µrad whereas some errors changed by more than 40 µrad between cycles of the day. A machine user conducting a calibration at a particular time of the day may draw conclusions about machine errors which are no longer valid later on that same day.

Input quantities uncertainty used pooled covariance matrices to either retain or remove the change in the machine errors between successive test cycles on a day so that the uncertainty on the estimated error can either include, or ignore, the likely change in the values of the measurands. Although good correspondence was found between the uncertainty values and estimated error ranges within a specific strategy, especially when including daily effect, it remains that the spread of the results and the corresponding large uncertainties calls for further studies in machine variations through the day, the impact of artefact facets' selection and, more

generally, the use of uncalibrated indigenous artefacts as opposed to current state of the art approaches using brought-in controlled artefacts.

5.8 Acknowledgements

Work funded by NSERC, CANRIMT, CRIAQ, Pratt & Whitney Canada, Meloche Group and SONACA Montreal. Authors are grateful for the experimental support of G. Gironne and V. Mayer.

5.9 References

[1] Test Code for Machine Tools-Part 1: Geometric accuracy of machines operating under no-load or quasistatic conditions, ISO 230-1:2012(E).

[2] Schwenke, H., Knapp, W., Haitjema, H., Weckenmann, A., Schmitt, R., Delbressine, F., 2008, Geometric error measurement and compensation of machines—An update, Annals of the CIRP, 57/1:660–675.

[3] Abbaszadeh-Mir, Y., Mayer, J. R. R., Cloutier, G., Fortin, C., 2002, Theory and simulation for the identification of the link geometric errors for a five-axis machine tool using a telescoping magnetic ball-bar, International Journal of Production Research, 40/18:4781-4797.

[4] Sharif Uddin, M., Ibaraki, S., Matsubara, A., Matsushita, T., 2009, Prediction and compensation of machining geometric errors of five-axis machining centers with kinematic errors, Precision Engineering 33:194–201.

[5] Bringmann, B., Knapp, W., 2006, Model-based ‘Chase-the-Ball’ Calibration of a 5-Axes Machining Center, Annals of the CIRP, 55/1:531-534.

[6] Mayer, J. R. R., 2012, Five-axis machine tool calibration by probing a scale enriched reconfigurable uncalibrated artefact, Annals of the CIRP, 61/1:515–518.

[7] Ibaraki, S., Iritani, T., Matsushita, T., 2012, Calibration of location errors of rotary axes on five-axis machine tools by on-the-machine measurement using a touch-trigger probe, International Journal of Machine Tools & Manufacture, 58:44–53.

[8] Rahman, M.M., Mayer, J.R.R., 2014, Five axis machine tool volumetric error prediction through an indirect estimation of intra and inter axis error parameters by probing facets on a scale enriched uncalibrated indigenous artefact, Precision Engineering, 40:94-105.

[9] Bringmann, B., Knapp, W., 2009, Machine tool calibration: Geometric test uncertainty depends on machine tool performance, Precision Engineering, 33:524–529.

[10] Alami Mchichi, N., Mayer, J.R.R., 2014, Axis location errors and error motions calibration for a five-axis machine tool using the SAMBA method, Procedia CIRP, 14:305–310.

[11] Knapp, W., 2002, Measurement Uncertainty and Machine Tool Testing, Annals of the CIRP, 51/1:459-462.

[12] GUM S2, Evaluation of measurement data – Supplement 2 to the "Guide to the expression of uncertainty in measurement" – Extension to any number of input quantities," ed, Joint Committee for Guides in Metrology, JCGM 102:2011

CHAPTER 6 ARTICLE 3: PERFORMANCE OF A FIVE-AXIS MACHINE TOOL AS A COORDINATE MEASURING MACHINE

Md Mizanur Rahman, J.R.R. Mayer

Mechanical Engineering Dept., Polytechnique Montréal, P.O. Box 6079, Station Downtown, H3C 3A7 Montréal (QC), Canada

The article is submitted to the Journal of Advanced Mechanical Design, Systems and Manufacturing, Japan Society of Mechanical Engineers (JSME) (under review)

6.1 Abstract

The use of machine tools for on-machine coordinate measurement on the workpiece is becoming commonplace. However, numerous errors can adversely affect the measurement accuracy. For instance, the inter-axis parameters are major contributors to the overall machine tool's inaccuracy hence estimation and compensation of such errors are prerequisite to fully exploit the machine's measurement capability. This paper presents a scheme to assess the accuracy of coordinate measurement by probing a precision sphere mounted on the machine table for different rotary axes indexations. The individual probing data, and not the computed sphere centre, are used for the assessment thus providing a richer data set. Machine readings are processed either directly, using the machine nominal model or using a compensated model. This provides a fast method to validate on-machine measurement before and after compensation with the exception of isotropic scale effects.

Key words: Machine tool, probing, coordinate metrology

6.2 Introduction

The use of on-machine probing is well established to correct workpiece setup errors to avoid excessive depths of cut resulting in damage to the tool or the workpiece (Mou and Liu 1995). There is growing industrial interest to expand such capability to inspecting the workpiece at various stages of its machining for finishing path compensation (Guiassa, Mayer et al. 2014) and

even finished dimensions control. Such capability allows immediate remedial action thus avoiding the production of scrap and can also reduce post-machining inspection of the workpiece on a coordinate measuring machine which requires time and increases cost. However, this requires an accurate or a calibrated geometric model capable of predicting the measurement errors so that machine indications can be compensated. It also raises the question of how to easily assess measurement accuracy on a five-axis machine tool.

Artefact measurement is a known technique to check co-ordinate measuring machines (CMMs) and machine tools performance. Measuring a test piece to verify the measuring performance of a CMM is described in ASME B89.4.10360.2-2008. Five different calibrated test lengths are placed in seven different positions and each length is measured three times. Test procedure and acceptance criteria are well explained under certain environmental and metrological requirements (ASME B89.4.10360.2 : 2008). Two different reference spheres of different diameters at two different heights are measured to verify CMM's performance. The center of the spheres is measured in three different directions: axial, tangential and radial. Test procedure and evaluation criteria are described in ISO 10360-3 (ISO 10360-3 : 2000).

Much research has been carried out for the performance verification of CMMs by measuring an artefact or workpiece. Cauchick-Miguel et al. performed an extensive survey on CMM verification techniques. The authors conclude that, among mechanical artefacts (gauge block, step gauge, ring gauge, ball bars, hole and ball plate, space frames etc.), optical techniques (laser interferometry, optical space frame etc.) and opto-mechanical (laser step gauge, terra-test etc.) methods, mechanical artefacts are the most widely used and well established techniques for CMM verification. Laser interferometry is a commonly used optical technique with the disadvantage of complexity and time of set-up. It also requires trained personnel (Castro and Burdekin 2003). Weckenmann and Lorz proposed an approach to track CMM's degradation by measuring a series of calibrated workpiece (shaft collet) from a sheet metal parts production line. A Similar measurement strategy is used for calibration as for the series workpiece measurements hence the technique does not required special programmation or artefact (Weckenmann and Lorz 2005).

Ibaraki et al. proposed an on-machine laser measurement technique for 3-D profile measurement to formulate the influence of the rotary axes errors on workpiece position and orientation on five-axis machine tools by using a laser displacement sensor. The method is validated by on-machine surface profile measurement of a precalibrated precision sphere (Ibaraki, Kimura et al. 2015). Nowadays most multi-axis machine tools have an integrated touch trigger probe for workpiece measurement. ISO/DIS 230-10 describes test procedure to determine the measuring performance of the probing system of CNC machine tools. For three dimensional (3D) workpiece, the test includes probing 25 points on a reference sphere in 3D radial vector directions which are evenly distributed over a hemisphere. For 1D and 2D, a reference ring of 25 mm bore diameter is measured (ISO/DIS 230-10 : 2011). Standardized tests for feature location repeatability (FLR) and feature measurement accuracy (FMA) of a machining center are described in ASME B5.54-2005 to assess the machine performance as a measuring tool equipped with a suitable probing system. A calibrated probing system is used to measure artefacts (ring gauge/precision sphere) to evaluate the machine tool's FLR and FMA to locate the workpiece (ASME B5.54 : 2005). The tests focus on the three linear axes of the machine and the measurements are conducted in a volume limited by the 25 mm diameter artefacts so that intra- (individual axis error motions) and inter-axis errors (alignments between axes etc.) have limited impact. In order to evaluate the test methods described in ISO/DIS 230-10: 2011 to investigate the measuring performance of a machine tools equipped with touch trigger probe Fesperman et al. performed several test procedure to assess the probing repeatability, two- and three-dimensional probing error, and workpiece coordinate system identification error in machine coordinate system of a CNC machining center. A touch probe is used to measure three reference artefact such as gauge block, ring gauge and a sphere. The authors concluded that, probing performance is better than linear positioning performance and machine's positioning errors may contribute 44% to the probing error (Fesperman, Moylan et al. 2010). Hence calibrating the error parameters prior to the procedures mentioned above can improve the measuring performance of machine tools.

This paper will exploit the idea of multidirectional sphere probing in order to perform a quick check on machine tool's measuring performance before and after its calibration by probing an indigenous artefact. In this research individual touch probing indications are gathered on a precision sphere at different rotary axes indexations in the machine working volume to assess the

accuracy of the machine tool for coordinate measurement in five-axis mode using the machine nominal or estimated kinematic models. For a perfect machine and the nominal model or an imperfect model and a perfectly representative model, the calculated points when expressed in a reference frame attached to the machine table are expected to lie on a perfect sphere. In this work, the compensated model includes the inter-axis errors, stylus tip offsets and linear axes scale gain errors.

6.3 **Probing Procedure**

For the machine inter-axis, scale and stylus tip offset error estimation the uncalibrated machine table (as an indigenous artefact) was measured to generate machine model estimation data (Rahman and Mayer 2015). A total of 28 C1- (spindle), B- and C-axis indexations were used to probe facets on the machine tool table. A total of 26 facets and a scale bar are measured in 2H41M (2 hours and 41 minutes). Figure 6-1 shows the C1-, B- and C-axis combinations.

The machine probing capability verification involves probing a precision sphere of ϕ19.05 mm using two different strategies. In strategy I, the sphere is probed at 20 B- and C-axis indexations which are also part of the machine model calibration indexation set. In strategy II, 21 new B- and C-axis orientations are used to acquire machine model validation data (Figure 6-2). As the sphere measurement is carried out to validate the machine tool's probing measurement performance, the spindle rotation is not changed as it would be the case during probing. A total of 33 target points with their local nominal normals have been defined on the sphere for touch probing purposes. The distribution of the point is similar to ISO/DIS 230-10 as they are evenly distributed over at least a hemisphere (ISO/DIS 230-10 : 2011).

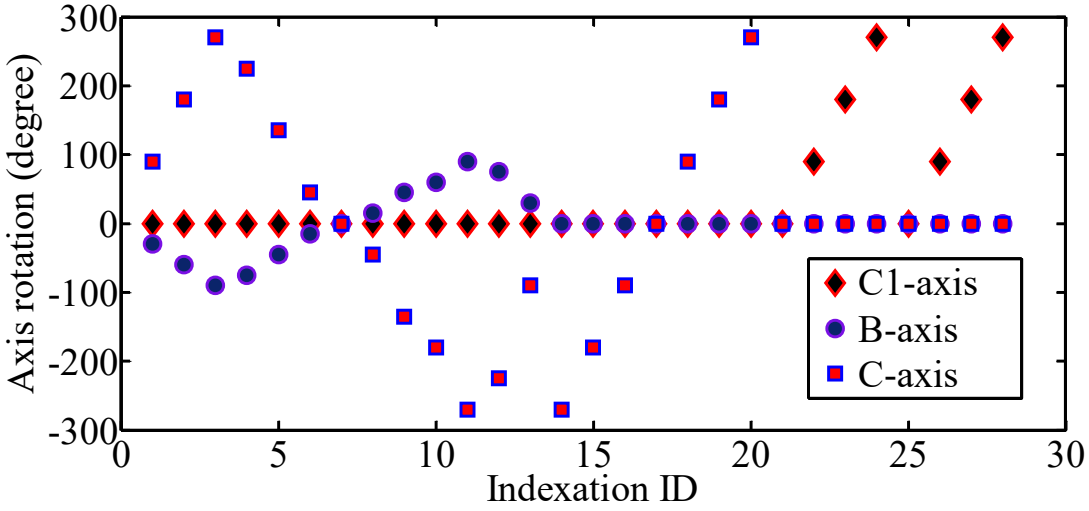

Figure 6-1 B- and C-axis combinations (calibration set). The first 20 B- and C- axis indexations are also used as Strategy I validation set

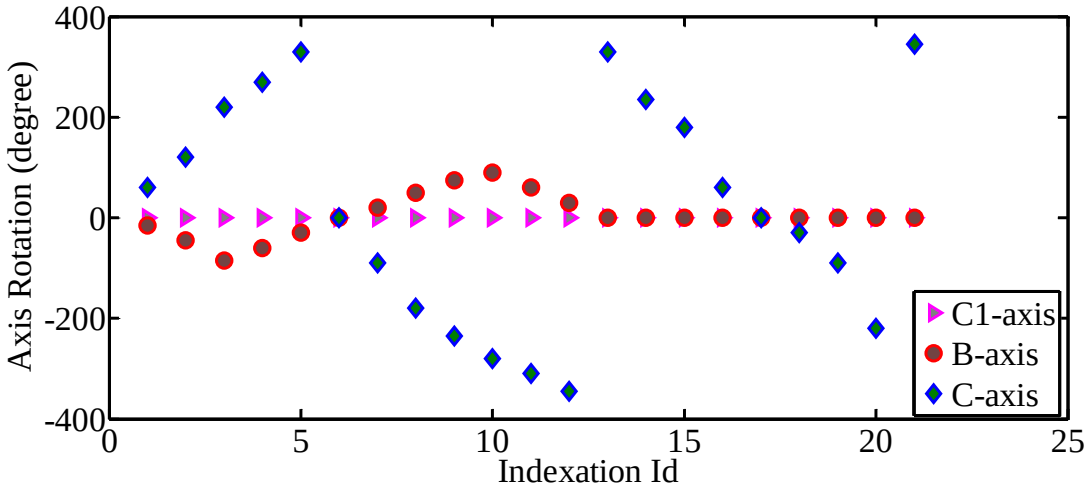

Figure 6-2 B- and C-axis combinations for Strategy II validation set

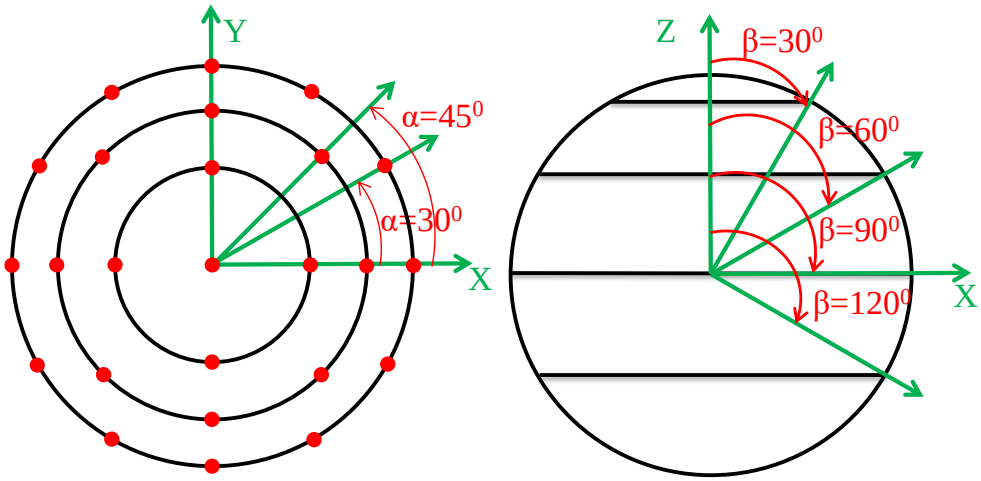

Figure 6-3 Points distribution on the test sphere for machine model validation purposes

The distribution of the points is as follows: equally spaced on each parallel, 12 points around the equator of the sphere, 8 points at +30° and -30° latitude, 4 points at 60° latitude and 1 point on the pole of the sphere. Figure 6-3 shows the points' distribution. A total of 424 data points are measured in 2H10M (Strategy I) and 453 data point are measured in 2H19M (Strategy II) using a Renishaw MP700 touch trigger probe on a Mitsui Seiki HU40T horizontal machining center with the topology wCBXfZY(C1)t (Figure 6-4) with a tool length of 326.674 mm.

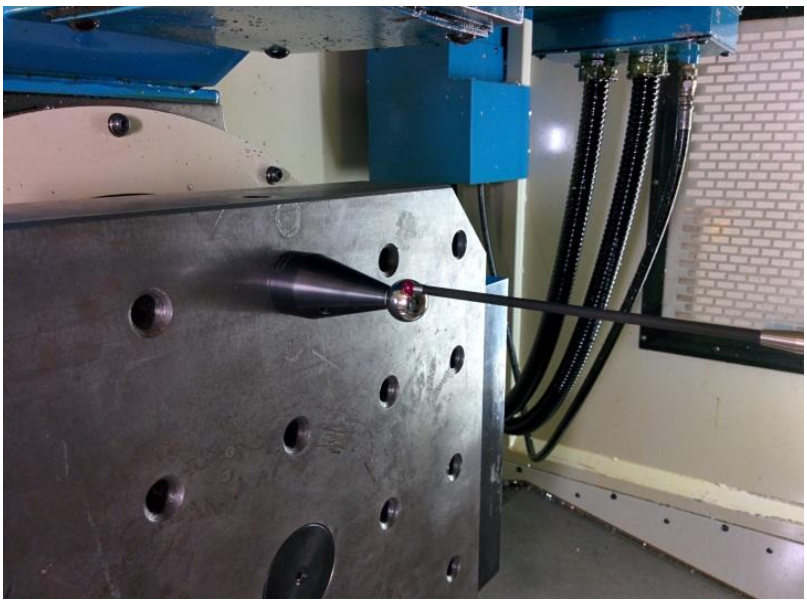

Figure 6-4 The precision sphere probing on the wCBXfZY(C1)t machine tool

6.4 **Mathematical Model**

For coordinate measurement, the stylus tip centre positions are calculated (predicted) in the machine table frame which coincides with the last workpiece branch frame (C-frame), to which the ball is assumed rigidly attached, using homogeneous transformation matrices (HTMs):

$$ {}^{\{C'\}}P_{si} = {}^{C'}T_{B'}\,{}^{B'}T_{X'}\,{}^{X'}T_{f}\,{}^{f}T_{Z'}\,{}^{Z'}T_{Y'}\,{}^{Y'}T_{C1'}\,{}^{\{C1'\}}P_{si} \tag{6-1} $$

where, ${}^{\{C'\}}P_{si}$ is the predicted (calculated) stylus tip centre position as seen from and projected in the C-axis reference frame, when touching the precision sphere, calculated using the recorded X-, Y- and Z-axis positions for the various B- and C-axis indexations. ${}^{\{C1\}'}P_{si}$ is the stylus tip position as seen from and projected in the spindle (C1) reference frame. The HTM for each machine tool axis is the product of four sub-HTMs: they are the nominal axis location, the inter-axis errors, the nominal axis motion and the intra-axis errors. For example the Y'-axis HTM is as follows:

$$ \begin{aligned} {}^{Z'}T_{Y'} &= {}^{Z'}T_{Y_0}\,{}^{Y_0}T_{Y_{0'}}\,{}^{Y_{0'}}T_{Y}\,{}^{Y}T_{Y'} \\ &= I_{4\times4}\begin{bmatrix} R\left(k_{Y_0}, E_{C0Y}\right)R\left(\hat{i}_{Y_0}, E_{A0Y}\right) & \begin{matrix}0\\0\\0\end{matrix} \\ 0_{1\times3} & 1 \end{bmatrix}\begin{bmatrix} I_{3\times3} & \begin{matrix}0\\0\\y\end{matrix} \\ 0_{1\times3} & 1 \end{bmatrix}\begin{bmatrix} I_{3\times3} & \begin{matrix}0\\E_{YY}\\0\end{matrix} \\ 0_{1\times3} & 1 \end{bmatrix} \end{aligned} \tag{6-2} $$

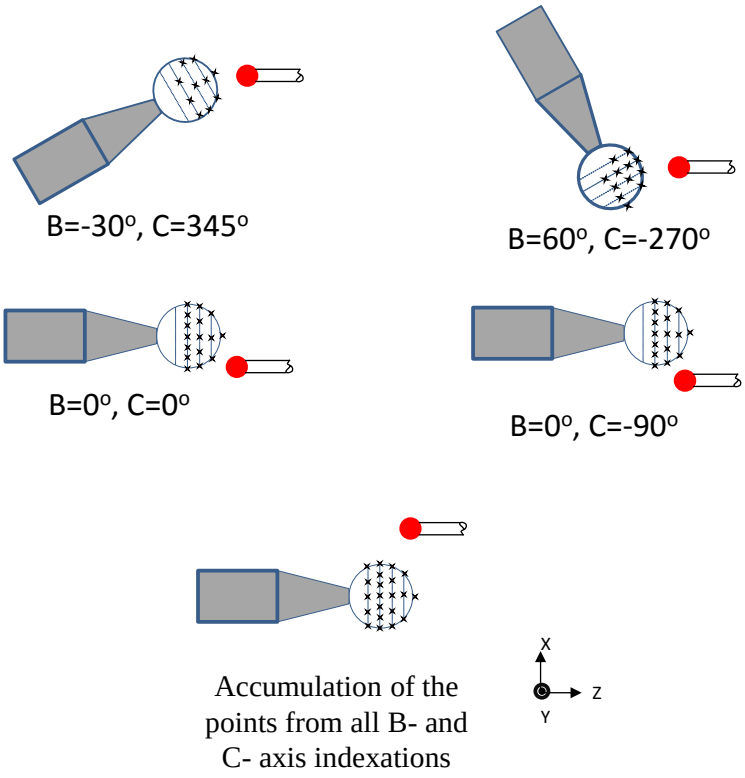

Figure 6-5 Merging the various indexations probing results. B- and C-rotary axis indexations are in degrees

Figure 6-5 illustrates conceptually how the coordinates (target points on the sphere) have been measured at different B- and C-axis indexations; as an example here (B=30^o, C=345^o), (B=60^o, C=-270^o), (B=0^o, C=0^o) and (B=0^o, C=-90^o). Then, all point measurements at the 20 (Strategy I) or the 21 (Strategy II) different B- and C-axis indexations are cumulated by calculating the coordinate measurements in the last workpiece branch frame (C-frame).

A sphere is then fitted to the points using a Gauss-Newton algorithm that minimizes the sum of the squares of the radial distances between each point and the fitted sphere. The position of the fitted sphere center and its radius are estimated.

6.5 **Results of simulations**

Prior to assess the out of sphericity of the experimental data using the uncompensated and compensated machine tool models, a study of the influence of the individual error parameters on

the out of sphericity was conducted through simulations. Only one error at a time is set to a non-zero value in the model and the out of sphericity is calculated. For error parameters in mm the parameter value is set to 0.001 mm or 1 μm and for angular errors the value is set to 0.001 mm divided by a length of 400 mm (0.0025 radian). This way the effect of linear and angular errors should be commensurate. The results are listed in Table 6-1.

Table 6-1 Effect of individual error parameters on measurement's out of sphericity

Parameter included in the model	Values [μm, μrad or μm/m]	Size Error ($r_{estimated} - r_{simulated}$) (mm)	Out of Sphericity (mm)
No parameters	0	7.11×10^{-15}	1.83×10^{-13}
E_{A0B} (μ rad)	2.5	-1.14×10^{-05}	9.54×10^{-04}
E_{A0C} (μ rad)	2.5	5.46×10^{-06}	8.21×10^{-04}
E_{A0Y} (μ rad)	2.5	-1.48×10^{-06}	2.04×10^{-03}
E_{B0C} (μ rad)	2.5	8.55×10^{-06}	8.63×10^{-04}
E_{B0Z} (μ rad)	2.5	-7.5×10^{-06}	6.14×10^{-04}
E_{C0B} (μ rad)	2.5	7.09×10^{-06}	9.08×10^{-04}
E_{C0Y} (μ rad)	2.5	1.72×10^{-06}	6.65×10^{-04}
E_{X0C} (μm)	1.0	-3.34×10^{-05}	2.42×10^{-03}
$E_{Y0(C1)}$ (μm)	1.0	-1.57×10^{-05}	2.43×10^{-03}
$E_{X0(C1)}$ (μm)	1.0	2.15×10^{-05}	2.49×10^{-03}
E_{XX} (μm/m)	2.5	-1.21×10^{-05}	5.16×10^{-04}
E_{YY} (μm/m)	2.5	-1.49×10^{-05}	4.54×10^{-04}
E_{ZZ} (μm/m)	2.5	-2.08×10^{-04}	1.72×10^{-03}

Results show that linear offsets of the spindle along Y- and Z-direction ($E_{Y0(C1)}$ and $E_{X0(C1)}$) and C-axis offsets in X-direction (E_{X0C}) influence the most the out of sphericity. The influence of Y-axis squareness error relative to Z-axis (E_{AOY}) and Z-axis positioning error (E_{ZZ}) are also prominent on out of sphericity and size error. However, all simulated parameters affected the out of sphericity significantly.

Figure 6-6, Figure 6-7, Figure 6-8 and Figure 6-9 shows the graphical representation of the individual error parameter's effect on the out of sphericity of the sphere.

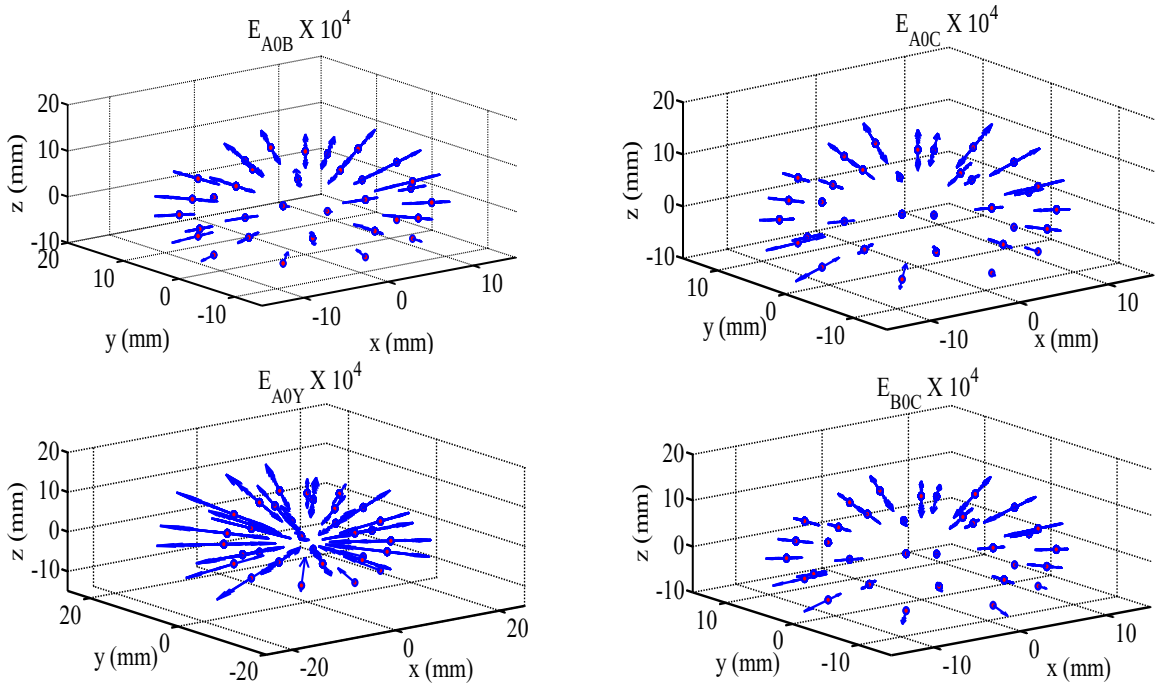

Figure 6-6 Effect of E_{A0B}, E_{A0C}, E_{A0}Y and E_{B0C} on the out of sphericity measurement

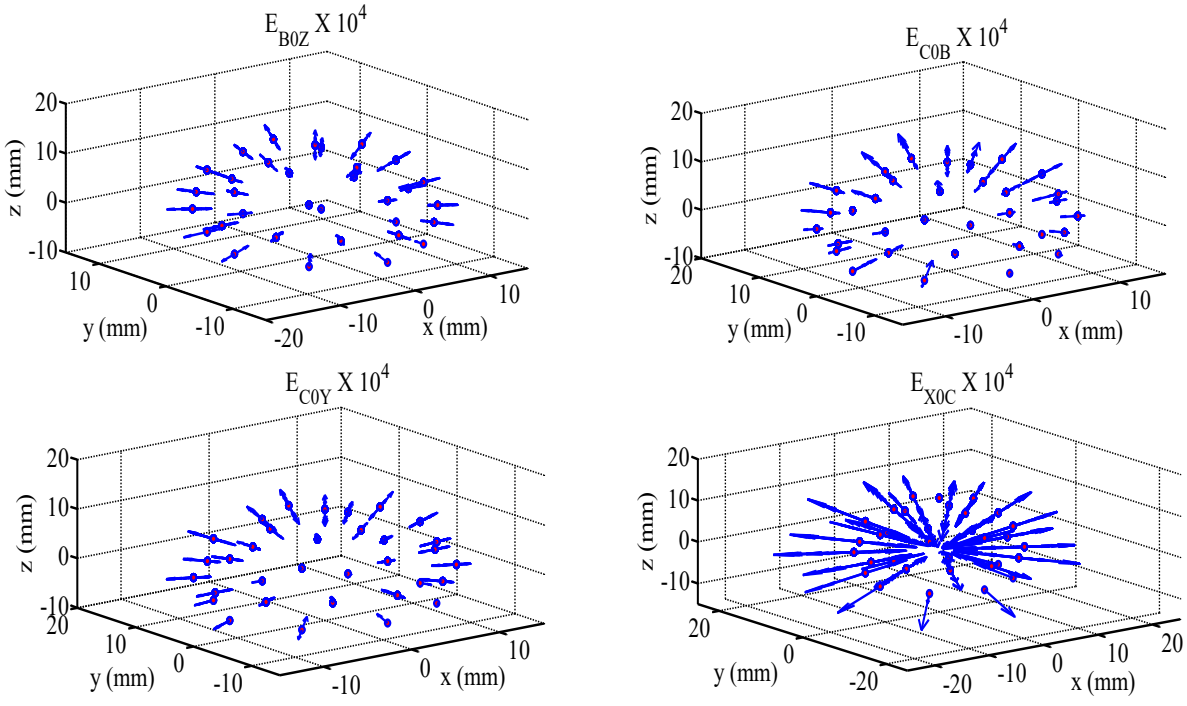

Figure 6-7 Effect of E_{B0Z}, E_{C0B}, E_{C0Y} and E_{X0C} on the out of sphericity measurement

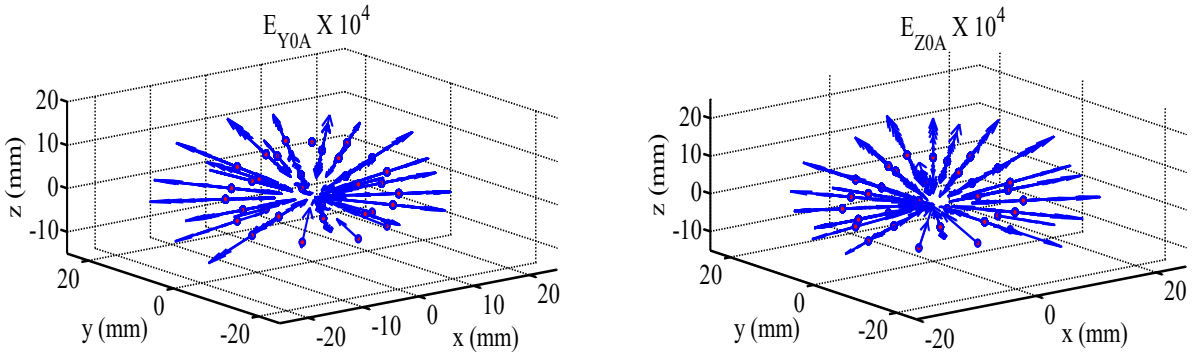

Figure 6-8 Effect of E_{Y0A} and E_{Z0A} on the out of sphericity measurement

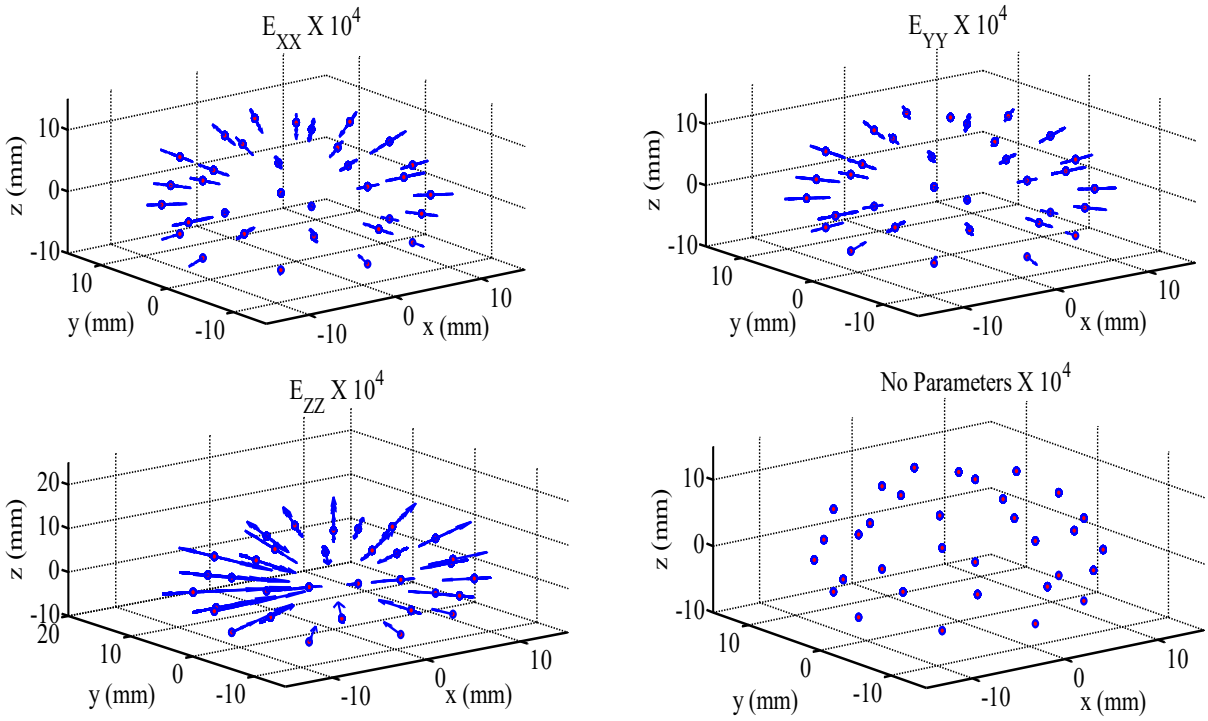

Figure 6-9 Effect of E_{XX}, E_{YY}, E_{ZZ} and No parameters on the out of sphericity measurement

6.6 **Measurement Results**

The machine model estimation data from the measurement of the uncalibrated indigenous artefact, i.e. the machine table, and a scale bar is processed as in (Rahman and Mayer 2015). The estimated parameters are shown in Table 6-2. Noticeable on this particular machine are the large cross rotary axis offset, a similar X spindle offset and also important values on most errors with

the exception of E_{BOC} which is normally easily adjusted by the machine operator using an offset on the B-axis. With such a collection of errors, we expect to see significant out of sphericity errors on the measurement of the sphere.

Table 6-2 Estimated machine error parameters by probing an uncalibrated indigenous artefact

Parameters descriptions		Values [µm, µrad or µm/m]
Symbol,	Description	
E_{AOB},	out-of-squareness of B- to Z-axis (µrad)	-29.1
E_{COB},	out-of-squareness of B- to X-axis (µrad)	-15.4
E_{YOS},	Y offset of the spindle to C-axis (µm)	27.4
E_{XOS},	X offset of the spindle to B-axis (µm)	-120.6
E_{BOZ},	Z-axis out-of-squareness to X-axis (µrad)	65.7
$E_{AOY,}$	Y-axis out-of-squareness to Z-axis (µrad)	-36.9
E_{COY},	Y-axis out-of-squareness to X-axis (µrad)	22.3
E_{XOC},	C-axis offset relative to B-axis (µm)	-111.0
E_{AOC},	C-axis out-of-squareness to B-axis (µrad)	-25.0
E_{BOC},	C-axis out-of-squareness to X-axis (µrad)	3.0
E_{XX},	X-axis positioning error gain (µm/m)	23.2
E_{YY},	Y-axis positioning error gain (µm/m)	45.6
E_{ZZ},	Z-axis positioning error gain (µm/m)	-46.3

Now let's consider the raw probing data gathered on the sphere at different rotary axis indexations. The data for strategy I was processed first using the nominal machine model (with zero machine errors) and then processed again using the estimated model in order to predict the stylus tip positions in the machine table frame. In both cases, a theoretical (ideal) sphere is fitted to the predicted stylus tip centres to investigate the nature of the measurement errors. In the absence of any error, all points should be on a sphere and the residuals should be null. Using the nominal machine model, the out of sphericity (maximum minus minimum residuals), maximum and minimum residuals and standard deviation of the residuals are as given in Table 6-3 and Figure 6-10.

Table 6-3 Out of sphericity of the probing results, maximum and minimum residuals and standard deviation when using the machine nominal model and estimated model to calculate the tool tip position in the machine table frame (Strategy I and Strategy II)

Variables	Values (nominal machine model)	Values (compensated machine model)	
	Strategy I	Strategy I	Strategy II
Out of sphericity (μm)	268.27	60.51	71.12
Maximum residual (μm)	145.98	37.08	47.08
Minimum residual (μm)	-122.29	-23.43	-24.04
Standard deviation of the residuals (μm)	41.80	10.36	11.3
Diameter of the sphere (mm)	19.04	19.045	19.045

Then, the stylus tip positions are calculated using the compensated machine model that includes the estimated error parameters. Two different measurement strategies are used to gather the sphere probing validation data.

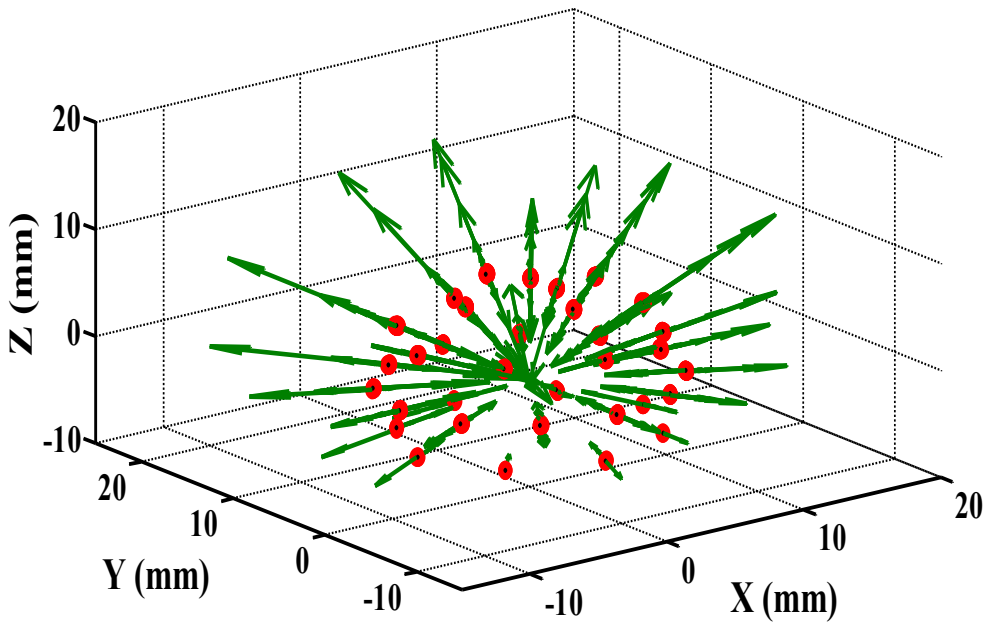

Figure 6-10 Residuals without machine compensation (100x)

For Strategy I, the out-of-sphericity (maximum minus minimum residuals), maximum and minimum residuals and standard deviation of the residuals of the estimated model are given in Table 6-3 and shown in Figure 6-11 and for Strategy II, results are also given in Table 6-3 and shown in Figure 6-12.

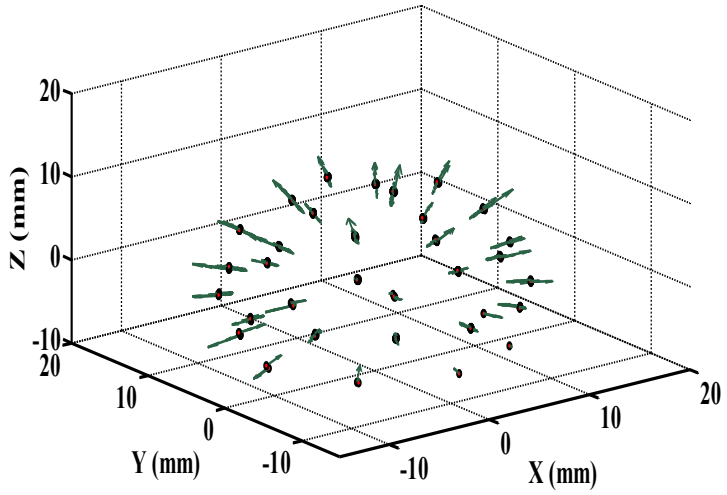

Figure 6-11 Residuals with machine compensation (100x). (Strategy I validation set)

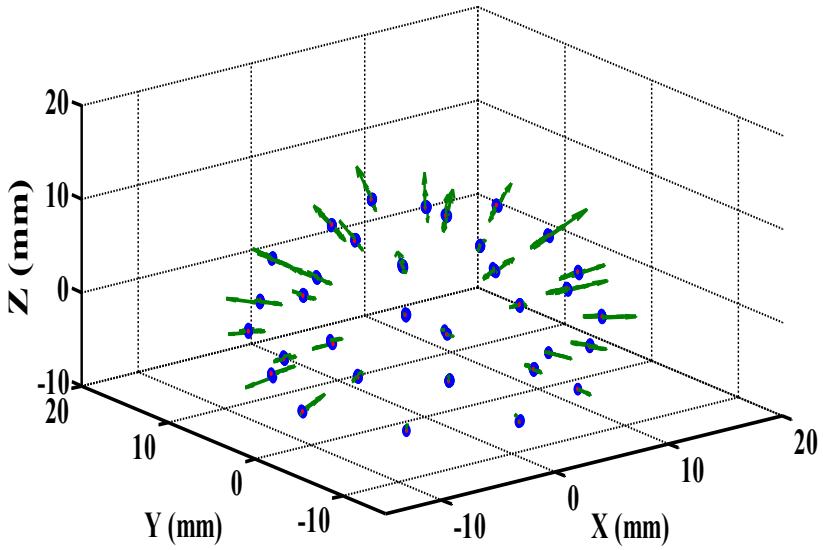

Figure 6-12 Residuals with machine compensation (100x). (Strategy II validation set)

In a separate test the systematic lobing error of the probing measurements is estimated by measuring a precision sphere of ϕ 19.05 mm without changing the rotary axes indexations. After fitting a sphere to the measurements, the out-of-sphericity of the sphere is calculated as 8.07 µm. This value may also include some errors from the machine such as backlash and short term thermal drift. This value is small compared to the out of sphericity of the validation data which suggests that for the machine tested the machine geometry has a significant impact on the accuracy of the probing measurements in five-axis mode. The improvement from using the calibrated model for data processing is by a factor of four.

6.7 Conclusion

A five-axis machine tool was tested for coordinate measurement by probing a precision sphere and processing the data with and without considering the machine's inter-axis and scale errors. The out of sphericity of the fitted data and the standard deviation of the residuals when using the nominal and calibrated models are reduced from 268.27 and 41.8 down to 60.51 and 10.36 µm respectively, when the validation data set uses the same B- and C-axis indexations set as for the calibration, and down to 71.12 and 11.3 µm respectively when the validation data set is obtained using a B- and C-axis indexations set different from the calibration indexations set. Thus the compensated model provides an improvement by a factor of about four. Simulations show that, spindle offsets, C-axis offsets in X-direction, squareness between Z- and Y-axis and Z-axis positioning errors can strongly impact the out of sphericity. The described procedure is a simple yet effective way to quickly assess the machine metrological capability when measuring objects with a combination of rotary axes indexations values.

6.8 Acknowledgement

Work funded by NSERC, CRIAQ, Pratt & Whitney Canada, Meloche Group and SONACA Montreal. Authors are grateful for the experimental support of Guy Gironne and Vincent Mayer.

6.9 References

ASME (B5.54 : 2005). Methods for performance evaluation of Computer Numerically Controlled machining centers (revision of ASME B.54-1992).

ASME (B89.4.10360.2 : 2008). Acceptance Test and Reverification Test for Coordinate Measuring Machines (CMMs). Part 2: CMMs Used for Measuring Linear Dimensions.

Castro, H. F. F. and M. Burdekin (2003). "Dynamic calibration of the positioning accuracy of machine tools and coordinate measuring machines using a laser interferometer." International Journal of Machine Tools & Manufacture **43**(9): 947-954.

Fesperman, R. R., S. P. Moylan, et al. (2010). Methods, practices, and standards for evaluating on-machine touch trigger probing of workpieces. 25th Annual Meeting of the American Society for Precision Engineering, ASPE 2010, October 31, 2010 - November 4, 2010, Atlanta, GA, United states, American Society for Precision Engineering, ASPE.

Guiassa, R., J. R. R. Mayer, et al. (2014). "Closed door machining error compensation of complex surfaces using the cutting compliance coefficient and on-machine measurement for a milling process."

Ibaraki, S., Y. Kimura, et al. (2015). "Formulation of influence of machine geometric errors on five-axis on-machine scanning measurement by using a laser displacement sensor." Journal of Manufacturing Science and Engineering, Transactions of the ASME **137**(2).

ISO (10360-3 : 2000). Geometrical Product Specifications (GPS) -- Acceptance and reverification tests for coordinate measuring machines (CMM) Part 3: CMMs with the axis of a rotary table as the fourth axis.

ISO/DIS (230-10 : 2011). Test code for machine tools Part 10: Determination of measuring performance of probing systems of numerically controlled machine tools.

Mou, J. and C. R. Liu (1995). "Adaptive methodology for machine tool error correction." Journal of Engineering for Industry, Transactions of the ASME **117**(3): 389-399.

Rahman, M. M. and J. R. R. Mayer (2015). "Five axis machine tool volumetric error prediction through an indirect estimation of intra- and inter-axis error parameters by probing facets on a scale enriched uncalibrated indigenous artefact." Precision Engineering **40**(0): 94-105.

Weckenmann, A. and J. Lorz (2005). Monitoring coordinate measuring machines by calibrated parts. Seventh International Sympsoium on Measurement Technology and Intelligent Instruments, 6-8 Sept. 2005, UK, IOP Publishing.

CHAPTER 7 ARTICLE 4: MEASUREMENT ACCURACY INVESTIGATION OF TOUCH TRIGGER PROBE WITH FIVE AXIS MACHINE TOOLS

Md Mizanur Rahman, J.R.R. Mayer

Mechanical Engineering Dept., Polytechnique Montréal, P.O. Box 6079, Station Downtown, H3C 3A7 Montréal (QC), Canada

Article submitted to the Archive of Mechanical Engineering (under review)

7.1 Abstract

The touch trigger probe plays an important role in modern metrology because of its robust and compact design with crash protection, long life and excellent repeatability. Aside from coordinate measuring machines (CMM), touch trigger probes are used for workpiece location on a machine tool and for the accuracy assessment of the machine tools. As a result, the accuracy of the measurement is a matter of interest to the users. The touch trigger probe itself as well as the measuring surface, the machine tool, measuring environment etc. contribute to measurement inaccuracies. The paper presents the effect of surface irregularities, surface wetness due to cutting fluid and probing direction on probing accuracy on a machine tool.

Keywords: Probing, machine tool, touch probe, repeatability, measurement inaccuracy

7.2 Introduction

Users of machine tools seek to integrate touch trigger probe measurements within the machine tool environment so that the machine tool can locate the part, perform self-checks and ultimately inspect the machined part at strategic points throughout the machining of a part. In general, a touch trigger probe provides a binary signal, when contact occurs with the workpiece surface, which is used to trigger readings of the machine's X-, Y- and Z-axis positions. The touch trigger probe temporarily replaces the cutting tool in the machine spindle. On-machine measurement of the workpiece allows to take corrective actions while the workpiece is still on the machine tool

[1]. Thus the accuracy of the measuring device (probe) has significant influence on the part produced.

Cauchick-Miguel and King studied the factors that affect probe accuracy including the approach direction, probe lobing, measuring speed, probe indexing angle and spring pressure by measuring a precision spheres [2]. Wozniak et al. considered probe pretravel variation as one of the major sources of probe inaccuracies. They experimentally demonstrated that configuration of the probe, triggering force, stylus length and stiffness influence the probe pretravel variation [3]. Later on, they proposed a new technique for the verification of CMM touch trigger probe accuracy by measuring the distance between a reference point and the triggering point for different directions. The reference point is defined by the axis of rotation of the most stable axis of any rotary table [4], using this technique they also showed that the measured object's shape, surface roughness and material stiffness contribute to the inaccuracies caused by a touch trigger probe [5].

Johnson et al. investigated the dynamic error characteristics of touch trigger probes on a CMM and found measurement speed, probe longitude, approach distance, probe latitude, stylus length/stylus tip diameter, probe orientation, operating mode (scanning and non-scanning), scan pitch, preload spring force (gauging force), probe type, and the surface approach angle had an important impact on probe accuracy. They also proposed some solution to avoid such error sources such as, optimizing the measurement speed along with a defined probe spring force and selection of probe type [6]

Fesperman et al. proposed an evaluation method for the standard of numerical control machines' measuring performance assessment furnished with touch trigger probe. Based on the designed tests, probing repeatability, two dimensional (2D) and three dimensional (3D) probing errors as well as the inaccuracies in distinguishing the WCS (workpiece coordinate system) in MCS (machine coordinate system) is also considered for this evaluation method [7]. This work aimed to create a baseline for on-machine measurement uncertainty budget data set [8] Jankowski et al. built a portable setup by using a master artefact with an inner hemisphere for the indirect assessment of the accuracy of the touch-trigger probe. This setup is used to estimate the triggering radius variation in 2D and 3D measurements as well as unidirectional repeatability of a touch-trigger probe [9].

All the above works was conducted for CMM probing. On a machine tool additional factors must be considered. Machining process requires coolant liquid for the cutting process that makes the surfaces wet. Also the surface might not be smooth. Hence, this paper focuses on the external influences that can yield inaccuracies of the probing measurements on a machine tool. Surface irregularities, wetness effect, repeatability of the probe and equivalent probe lobing are experimentally evaluated.

7.3 **Measurement methods and results**

For the tests, the table of a five axis WCBXFZYT horizontal machine tool is probed as shown

Figure 7-1 is with a Renishaw machine touch trigger probe MP700 is used with a 100 mm stylus. Four different test procedures have been followed.

In procedure I, the unidirectional repeatability of the probe is evaluated by measuring a surface point 300 times in X-, Y-, Z-, 2D- (an inclined XY plane 45^0 with the horizontal axis) and 3D-directions (all the linear axes need to move simultaneously). The surface is cleaned and dried before the measurements commence.

Figure 7-1 Probing on a WCBXFZYT machine tool

In Procedure I, total time required for 300 probing with the respective direction is 1H45M approximately with the full retraction of the probe in Z-axis by 300mm after each probing. Figure 7-2 shows the presence of a drift for an unknow reason although thermal drift of the machine is suspected. Table 7-1 shows the results for the Procedure I (unidirectional repeatability of the probe).

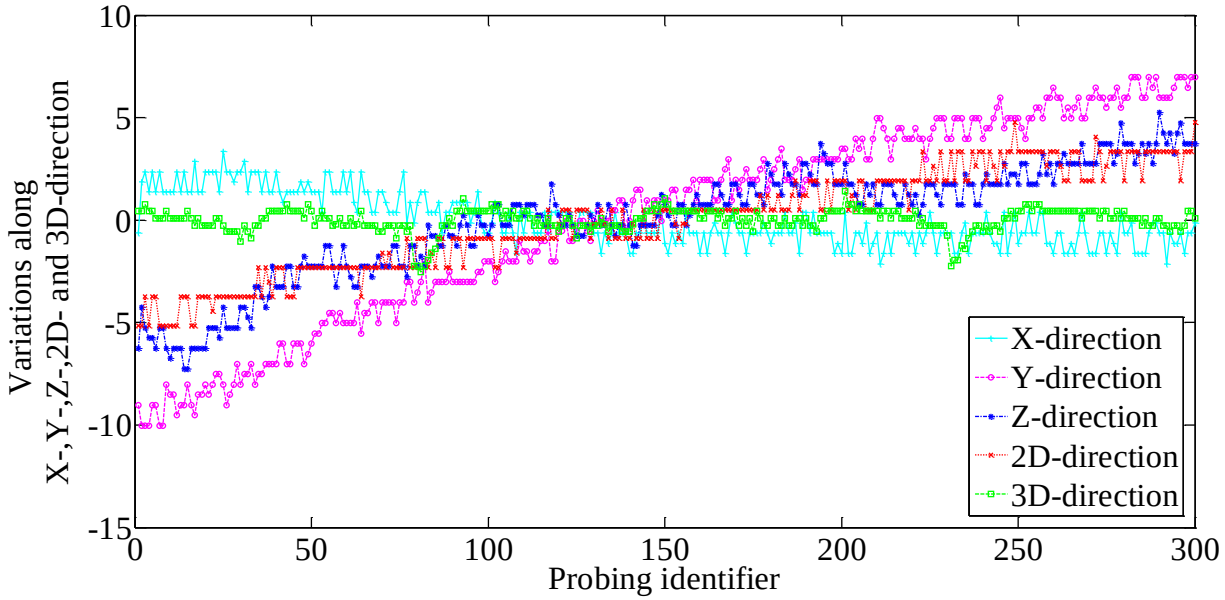

Figure 7-2 Procedure I (Unidirectional repeatability)

The drift could be responsible for the larger variation range of Y-, Z- and 2D-directional measurements. The standard deviation of the measurement in 3D direction is unexpectedly lower primarily because no drift is apparent.

Table 7-1 Range and standard deviation of the probing measurements for 300 repetitions in each of the selected directions

	X	Y	Z	2D	3D
Range (μm)	5.5	17.0	12.5	9.9	3.9
Standard deviation (μm)	1.2	4.9	2.7	2.5	0.6

To remove the effect of the drift on the statistical results, pooled standard deviation is calculated for these five directional measurement. For pooled standard deviation calculation, 12 small

windows of 25 probings are defined. From these 12 populations, the pooled standard deviation is calculated by using the following formula:

If the populations are indexed as i=1, 2… m, then the pooled variance s_p^2 can be estimated by the mean of the variances s_i^2

$$s_{p,k}^2 = \frac{\sum_{i=1}^{m}(n_i-1)s_{i,k}^2}{\sum_{i=1}^{m}(n_i-1)}; \quad (7\text{-}1)$$

where n_i is the sample size of population i and k refers to the X-, Y-, Z-, 2D- and 3D-directions. The pooled standard deviations are given in Table 7-2. Hence, a significant reduction in the calculated measurement repeatability is gained which confirms the significant contribution of the observed drift on the standard deviation of the measurements.

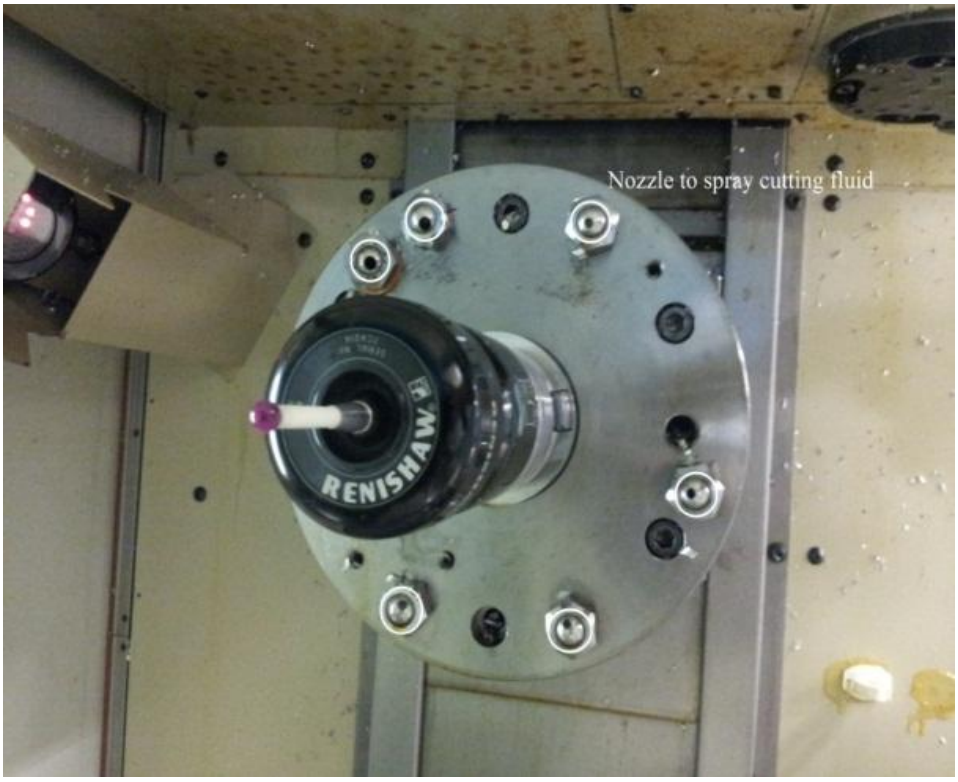

Figure 7-3 Spindle with nozzle to spray cutting fluid holding the probe

Table 7-2 Pooled standard deviation for a window of 25 probing measurements based on the probing measurements for 300 repetitions in each of the selected directions

	X	Y	Z	2D	3D
Pooled standard deviations (μm)	0.63	0.59	0.63	0.64	0.46

In procedure II, surface wetness effect on probing is assessed by measuring a single surface point in the Z- and 3D- directions. Procedure II includes four different approaches, named A, B, C and D. For Approach A, a surface point with the local surface normal aligned with the machine Z-axis is measured 600 times. For the first 100 touches the surface is dry and clean, for the second 100 touches the cutting fluid (4-6% of CIMSTAR 60 semi-synthetic metal working fluid added to water) is sprayed manually on the surface to make it wet and this cycle is repeated for the remaining 600 measurements. Approach B is similar to Approach A but instead of manually wetting the surface the machines' own system (Figure 7-3) is used to apply the cutting fluid on the surface. The cutting fluid passes through the machine spindle to the targeted surface area.

In Approach C, the same surface point as approach A and B is measured 600 times without using cutting fluid and the surface is kept clean and dry. Finally, in Approach D a surface point is measured with its normal at an oblique 3D angle of the machine tool for 600 times but with the same manner than Approach A. Figure 7-4 shows the measurement variation over 600 probing for Approach A, B, C and D. Total time required for the measurements of each Approach is 1H53M approximately.

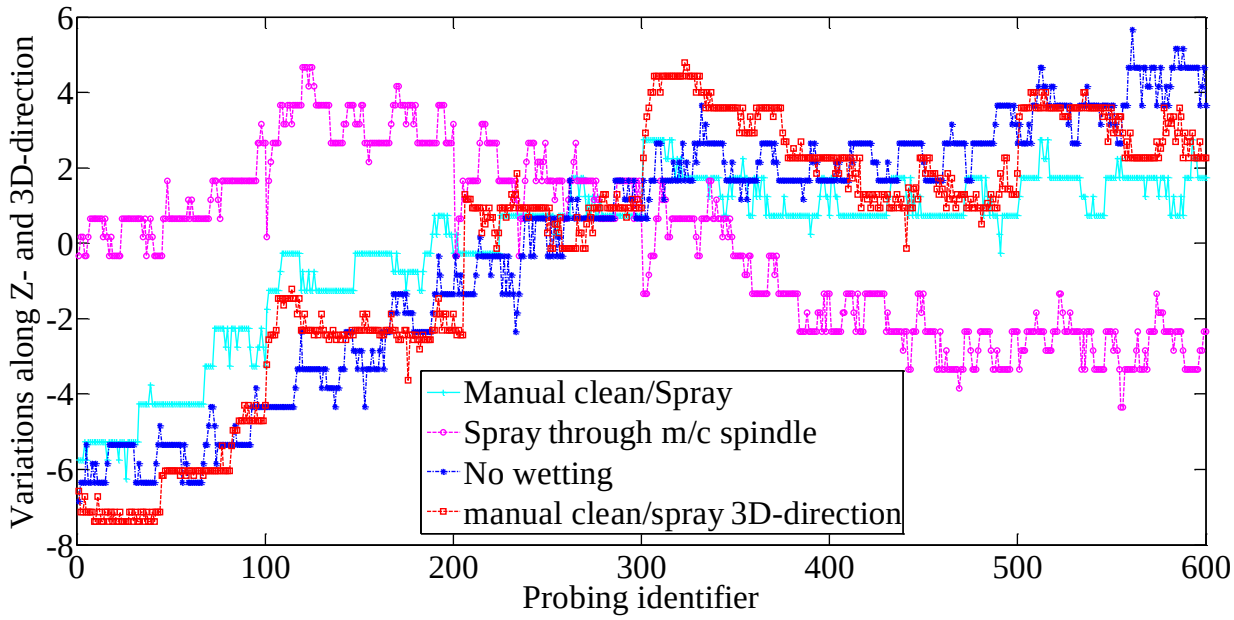

Figure 7-4 Procedure II (Approaches A, B, C and D)

Table 7-3 shows the range and standard deviation for Procedure II. Figure 7-4 shows that, the results seems to be stabilized after 300 probing for approach A, C and D. For Approach B, the cutting fluid was sprayed through the machine spindle, as shown in Figure 7-3, which may cause thermal effects. Plateaus corresponding to the dry and wet cycles are apparent for Approach D only.

Table 7-3 Range and standard deviation for all four approaches in Procedure II

	Approach A	Approach B	Approach C	Approach D
Range (µm)	9.0	9.0	12.5	12.2
Standard deviation (µm)	2.1	2.3	3.4	3.5

Procedure III is for surface irregularity assessment. A 5x5 spatial grid of 2 by 2 mm total size with n=25 regularly spaced points P_i, $i = 1$ to n, measured along direction k with k= X, Y, Z, 2D and 3D. The grid is measured $j = 1$ to m times, with m=19, for the respective direction hence each point on the grid is revisited m times. Then the effect of surface irregularities is observed by calculating the mean of each point i and for a specific direction k, $\hat{P}_{i,k}$, over all m cycles. By doing this, the effect of repeatability and drift can be removed and the graphical representation of the surface irregularity effect is given in Figure 7-5. For an indirect machine tool inspection

technique like [10], the measured surface can influence the overall measurement inaccuracies as measurements are conducted directly on the machine tool table.

Grid measurement cycle start with measuring the spatial grid along the X-direction followed by the Y-, Z-, 2D- and 3D-directions. The means $\hat{P}_{i,k}$ over all m cycles for a particular direction k is,

$$\hat{P}_{i,k} = \frac{1}{m}\sum_{j=1}^{m} P_{i,j,k}; \quad (7\text{-}2)$$

The standard deviation of the n=25 grid points means is then calculated for each respective direction.

$$S_k^2 = \sum_{i=1}^{n} \frac{(\hat{P}_{i,k} - \hat{T}_k)^2}{n-1}; \quad (7\text{-}3)$$

where, $\hat{T}_k = \frac{1}{n}\sum_{i=1}^{n} \hat{P}_{i,k}$; (7-4)

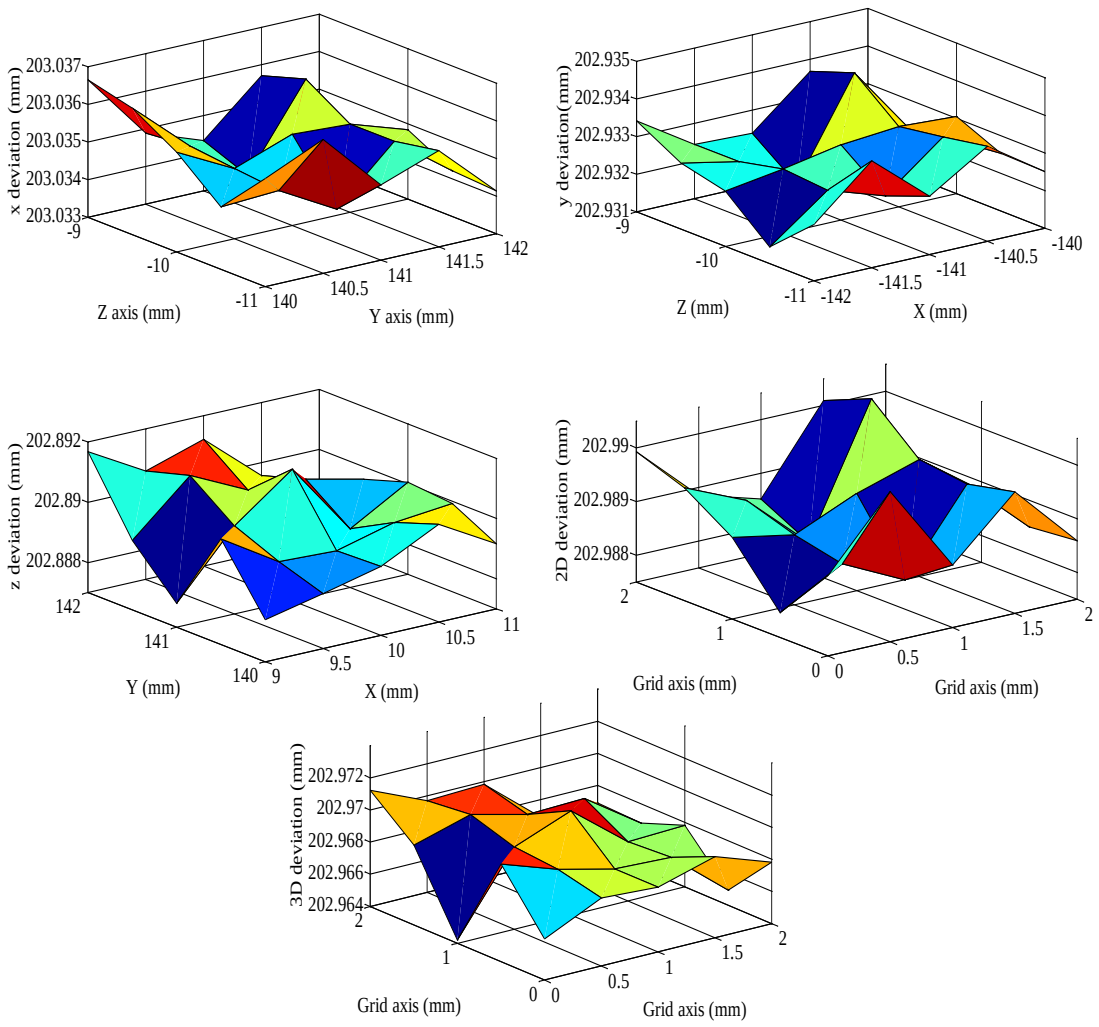

Figure 7-5 Effect of surface irregularities on probing of a 2 by 2 mm spatial grid along the X-, Y-, Z-, 2D- and 3D-directions

Table 7-4 Range and standard deviation of the 5×5 spatial grid probing

	X	Y	Z	2D	3D
Range (µm)	2.9	2.7	3.9	2.5	7.0
Standard deviation (µm)	0.86	0.68	0.97	0.73	1.7

Table 7-4 shows the range of the $\hat{P}_{i,k}$ and standard deviations for each grid point along the k directions. It shows the measurements variation attributed to surface irregularities. The probing in Z- and 3D-directions is shows the largest variations with [range, standard deviation] of [3.9, 0.97] µm and [7.0, 1.7] µm respectively.

If we look closer to the individual grid point analysis as given in Table 7-5 and Figure 7-6 (a, b, c, d and e), it shows that the measurements are affected by surface irregularities mostly in X- and 3D-direction by a (maximum, minimum) standard deviation of (5.3, 4.7) and (6.1, 0.92) µm. As mentioned earlier, there is an unknown drift affects the measurement results for the first hour. Hence, X- and 3D- direction can also be affected by the drift and results in a larger variation in the measurements. Random variation in 3D-probing has been observed and the reason is unknown. The pooled standard deviation in 3D-probing is 0.95 µm which is noticeably smaller.

Table 7-5 Individual standard deviation for each grid point

Grid Points ID	X (µm)	Y (µm)	Z (µm)	2D (µm)	3D (µm)
1	5	2.6	1.7	2.3	5.5
2	4.9	2.5	1.6	2.2	1.2
3	5.1	2.6	1.9	2.1	6.1
4	5.2	2.4	1.7	2.3	1.2
5	5.1	2.5	2	2.2	1.1
6	5.1	2.3	1.7	2.2	1.2
7	5.2	2.3	2	2.1	1.3
8	4.9	2.5	1.7	2.3	1.3
9	5.2	2.4	1.7	2.1	1.2
10	5.2	2.3	1.9	2.3	1.2
11	5.2	2.2	1.8	2.2	1.1
12	5.1	2.3	1.8	2.3	1.1
13	5.1	2.3	1.9	2.2	1.7
14	5.1	2.4	1.8	2.2	1.1
15	5.1	2.5	1.8	2.2	1
16	5.1	2.5	1.8	2.2	1.1
17	5.3	2.6	1.8	2.2	0.9
18	5.2	2.6	1.9	2.2	1
19	5.1	2.5	1.9	2.1	1
20	5.1	2.8	1.8	2.4	3.9
21	4.9	2.8	1.6	2.2	1
22	4.9	2.9	1.6	2.2	5.5
23	4.9	2.6	1.7	2.2	1.5
24	4.8	2.6	1.6	2.2	3.7
25	4.7	2.7	1.4	2.3	1.4
Maximum	5.3	2.9	1.9	2.4	6.1
Minimum	4.7	2.3	1.4	2	0.92
Pooled Standard	5.1	2.4	1.8	2.1	0.95

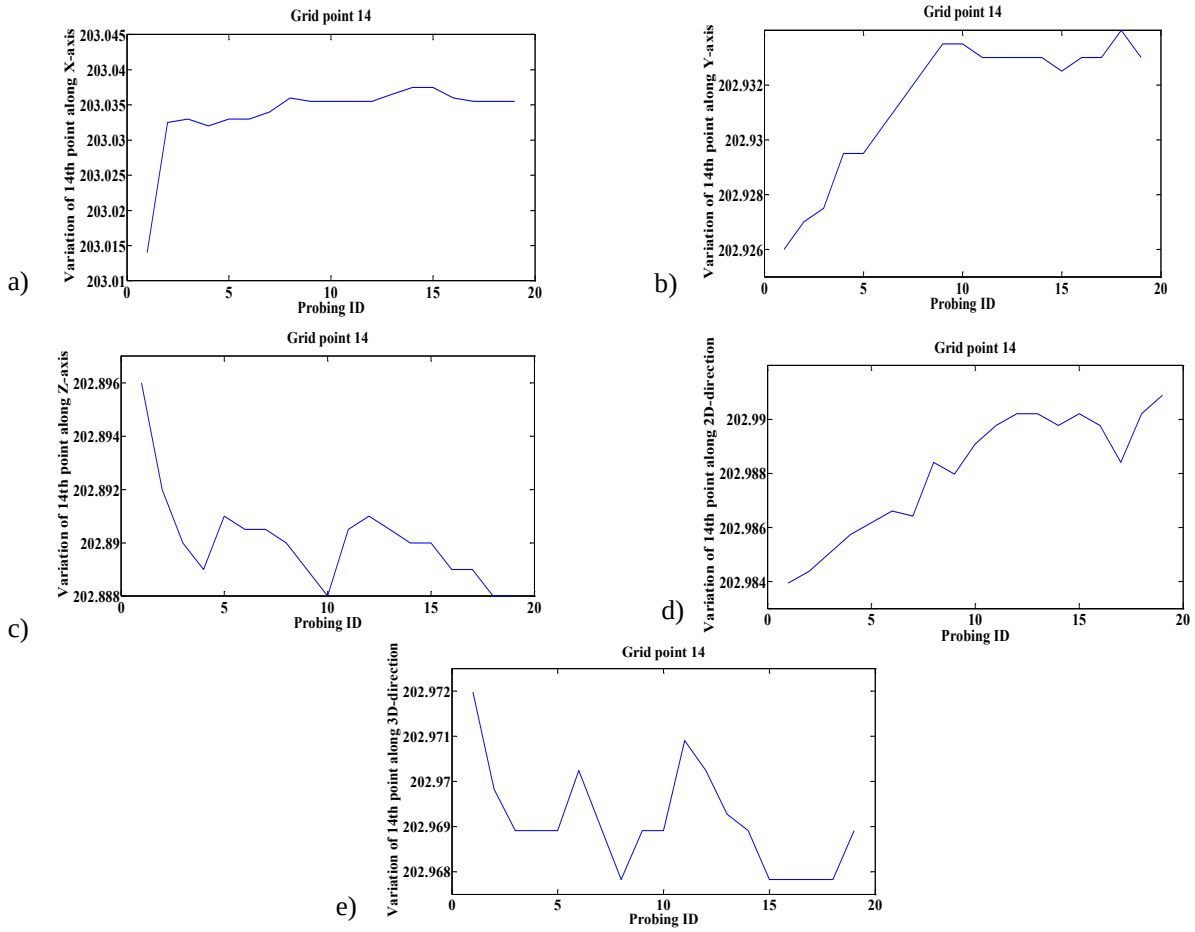

Figure 7-6 A typical trends for spatial grid measurement along X-, Y-, Z-, 2D- and 3D- direction (14th grid point) denoted by a, b, c, d and e respectively. As the spatial grids measurement repeats for 19 times hence the point is measured for 19 times. The variations are in "***mm***"

To observe the effect of the machine state on the grid measurements, a random grid points are considered and a typical trend of measurement variation is given in Figure 7-6. The X-axis measurements are affected the most for first and second cycle by approximately 20 µm while the measurements variation along other direction remains below 10.0 µm (approximately) The grid measurement started in the morning with the machine's cold state hence machine hysteresis as well as the machine's state change can be responsible for the drift on X-axis measurements.

In Procedure III, surface irregularity test was carried out in the machine tool hence the machine tool itself can contribute to the measurement variability. To isolate the effect of the surface on the measurements, the machine table was measured on an accurate Coordinate Measuring Machine

(CMM). To do so, six different spatial grids of 0.2 mm × 0.2 mm are defined that represents typical surface quality regions with surface normals along X-, Y- and Z- direction as illustrated in Figure 7-7. One spatial grid at both positive and negative X- and Y- direction and two on the negative Z-axis direction since the probe has only negative Z approach capability.

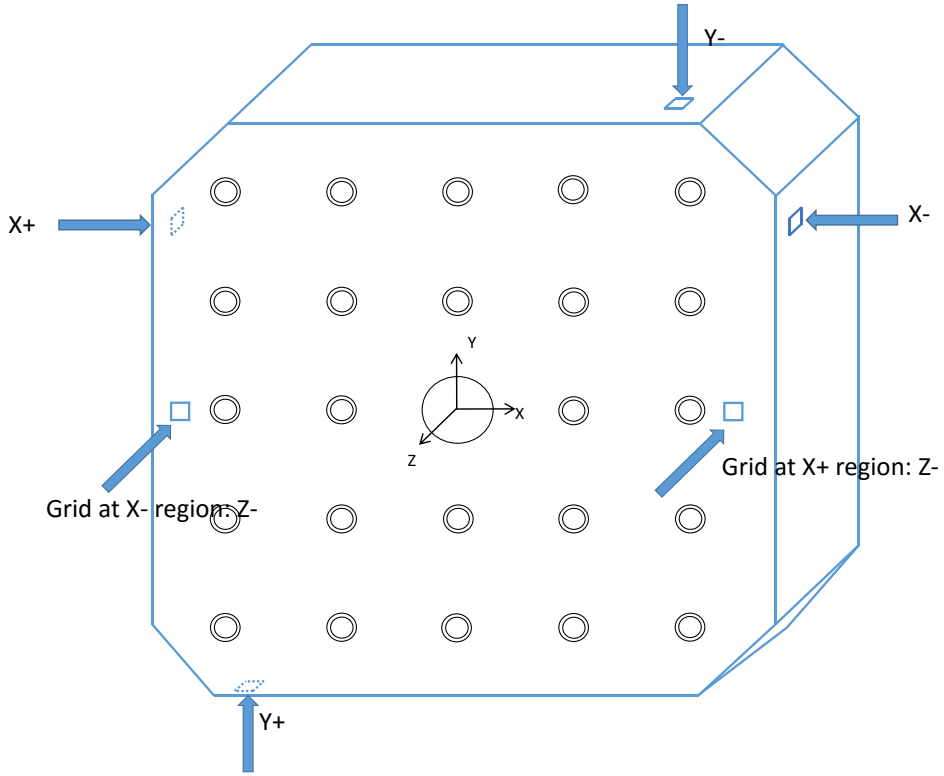

Figure 7-7 Spatial grid probing on a CMM (grid size is 200 µm × 200 µm)

Each grid measurements was repeated three times. The average of each point measurement is used to calculate the range and the standard deviation of the measurement variation in each measuring direction. Figure 7-7 and Figure 7-8 shows the location, direction and the quality of the measured surface and Table 7-6 shows the results.

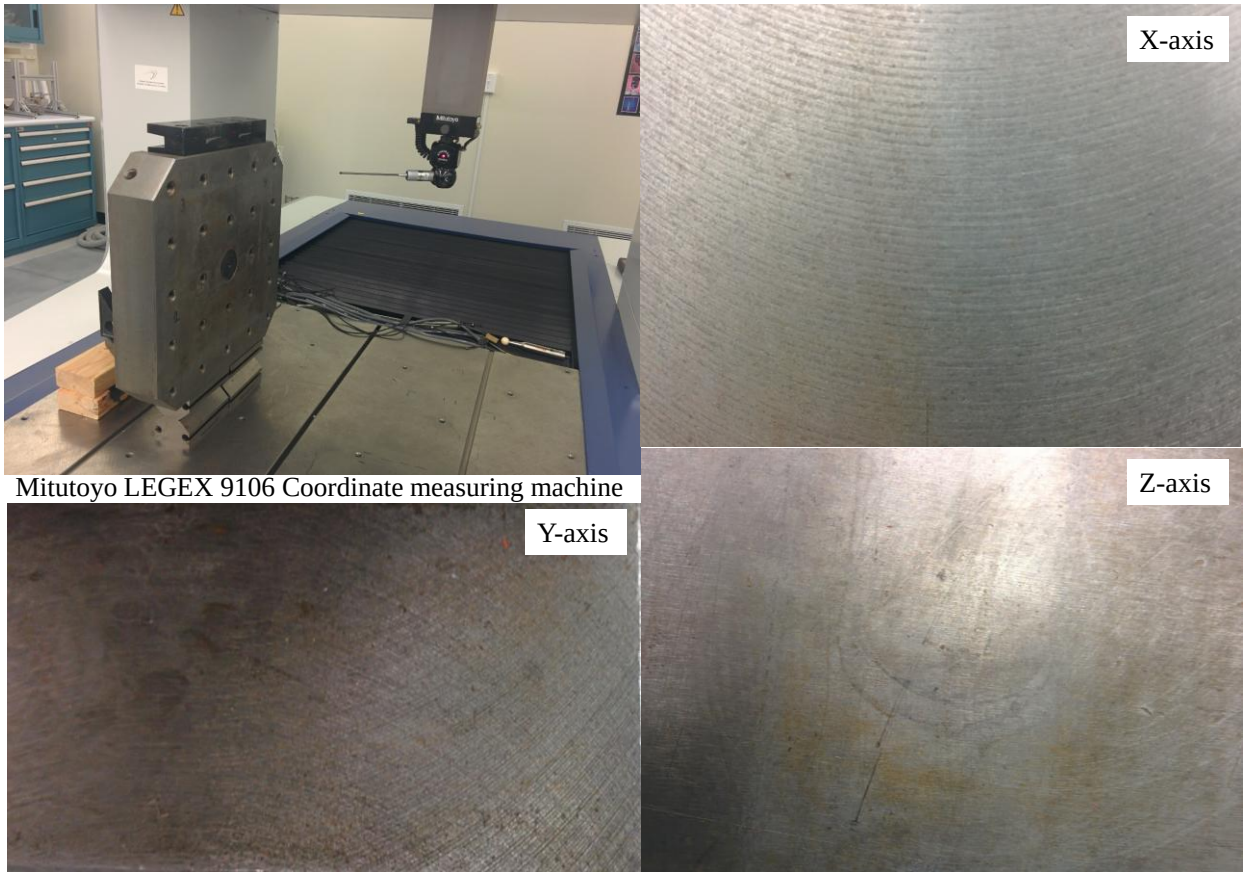

Figure 7-8 The Coordinate Measuring Machine (CMM) and surface quality at X-, Y- and Z-direction

The range and standard deviation of X- and Y-axis measurements in Table 7-4 and Table 7-6 are similar in magnitude but for the Z-axis measurements the CMM results show much less variation; about 1 µm on the CMM instead of 3 on the machine tools. Figure 7-9 shows the variation of the measurements for the six different spatial grid as shown in Figure 7-7.

Table 7-6 The range and standard deviations of six spatial grid probing in CMM

	X+	X-	Y+	Y-	Z (in X+ region)	Z (in X- region)
Range (µm)	3.13	3.23	2.97	2.00	1.07	1.27
Standard deviation	0.71	0.91	0.94	0.53	0.34	0.33

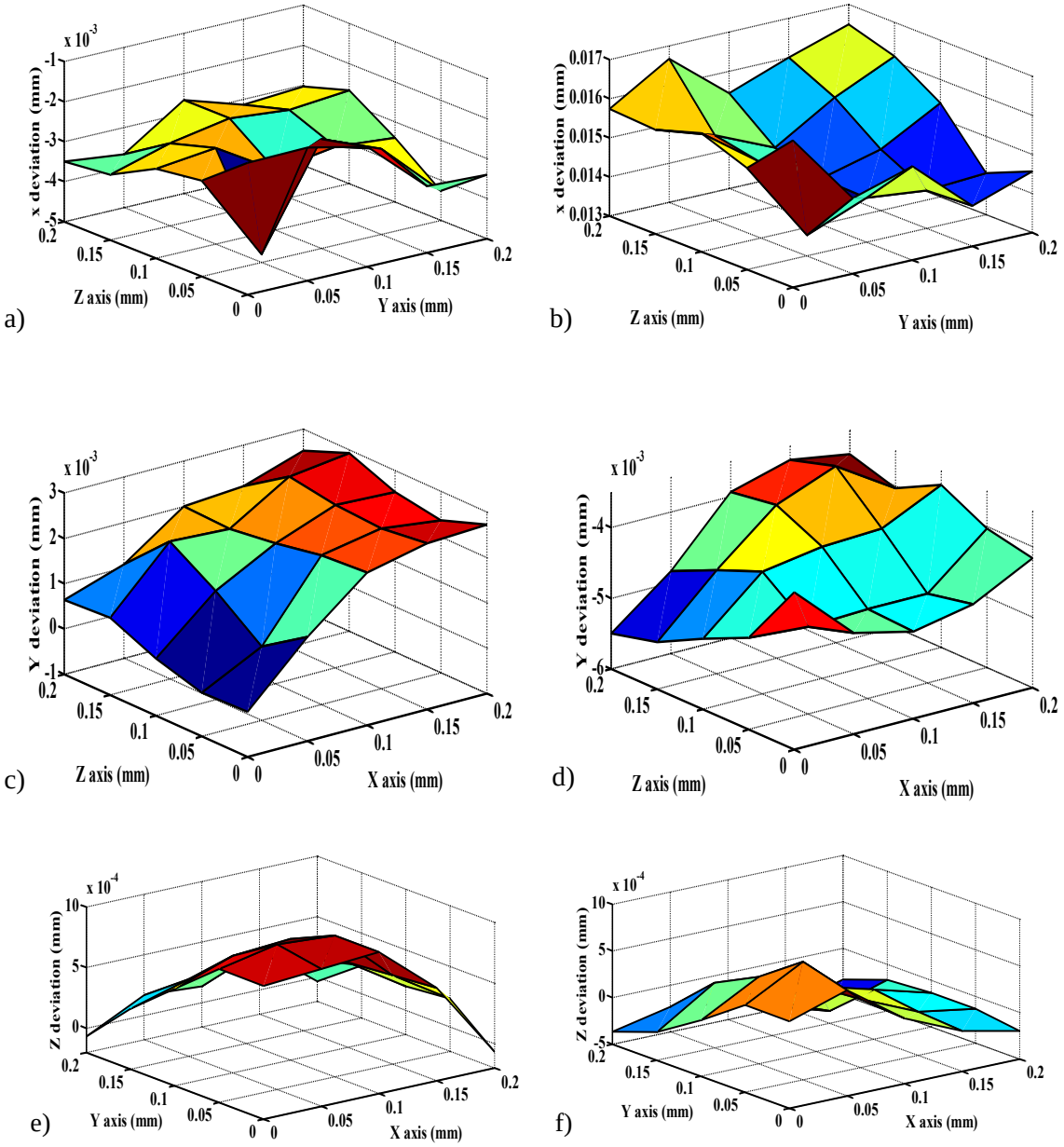

Figure 7-9 Surface irregularity effect on a 200 µm × 200 µm spatial grid. a) Negative X-probing, b) positive X-probing, c) positive Y-probing, d) negative Y-probing, e) negative Z-probing in X+ region and f) negative Z-probing in X- region of the artefact

A scanning probe Mitutoyo MPP-300 is used to scan a 15 mm by 15 mm spatial grid at the X- and Y-direction as shown in Figure 7-7 in order to observe the surface irregularities. Since the

surface on Z-direction is polished and CMM tests shows that it has negligible contribution hence, the grid on X- and Y-axis are taken into consideration for this test.

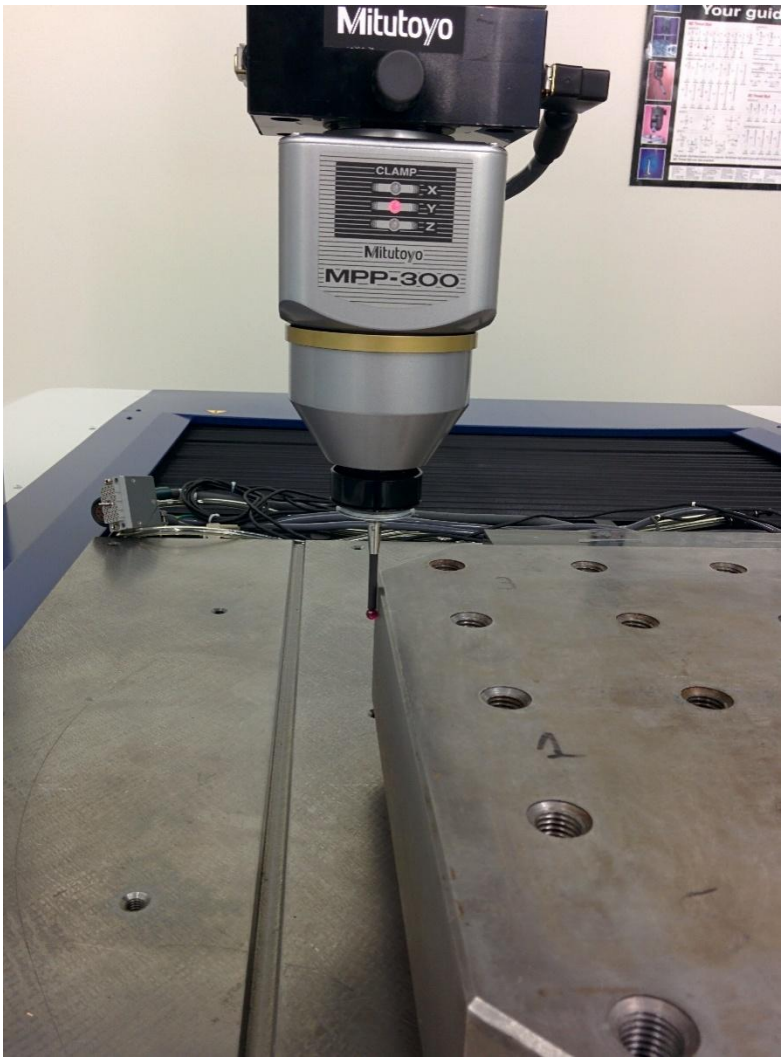

Figure 7-10 Mitutoyo MPP-300 scanning probe to measure 15 mm by 15 mm spatial grid on CMM

Figure 7-10 shows the scanning probing is in operation on a Legex 910 coordinate measuring machine and Table 7-7 shows the results of the measurements. Result shows that, the grid on the –X direction has maximum standard deviation of 1.49 µm.

Table 7-7 The range and standard deviations of six spatial grid obtained by a Mitutoyo MPP-300 scanning probe on CMM

	X+	X-	Y+	Y-
Range (µm)	3.67	6.27	2.58	3.66
Standard deviation (µm)	0.85	1.49	0.62	0.84

Procedure IV focused on the effect of the probe and machine. Systematic lobing of the probing results is estimated by probing a precision sphere with a sphericity of 1.6 µm. The on machine tool probing is done every 30 degrees longitudinally and every 10 degree latitudinally. Then a sphere is fitted to the measurements. The maximum and minimum residuals, out of sphericity as well as the standard deviation of the residuals are 4.71, -3.37, 8.1 and 1.7 µm respectively.

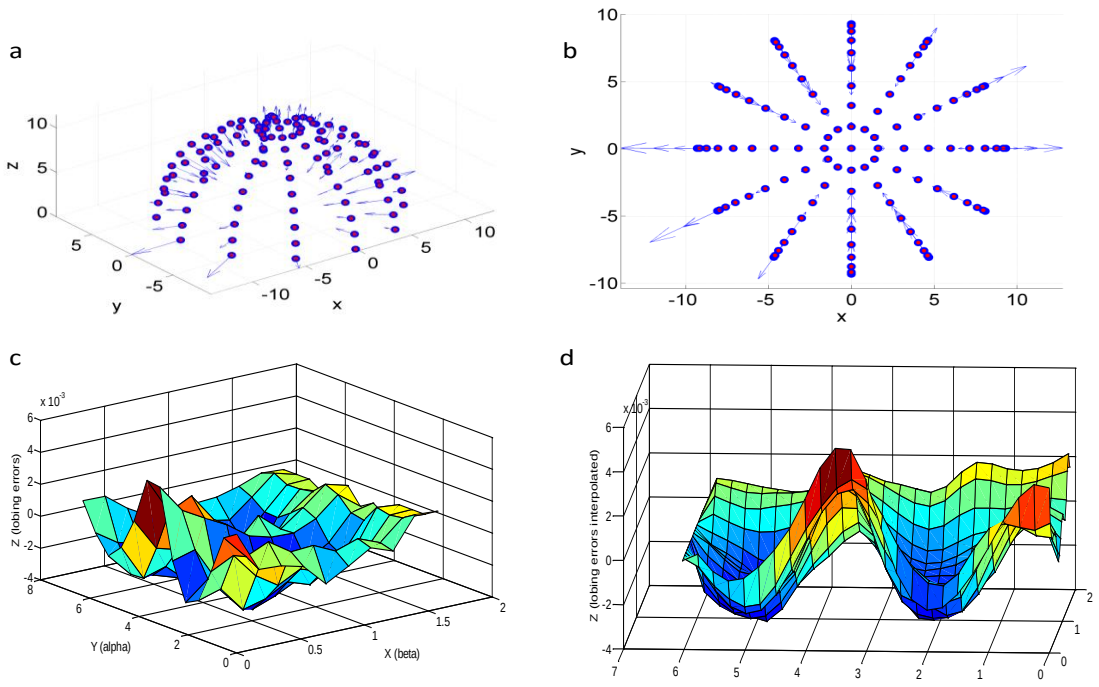

Figure 7-11 Residuals for a sphere probing (1000x) (a) and (b), probe lobing error (c) and interpolated lobing error (d)

Figure 7-11 (b) shows that, there is an elliptical trend over the residuals with two visible lobes also visible in Figure 7-11 (c and d). This error can be the combined effect of the probe, sphere and the machine itself

7.4 Conclusions

Machine tool's probing accuracy is affected by the probe, the machine as well as the measurement environment. Results show that, there is an unknown drift of approximately 10 µm for the first hour while the measurements are performed. Surface irregularities are the major contributor to the inaccuracy of the probing when the probe approaches in Z and 3D directions with a deviation range of 3.9 and 7 µm in the machine tool while the CMM measurements shows that surface on X- and Y-axis contribute the most (3.23 and 2.97 µm). Since the measurement on CMM takes a short amount of time hence the measurement variation can considered to be solely the surface contribution. In contrast to CMM, on the machine tool the drift might contribute to the inaccuracies of the surface measured in different directions since the measurement was conducted over a longer period of time (7 hours and 30 minutes). Disregarding the drift, surface wetness does not have observable effect on probing measurements unless cutting fluid is supplied through the machine's system to wet the surface which may cause a thermal effect on the machine. Thus it can also affect the accuracy of the probing measurement. Repeatability of the probe causes significant effects on the measurements. The worst case is the repeatability for the Y-axis measurement with a standard deviation of 4.9 µm while the 3D measurement has unexpectedly lower standard deviation of 0.6 µm. Out of sphericity of the probing results was significant at 8.1 µm.

7.5 Acknowledgments

This research work is funded by NSERC, CRIAQ, Pratt & Whitney Canada, Meloche Group and SONACA Montreal. The authors are very grateful for the experimental support of Guy Gironne and Vincent Mayer.

7.6 References

[1] Guiassa, R., Mayer, J. R. R., Balazinski, M., Engin, S., and Delorme, F. E., 2014, "Closed door machining error compensation of complex surfaces using the cutting compliance coefficient and on-machine measurement for a milling process". International Journal of Computer Integrated Manufacturing, Volume 27, Issue 11, 2014

[2] Cauchick-Miguel, P. A., and Kings, T. G., 1998, "Factors which influence CMM touch trigger probe performance," International Journal of Machine Tools and Manufacture, 38(4), pp. 363-374.

[3] Wozniak, A., and Dobosz, M., 2005, "Factors influencing probing accuracy of a coordinate measuring machine," IEEE Transactions on Instrumentation and Measurement, 54(6), pp. 2540-2548.

[4] Dobosz, M., and Wozniak, A., 2005, "CMM touch trigger probes testing using a reference axis," Precision Engineering, 29(3), pp. 281-289.

[5] Wozniak, A., and Dobosz, M., 2005, "Influence of measured objects parameters on CMM touch trigger probe accuracy of probing," Precision Engineering, 29(3), pp. 290-297.

[6] Johnson, R. P., Qingping, Y., and Butler, C., "Dynamic error characteristics of touch trigger probes fitted to coordinate measuring machines," Proc. IMTC/98 Conference. IEEE Instrumentation and Measurement Technology Conference.18-21 May 1998, IEEE, pp. 1168-1172.

[7] Fesperman, R. R., Moylan, S. P., and Donmez, M. A., "Methods, practices, and standards for evaluating on-machine touch trigger probing of workpieces," Proc. 25th Annual Meeting of the American Society for Precision Engineering, ASPE 2010, October 31, 2010 - November 4, 2010, American Society for Precision Engineering, ASPE, pp. 309-312.

[8] ISO/DIS, 2011, "Test code for machine tools-Part 10: Determination of measuring performance of probing systems of numerically controlled machine tools," 230-10.

[9] Jankowski, M., Wozniak, A., and Byszewski, M., 2014, "Machine tool probes testing using a moving inner hemispherical master artefact," Precision Engineering, 38(2), pp. 421-427

[10] Rahman, M.M., Mayer, J.R.R., 2014, “Five axis machine tool volumetric error prediction through an indirect estimation of intra and inter axis error parameters by probing facets on a scale enriched uncalibrated indigenous artefact”, Precision Engineering, 40:94-105

CHAPTER 8 ARTICLE 5: CALIBRATION PERFORMANCE INVESTIGATION OF AN UNCALIBRATED INDIGENOUS ARTEFACT PROBING FOR FIVE-AXIS MACHINE TOOL

Md Mizanur Rahman, J.R.R. Mayer

Mechanical Engineering Dept., Polytechnique Montréal, P.O. Box 6079, Station Downtown, H3C 3A7 Montréal (QC), Canada

Published in Journal of Machine Engineering, Vol. 16, No. 1, 2016

8.1 Abstract

On machine measurement of artefacts such as single ball, multiple balls or even prismatic shape artefact is gaining popularity for the calibration of five-axis machine tools. However, calibration results can be degraded due to errors from different process variables such as the measurement strategies, rotary axes indexations and artefact dismount and remount cycles. This research investigates the repeatability of uncalibrated indigenous artefact probing and machine tool error parameters calibration against a number of process variables. Uncertainties of the estimated parameters are estimated to quantify the calibration quality.

Keywords: Robustness, machine tools, artefact, uncertainty

8.2 Introduction

Five-axis machine tools offer numerous opportunities to produce complex parts because of their ability to orient the tool with respect to the workpiece. Due to the existence of two rotary axes, direct calibration, such as laser interferometry, are difficult, time consuming, require trained personnel and are sometimes complicated to implement. In contrast, indirect calibration techniques are comparatively easy to adapt and can often be automated [1]. Since CNC machine tools are usually equipped with a touch trigger probe, some researchers have developed indirect calibration technique involving the measurement of different artefacts to gather machine tools geometric information. Hence, the measuring capability of the machine tool becomes a prior concern.

In [1] - [6], much work is presented to estimate geometric and dynamic error parameters for CNC machine tools using indirect approaches but the variability of these approaches against process variables has not been addressed except for Verma et al. [12] whom investigated the influence of the most significant variable on the measurement accuracy of a CNC machine tool and found that tool change and machine tool warm up cycles are major contributors.

Some research [7] - [12] considered the measurement inaccuracies introduced by the measuring instruments (touch trigger probe etc.) for Coordinate Measuring Machines (CMMs) and CNCs with detail error modelling.

Machine tool's moving parts such as: bearings, gear and hydraulic oil, drives and clutches, pumps and motors, guide ways, cutting action and swarf, external heat sources etc. generate heat while the machine tool is in continuous operation [13]. Martin et al. found that over 50% of the overall machine tool inaccuracy was caused by these internal or external heat sources. They proposed a thermal error compensation model where the displacement of the tool center point (TCP) can be calculated by a transfer function (TF) that contains models based on heat transfer principles. The TF modeling approach was applied to different machine tools with similar components and structures but different initial expansion in individual parts. The improvement was 87% compared to the uncompensated state. The improvement in calibration performance between the machine tools varies only 1% which implies the TF model's portability among variety of machine tools [14]. Jerzy and Wojciech reviewed the integration of intelligent functions such as active vibration control, intelligent thermal shield, safety shield, voice adviser, intelligent performance spindle, maintenance support and balance analyzer in machine tools in order to make them autonomous (self-supervision, self-diagnosis, etc.). For high performance machine tools, the authors attach importance to holistic modeling and numerical simulation of machine tool's operational properties during the entire machining process in order to enhance the capabilities and effectiveness of identifying and minimizing the disturbance and error compensation. They concluded that integrating these intelligent functions will increase efficiency and precision while minimizing production costs [15].

Authors investigated the influence of machine tools status change during a day period and between consecutive days on the calibration performance of an on-machine probing of an

uncalibrated indigenous artefact on a five-axis machine tool [16]. This research investigates the influence of variables such as the measurement strategy, rotary axes indexations and artefact dismount and remount cycles on the performance of calibration. Uncertainty estimates of the calibrated parameters will be considered for this analysis.

8.3 Mathematical background

A similar artefact probing strategy to those described in [1] is used where facets are probed based on their nominal position and nominal local normals. Homogeneous transformation matrices (HTMs) transform axis command into the position of the stylus tip with respect to the facets from which linear equations are produced in order to estimate the error parameters.

$$\boldsymbol{\delta d} = \boldsymbol{J}.\boldsymbol{\delta E} \tag{8-1}$$

Where, $\boldsymbol{\delta d}$ are the distance between facets and stylus tip calculated using the nominal model, $\boldsymbol{J}$ is the Jacobian sensitivity matrix of the facets to stylus tip for small change is distances and $\boldsymbol{\delta E}$ are the estimated error parameters. In this study, inter-axis errors, scale gains and backlash will be estimated. For the parameter uncertainty estimation, GUM uncertainty framework (GUF) is used. The estimation process is based on a multi-input and multi-output model and the covariance of the input quantities is required [16]. For an output quantity $\boldsymbol{Y} = (Y_{1,\ldots}, Y_{\mathrm{m}})^{\mathrm{T}}$ and an input quantity $\boldsymbol{X} = (X_{1,\ldots}, X_{\mathrm{N}})^{\mathrm{T}}$, with

$$Y = \boldsymbol{f}(X) \tag{8-2}$$

where $f = (f_1, \ldots, f_{\mathrm{m}})^{\mathrm{T}}$.

Then, the output uncertainties, as a covariance matrix, can be calculated using the following formula [17]

$$\boldsymbol{U_y} = \boldsymbol{C_x U_x C_x^{\mathrm{T}}} \tag{8-3}$$

8.4 Calibration performance analysis

In this section, performance of the indirect calibration technique by probing an indigenous artefact is investigated against probing strategies, change in machine tool status during a day and between consecutive days, artefact dismount and remount cycle and rotary axis indexations.

8.4.1 Influence of the probing strategies

Calibration was done for four different probing strategies while the rotary axes indexations remains the same but the facets location was changed. The total number of 251 probing points remains the same for all the strategies. A particular strategy is conducted during a specific day. Each day has a different strategy. There are four strategies and so four days of test. So, for four consecutive days, each strategy repeats for four cycles each day as shown in Table 8-1. The time required for four repeated cycles is 6h. 6 min. for each strategy hence each cycle takes approximately 1h. 30min.

Table 8-1 Effect of strategies: Analysis criteria

	Four repeated cycles per strategy				Strategy-wise analysis
Day-1, Strategy 1	Cycle 1	Cycle 2	Cycle 3	Cycle 4	Mean values of the estimated parameters at each strategy for four repeated cycles
Day-2, Strategy 2	Cycle 1	Cycle 2	Cycle 3	Cycle 4	
Day-3: Strategy 3	Cycle 1	Cycle 2	Cycle 3	Cycle 4	
Day-4, Strategy 4	Cycle 1	Cycle 2	Cycle 3	Cycle 4	

In order to observe the effect of the strategies, the means of the estimated parameters for four repeated cycles at each strategy are calculated and compared (Table 8-1). Results are shown in Table 8-2. The overall mean of the parameters for all the strategies has also been calculated and compared with the mean of the individual strategies.

Table 8-2 Effect of change in probing strategy (change in facets location). Mean values of the estimated parameters of all strategies, individual strategy and the range of means of the strategies

Estimated Parameters	Overall mean (all strategies)	Strategy-wise mean values				Range of means
		Day 1	Day 2	Day 3	Day 4	
		Strategy 1	Strategy 2	Strategy 3	Strategy 4	
E_{XXb} (µm)	5.82	5.18	6.16	5.38	5.65	0.98
E_{AOB} (µrad)	-36.51	-41.15	-38.06	-36.98	-33.78	7.37
E_{COB} (µrad)	-7.35	-6.57	-7.37	-6.51	-9.65	3.14
E_{XOS} (µm)	-132.87	-125.83	-128.00	-128.08	-127.23	2.25
E_{YOS} (µm)	24.51	26.08	25.02	24.48	24.89	1.59
E_{YY} (µm/m)	-29.86	-26.42	-28.91	-27.42	-27.62	2.49
E_{YYb} (µm)	-5.92	-6.33	-5.62	-5.58	-5.48	0.85
E_{BOZ} (µrad)	84.96	63.40	66.98	67.11	64.51	3.71
E_{ZZ} (µm/m)	-52.12	-52.19	-57.42	-56.55	-51.00	6.42
E_{AOY} (µrad)	-17.27	-22.03	-21.28	-15.45	-16.25	6.58
E_{COY} (µrad)	14.79	13.50	15.19	15.08	14.54	1.70
E_{XOC} (µm)	-109.10	-109.43	-109.59	-110.10	-110.19	0.76
E_{AOC} (µrad)	8.78	-3.38	-4.80	-1.88	-8.78	6.90
E_{BOC} (µrad)	11.58	5.46	5.89	6.69	5.76	1.23
E_{BBb} (µrad)	8.93	7.99	8.88	8.43	8.89	0.90
E_{CCb} (µrad)	-0.19	-0.22	0.57	-0.69	-0.48	1.26
E_{XX} (µm/m)	-9.89	-7.18	-10.05	-10.25	-8.82	3.07

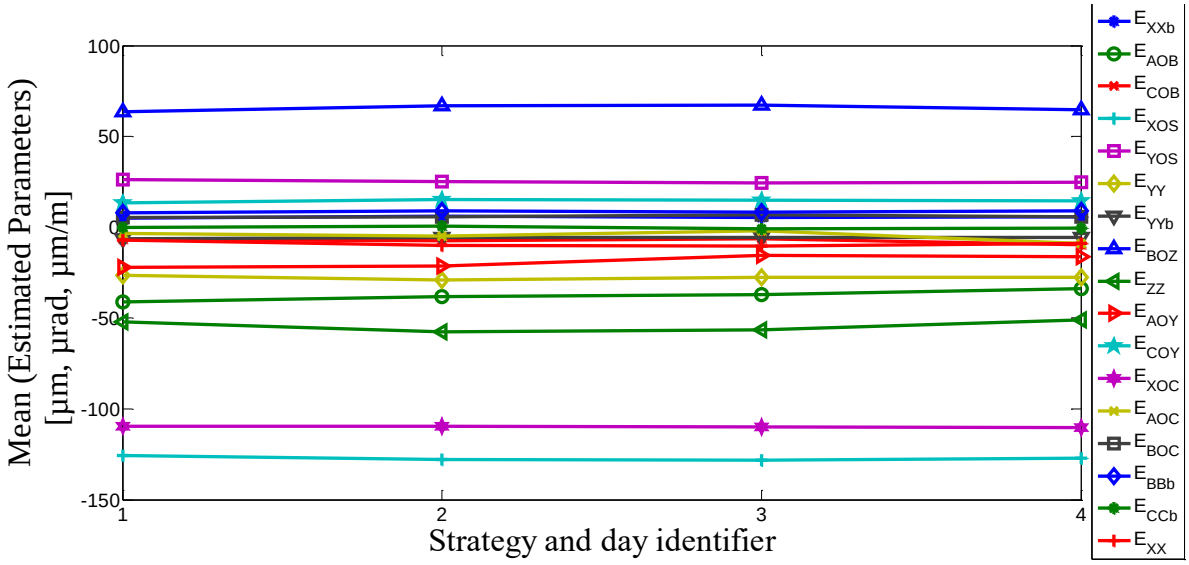

Figure 8-1 Effect of change in probing strategy (change in facets location). Mean values of the estimated parameters of all strategies

Table 8-2 shows the overall mean, strategy wise mean and the range of means for different strategies of the estimated parameters while Figure 8-1 shows the change in mean values throughout the strategies. Result shows that, E_{A0B}, E_{ZZ}, E_{AOY} and E_{AOC} have noticeable variation in range of means otherwise the range of mean values of the parameters at different strategies are considerably smaller.

8.4.2 Influence of artefact dismount and remount cycle

The artefact used in this work is the original machine tool table. In this section, the effect of artefact dismount and remount on the parameters estimation is analysed. The machine tool undergoes three different phases. The warm-up phase is approximately two hours from the machine tool cold condition and no measurements has been done in this phase, then the first measurement cycle is ran before artefact change followed by a second measurement cycle. Each measurement cycle takes approximately 1H30. During artefact change, the artefact is dismounted and put back into the machine tool's table depot then brought back and remounted again in the machine tool workspace. These operations are automated. The artefact dismount and remount cycle takes 3M30 approximately. This procedure was repeated the following day and the results are given in Table 8-3**.**

Table 8-3 Effect of artefact dismount and remount cycle in parameter estimation

Estimated Parameters	Day 1 Before artefact change	Day 2 Before artefact change	Range	Day 1 After artefact change	Day 2 After artefact change	Range	ΔRange
E_{XXb} (μm)	4.68	9.30	4.62	4.28	6.40	2.12	2.5
E_{AOB} (μrad)	-55.16	-47.78	7.38	-45.15	-40.16	4.99	2.39
E_{COB} (μrad)	-0.80	-5.84	5.04	-3.47	-5.85	2.38	2.66
E_{XOS} (μm)	-130.98	-127.83	3.15	-130.42	-132.57	2.15	1
E_{YOS} (μm)	30.25	25.08	5.17	26.89	23.97	2.92	2.25
E_{YY} (μm/m)	-25.04	-36.46	11.42	-12.58	-22.78	10.2	1.22
E_{YYb} (μm)	-5.82	-3.53	2.29	-4.98	-3.91	1.07	1.22
E_{BOZ} (μrad)	71.75	63.88	7.87	66.06	69.75	3.69	4.18
E_{ZZ} (μm/m)	-60.44	-66.75	6.31	-50.77	-55.64	4.87	1.44
E_{AOY} (μrad)	-34.29	-35.35	1.06	-22.53	-23.93	1.4	0.34
E_{COY} (μrad)	20.58	17.59	2.99	16.94	15.44	1.5	1.49
E_{XOC} (μm)	-105.42	-102.84	2.58	-104.70	-105.01	0.31	2.27
E_{AOC} (μrad)	-3.65	-7.60	3.95	-2.16	-5.44	3.28	0.67
E_{BOC} (μrad)	16.98	16.62	0.36	16.59	16.69	0.1	0.26
E_{BBb} (μrad)	8.49	7.96	0.53	7.32	7.17	0.15	0.38
E_{CCb} (μrad)	2.42	2.24	0.18	0.29	1.80	1.51	1.33
E_{XX} (μm/m)	-7.37	-6.56	0.81	0.01	-1.64	1.65	0.84

Result shows that artefact mount dismount cycle has no significant effect. This is expected for two reasons. One is that the mechanism for table mounting was found to be relatively repeatable,

and the other reason is that the mathematical model includes the artefact and tool setup errors as separately estimated variables. The test is affected by variability due to the change between the cycles during a day period and change between days for consecutive days as described in authors' previous work [16].

8.4.3 Influence of rotary axes indexations change

Measuring an artefact at different rotary axes indexation provides rich information about the machine tools geometry. But change in probing strategy by changing the number of rotary axes indexations may affect the parameters estimation. Since the artefact is measured at every rotary axes combination hence the higher the number of rotary axes combination the more measurement points are gathered. However, this also means more non-productive time for the machine tool so it is worth investigating the effect of increasing the number of indexations in the strategy on the estimated error parameters. For this purpose, a particularly rich probing strategy was repeated five times per day for four consecutive days. The probing strategy includes 28 combinations of Spindle-B-C (ABC) axes indexations. Out of these 28 indexations, five different subsets of ABC indexations have been chosen to evaluate the influence of rotary axes indexation on parameter estimation. The subsets are chosen based on the condition number of the Jacobian matrix by simulating the measurement subsets.

The condition number is a mathematical quantity to determine the numerical quality of the estimation. A low condition number provide better estimates. In this investigation, more than 10 different measurement strategies were analyzed with different ABC subsets and found that measurement strategy with higher number of ABC indexations does not necessarily means better estimates. Five indexation subsets are selected for this analysis.

Table 8-4 Condition number for different ABC indexation sets

	ABC sets					
	Complete ABC sets	Subset 1	Subset 2	Subset 3	Subset 4	Subset 5
	28	23	24	25	22	21
Condition Number	10073	10011	9143	9678	9230	8975

Table 8-4shows the condition number of the selected ABC indexation subsets. During the simulation, 17 machine error parameters are included in the model as shown in Table 8-2**.**

The selected subsets have been applied to the 20 measurement cycles (five cycles per day for four consecutive days). The standard deviations of the estimated parameters for each subset are calculated; mean and range of the standard deviations are also calculated and given in Table 8-5. Figure 8-2 shows the mean values of the estimated parameters for the five subsets.

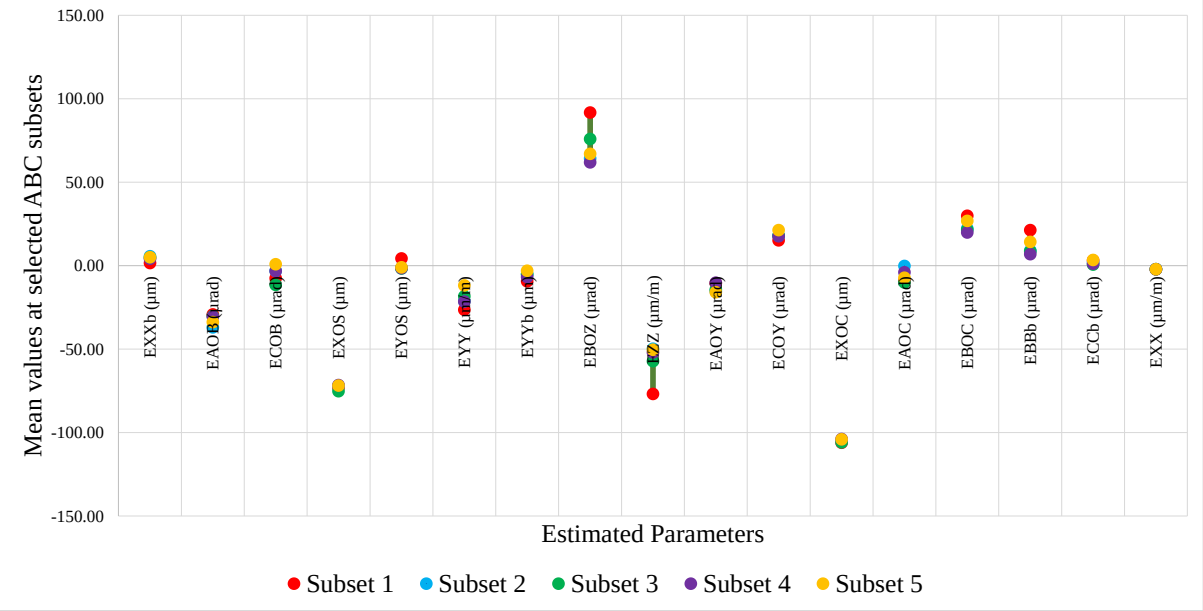

Figure 8-2 Mean values of the estimated parameters for the five ABC subsets applied to the 20 measurement cycles

From Figure 8-2 it is observed that the mean values for the subsets have similar trends in terms of parameter values. E_{B0Z} and E_{ZZ} has noticeable amount of standard deviation while others are significantly smaller (around or below 5 µm, µrad or µm/m). E_{XX} and E_{X0C} are the most stable parameters.

Table 8-5 Mean and standard deviations of the estimated parameters for the five ABC subsets applied to the 20 measurement cycles

	Subset 1 (23 ABC sets)	Subset 2 (24 ABC sets)	Subset 3 (25 ABC sets)	Subset 4 (22 ABC sets)	Subset 5 (21 ABC sets)	Standard Deviations
E_{XXb} (µm)	1.47	5.55	4.80	4.04	4.93	1.43
E_{AOB} (µrad)	-29.31	-37.04	-30.27	-30.60	-33.91	2.86
E_{COB} (µrad)	-7.59	-3.19	-11.59	-3.37	0.76	4.22
E_{XOS} (µm)	-73.13	-72.04	-75.28	-71.64	-71.87	1.35
E_{YOS} (µm)	4.25	-1.40	-1.74	-1.56	-1.12	2.29
E_{YY} (µm/m)	-26.49	-21.28	-18.44	-21.59	-11.86	4.80
E_{YYb} (µm)	-9.44	-5.28	-5.28	-6.86	-3.12	2.09
E_{BOZ} (µrad)	91.66	64.11	75.82	61.82	66.95	10.88
E_{ZZ} (µm/m)	-76.95	-49.88	-57.33	-52.04	-50.48	10.15
E_{AOY} (µrad)	-10.55	-15.35	-14.35	-10.22	-15.97	2.43
E_{COY} (µrad)	15.13	17.81	17.90	17.51	21.21	1.94
E_{XOC} (µm)	-106.12	-104.76	-105.96	-103.95	-104.16	0.90
E_{AOC} (µrad)	-9.09	-0.27	-10.15	-3.99	-7.25	3.61
E_{BOC} (µrad)	29.80	22.13	21.40	19.81	26.75	3.72
E_{BBb} (µrad)	21.23	8.92	8.58	6.82	14.16	5.25
E_{CCb} (µrad)	3.00	1.86	0.52	1.04	3.28	1.07
E_{XX} (µm/m)	-2.24	-2.23	-2.24	-2.23	-2.23	0.01

8.4.4 Uncertainties of the estimated parameters

Uncertainties of the estimated parameters were estimated using a covariance matrix generated from the measurement data obtained from the five repeated measurement cycles of a particular measurement strategy for four consecutive days. The uncertainty values are given in Table 8-6.

Table 8-6 Uncertainties of the estimated parameters

Parameters' names	E_{XXb} (µm)	E_{AOB} (µrad)	E_{COB} (µrad)	E_{XOS} (µm)	E_{YOS} (µm)	E_{YY} (µm/m)	E_{YYb} (µm)	E_{BOZ} (µrad)	E_{ZZ} (µm/m)
Uncertainties	2.22	2.43	1.42	3.28	1.07	5.16	0.87	4.51	5.18

Parameters' names	E_{AOY} (µrad)	E_{COY} (µrad)	E_{XOC} (µm)	E_{AOC} (µrad)	E_{BOC} (µrad)	E_{BBb} (µrad)	E_{CCb} (µrad)	E_{XX} (µm/m)
Uncertainties	3.18	1.63	0.86	1.41	7.49	0.56	0.85	3.28

Results shows that C-axis out of squareness to X-axis (E_{BOC}), Y- and Z-axis scale gains (E_{YY} and E_{ZZ}) and Z-axis out of squareness to X-axis (E_{B0Z}) have noticeably higher uncertainty values. Figure 8-3 shows the uncertainties versus standard deviations obtained in section 8.4.3. Similar trends are observed between the standard deviation and uncertainties but

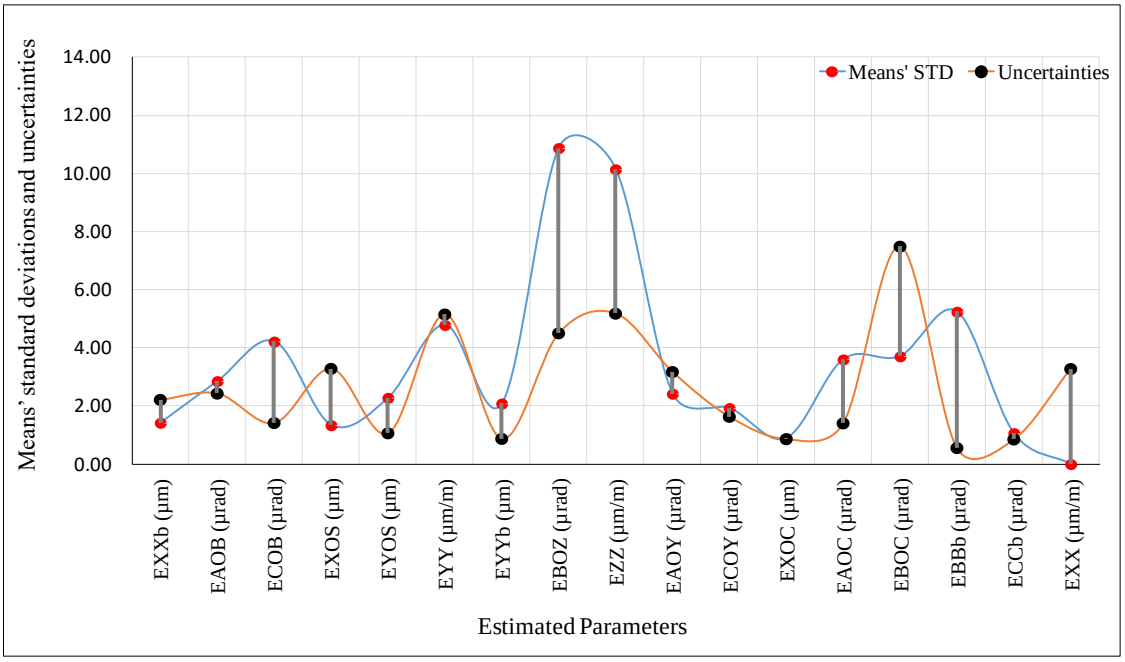

Figure 8-3 Uncertainties vs standard deviaiton of the estimated parameters

8.5 Conclusion

Performance of an indirect calibration technique by probing an indigenous artefact against some measurement process variables has been investigated in this work. Result shows that E_{A0B}, E_{ZZ},

E_{A0Y} and E_{A0C} are influenced by change in measurement strategy with ranges of 7.37 µrad, 6.42 µm/m, 6.58 µrad and 6.9 µrad while others are around or below 3 (µrad, µm or µm/m). As expected, the artefact dismount and remount cycle does not have significant effects on the estimation since this effect is considered in the estimation process. The selection of measurement strategy in terms of rotary axes indexation combinations plays an important role in calibration. The strategy can be optimized by observing the condition number which can reduce the time of the measurements. Standard deviation of the estimated parameters obtained for the indexation subsets are below the uncertainties. E_{B0C}, E_{YY}, E_{B0Z} and E_{ZZ} have noticeably higher standard deviation and uncertainties.

8.6 Acknowledgments

Work funded by NSERC, CRIAQ, Pratt & Whitney Canada, Meloche Group and SONACA Montreal. Authors are grateful for the experimental support of G. Gironne and V. Mayer.

8.7 References

[1] Rahman, M.M., Mayer, J.R.R., 2014, Five axis machine tool volumetric error prediction through an indirect estimation of intra and inter axis error parameters by probing facets on a scale enriched uncalibrated indigenous artefact, Precision Engineering, 40:94-105.

[2] Schwenke, H., Knapp, W., Haitjema, H., Weckenmann, A., Schmitt, R., and Delbressine, F., 2008, "Geometric error measurement and compensation of machines—An update," CIRP Annals - Manufacturing Technology, 57(2), pp. 660-675.

[3] Erkan, T., Mayer, J. R. R., and Dupont, Y., 2011, "Volumetric distortion assessment of a five-axis machine by probing a 3D reconfigurable uncalibrated master ball artefact," Precision Engineering, 35(1), pp. 116-125.

[4] Mayer, J. R. R., 2012, "Five-axis machine tool calibration by probing a scale enriched reconfigurable uncalibrated master balls artefact," CIRP Annals - Manufacturing Technology, 61(1), pp. 515-518

[5] Weikert, S., and Knapp, W., 2004, "R-test, a new device for accuracy measurements on five axis machine tools," CIRP Annals - Manufacturing Technology, 53(1), pp. 429-432

[6] Ibaraki, S., Iritani, T., and Matsushita, T., 2012, "Calibration of location errors of rotary axes on five-axis machine tools by on-the-machine measurement using a touch-trigger probe," International Journal of Machine Tools and Manufacture, 58, pp. 44-53.

[7] Cauchick-Miguel, P. A., and Kings, T. G., 1998, "Factors which influence CMM touch trigger probe performance," International Journal of Machine Tools and Manufacture, 38(4), pp. 363-374.

[8] Wozniak, A., and Dobosz, M., 2005, "Factors influencing probing accuracy of a coordinate measuring machine," IEEE Transactions on Instrumentation and Measurement, 54(6), pp. 2540-2548

[9] Johnson, R. P., Qingping, Y., and Butler, C., "Dynamic error characteristics of touch trigger probes fitted to coordinate measuring machines," Proc. IMTC/98 Conference. IEEE Instrumentation and Measurement Technology Conference. Where Instrumentation is going (Cat. No.98CH36222), 18-21 May 1998, IEEE, pp. 1168-1172

[10] Jankowski, M., Wozniak, A., and Byszewski, M., 2014, "Machine tool probes testing using a moving inner hemispherical master artefact," Precision Engineering, 38(2), pp. 421-427.

[11] Jankowski, M., and Wozniak, A., 2016, "Mechanical model of errors of probes for numerical controlled machine tools," Measurement: Journal of the International Measurement Confederation, 77, pp. 317-326.

[12] Verma, M. R., Chatzivagiannis, E., Jones, D., and Maropoulos, P. G., "Comparison of the measurement performance of high precision multi-axis metal cutting machine tools," Proc. International Conference on Digital Enterprise Technology - DET 2014 Disruptive Innovation in Manufacturing Engineering towards the 4th Industrial Revolution, March 25, 2014 - March 28, 2014, Elsevier, pp. 138-145.

[13] Ramesh, R., Mannan, M. A., and Poo, A. N., 2000, "Error compensation in machine tools - a review. Part II: Thermal errors," International Journal of Machine Tools and Manufacture, 40(9), pp. 1257-1284

[14] MARES Martin, HOREJS Otakar, HORNYCH Jan, SMOLIK Jan, “Robustness and portability of machine tool thermal error compensation model based on control of participating thermal sources”. Journal of Machine Engineering, Vol 13, No 1, 2013.

[15] JEDRZEJEWSKI Jerzy, KWASNY Wojciech, "Development Of Machine Tool Operational Properties". Journal of Machine Engineering, Vol 15, No 1, 2015.

[16] Mayer, J.R.R., Rahman, M.M., Los A., “An uncalibrated cylindrical indigenous artefact for measuring inter-axis errors of a five-axis machine tool”. CIRP Annals- Manufacturing Technology, Volume 64, Issue 1, 2015, Pages 487–490.

[17] JCGM, 102:2011, "Evaluation of measurement data – Supplement 2 to the “Guide to the expression of uncertainty in measurement” – Extension to any number of output quantities," GUM uncertainty framework.

CHAPTER 9 GENERAL DISCUSSION

The general discussion of the thesis highlights the significant outcomes of every stage of the study. The outcomes are discussed below in a chronological order.

In the first stage of this work, an on-machine probing approach called TANGO (Touch ANd GO) is proposed to probe facets on an existing machine tool table in order to gather machine geometric information. 28 rotary axes (A-, B- and C-axis) combinations are used to enrich the machine tool data. Primarily the TANGO method is applied to the machine table with flat surfaces followed by a machine tool table with cylindrical surfaces. Total 86 inter- and intra-axis error parameters are calibrated with and without a calibrated scale bar measurement. Four different parameter subsets are studied in the estimation process to observe the relative usefulness of the subgroups. TANGO is a self-calibration technique so the model also estimates the artefact. Hence, for the validation purpose the subsequent steps are followed:

- First, the artefact is measured by a CMM and then the TANGO estimated artefact is compared with the CMM artefact. The maximum value of the residual found is 3.43 μm with a standard deviation of 3.72 μm. The estimation model includes 86 inter- and intra-axis error parameters.
- In order to evaluate the predictability of the model, the probe stylus tip positions are calculated on the last workpiece branch frame (C-frame, firmly attached with the machine tool table) using the axis command of the facet probing and the estimated machine model for four different parameter subsets. Then the facet positions are compared with the CMM measured facets. The maximum residual distance found is 139.50 μm with standard deviation of 34.69 μm for the subset 01 (no parameters are included in the model) and the maximum residual distance found is 6.92 μm with standard deviation of 4.28 μm for the subset 04 (86 parameters are included in the model). Hence the estimation improves the model predictability significantly.
- To provide additional support to the predictability of the model, out of 28 ABC sets, 23 are used to estimate the parameters and the rest are used to predict the stylus tip position for the parameter subsets. The maximum residual distance is 80.27 with standard

deviation of 16.25 for the subset 01 and the maximum residual distance is 6.92 μm with standard deviation of 4.28 μm for the subset 04 hence a significant improvement is observed.

- The mean unexplained volumetric error norm is explained down from 25.93 μm to 1.38 μm (subset 01 to subset 04).

During the second stage of this work, the TANGO method is applied to a five-axis machine tool with an existing cylindrical machine table. Inter-axis error parameters are modelled (as scalar values acting at the different joints) and estimated. Different probing strategies are studied to observe the effect of probing point distribution. Effect of the machine tool status change on the parameter estimation at different period of the day and between consecutive days is also investigated. The key findings are:

- Distribution of the facets only in a shallow cylindrical section cannot alone estimate the machine parameters. The facets are requires to be distributed over at least two layers in the cylindrical section and the distance between the layers should be sufficiently large but adding a point on the surface of the cylinder improves the estimation. This implies that, constraining the artefact's degree of freedom is an important factor.
- Variation of the estimated parameters throughout a day period is higher compared to the variation of the parameters estimated at a particular time for consecutive days. The largest variation between days is around 10 μm where the variation throughout a day is over 40 μm.
- Parameter uncertainties show the similar tendency i.e. uncertainties pooled by cycles has the smaller values than those pooled by days. The least variation observed for E_{C0X} and E_{A0Z} where E_{B0C} shows the maximum variability.

In the third stage of this work, TANGO method is applied to a wCBXfZY(C1)t machine tool to investigate its performance as a coordinate measuring machine. The procedure described in this stage provides a simple and effective way to assess the machine's metrological capability by measuring objects using the rotary axes indexation combinations. Total 33 facets are measured on a precision sphere of 19.05 mm diameter using TANGO at 28 different Spindle-B-C axis

combinations. The measured coordinates are calculated on the table frame (firmly attached with the machine's last workpiece branch frame) using an uncompensated or nominal machine model and a compensated machine model. A perfect sphere is then fitted to the points using a Gauss-Newton algorithm that minimizes the sum of the squares of the radial distances between each point and the fitted sphere. The out of sphericity of the best fit sphere is analyzed. Two different probing strategies are studied to obtain the compensated model. In the first strategy 20 Spindle-B-C combinations are used which are also the subset of the machine calibration strategy and the other strategy has different Spindle-B-C combinations than the calibration strategy. The outcomes are as follows:

- Simulation shows that, squareness error of X-axis relative to Y-axis, the spindle offsets, X-offset of C-axis and the positioning error of Z-axis has significant influence on the out of sphericity of the sphere measured in a wCBXfZY(C1)t machine tools using TANGO method.
- Among the estimated parameters, the contribution of E_{X0S}, E_{Y0S}, E_{X0C}, E_{A0Y} and E_{ZZ} is higher compared to the other parameters to the overall machine errors hence their contribution to the out of sphericity is expected to be higher than the others. A good agreement is observed between the simulated results and the calibrated parameters.
- The out of sphericity and the standard deviation of the residuals are (268.27, 41.8) μm and (60.51, 10.36) μm for the nominal and the calibrated model respectively for strategy I.
- For the second strategy, the out of sphericity and the standard deviation of the residuals are (268.27, 41.8) μm and (71.12, 11.3) μm for the nominal and the calibrated model.

The factors that influence the measurement accuracy of the machine tools and the calibration performance are also investigated in this work. The remarks are given below.

- Machine tool's status change during the time of operation starting from the cold condition to the stable condition is approximately 10 μm.
- Surface irregularities contribute significant amount on the measurement inaccuracy when the surfaces on the X- and Y- direction are used. The value is around 3 to 6 μm.
- Surface wetness effect is significantly smaller or negligible.

- Directional repeatability of the probe has maximum standard deviation along Y-axis by 4.9 μm.
- Change in probing strategy by changing the facet locations affects E_{A0B}, E_{ZZ}, E_{A0Y} and E_{A0C} by a range of 7.37 μrad, 6.42 μm/m, 6.58 μrad and 6.9 μrad while the influence on other parameters are around or below 3 (μrad, μm or μm/m).
- Artefact dismount and remount cycle does not affects the parameter estimation since the artefact and tool setup errors are included in the mathematical model while estimating the error parameters and the dismount-remount cycles are quite repeatable.
- Probing strategy can be enhanced by optimizing the rotary axes indexation subsets. Condition number of the sensitivity matrix (Jacobian) for different probing strategy with the respective indexation subsets are used for this purpose. After studying more than 10 different rotary axes indexation subsets, E_{B0C}, E_{YY}, E_{B0Z} and E_{ZZ} shows noticeably higher standard deviation and uncertainties.

CHAPTER 10 CONCLUSION AND SCOPE OF FUTURE WORKS

10.1 Conclusion and original contribution

On-machine calibration of five-axis machine tool without the operator intervention is one of the most significant drawbacks found in the literature. Aside from this, almost all existing calibration techniques require external artefact or instruments. Mounting/dismounting these artefacts require precise setups and trained personnel; thus the overall calibration process increases the production down time. To facilitate uninterrupted manufacturing, this research work focused on developing a fully automated indirect machine tool inspection technique based on "in-situ" probing of an uncalibrated indigenous artefact. Several analytical and experimental investigations are performed throughout the development of the technique. The main contributions of this work are as follows:

- A new technique to probe facets on the indigenous (local) artefact is proposed and investigated based on the nominal geometry of the facets. The measured translational displacement between the probe stylus tip centers and the target facets as a constraint to estimate the error parameters. Facet probing requires a single measurement and the artefact is probed at different rotary axes combination to cover the axes motion range. The technique is new and never tested before.
- The proposed method is artefact geometry independent because the facets have a small used area where the geometric variations are negligible. The probing time is approximately 1 hour 30 minutes.
- A new strategy is proposed and tested to observe the machines' performance throughout a day and between consecutive days. Changes in calibrated parameters are larger throughout a day while the changes are significantly less between consecutive days. This can assists the machine user to conclude that, the machine errors estimated in a particular time of the day is no longer valid later or earlier on the same day.
- An out of sphericity test of a precision ball is proposed to assess the metrological capability of the machine tool. Facets on a precision sphere are measured in five-axis and

the data is processed with nominal and compensated model. The compensated model provides an improvement by a factor of 4.

- A detail investigation of the influence of calibration process variables such as probing strategy selection, facet location selection, artefact dismount/remount etc. on calibration repeatability is preformed which has never been addressed in literature.
- The inaccuracies of the measuring instrument, machine tool's status change over the time of operation, wet effect due to cutting fluid, probing repeatability, surface of the artefact etc. is also investigated.
- The proposed calibration method was adapted to the two laboratory machine tools successfully. Error model and measurement strategy is simulated for an industrial mill turn machine tool and the simulated results are satisfactory (simulation results are not presented here due to the confidential agreement with the industrial partners).
- The new calibration technique developed in this research is ready to implement in the increasingly popular mill turn machine tools with adjustable workpiece and tool branch for the aerospace manufacturing industries.

10.2 Scope of future works

As for most research work, there are always some prospects of improvements or further implementations. The following points associated with this research that can be suggested as future work:

- Even though the facet probing is artefact geometry independent, there is a possibility of cosine error when the probing is on a cylindrical surface. Hence a detail investigation of the influence of this cosine error can be conducted.
- Direct measurement methods can be applied to measure the maximum number of machine errors and compared with the calibrated parameters of the proposed technique. Laser interferometer can be used to measure linear axis positioning errors, Wollaston prism and a reflector with laser interferometer to measure straightness errors, angular interferometer

to measure angular errors and dial gauge to measure rotary axes radial and offset measurement.

- A comprehensive investigation can be done to optimize the probing strategy. The optimal distribution of the facets, number of facets at each machine pose and the optimized number of rotary axis indexation combinations can facilitate faster and effective calibration.
- Real time compensation of the calibrated parameters can be a milestone in automated manufacturing arena. An interface can be developed to correct the encoder readings of the axis movement based on the calibrated parameters and investigate the improvement on the machined parts.
- The proposed method was applied to the laboratory machine tools and proposed for industrial application. Error modeling and probing strategies are studied and verified through simulation but yet to be implemented. Since so many different factors (such as: vibration, ambient temperature etc.) can affect the calibration in an industrial environment therefore performance of the calibration by probing an indigenous artefact can be studied.

BIBLIOGRAPHY

(Renishaw plc - 2015). "Renishaw plc - Company Profile." Engineering and Management Services Retrieved 05-11-2015, 2015, from http://www.referenceforbusiness.com/history2/94/Renishaw-plc.html.

Abbaszadeh-Mir, Y., J. R. R. Mayer, et al. (2002). "Theory and simulation for the identification of the link geometric errors for a five-axis machine tool using a telescoping magnetic ball-bar." International Journal of Production Research **40**(18): 4781-4797.

Andolfatto, L., J. R. R. Mayer, et al. (2011). "Adaptive Monte Carlo applied to uncertainty estimation in five axis machine tool link errors identification with thermal disturbance." International Journal of Machine Tools and Manufacture **51**(7-8): 618-627.

Archenti, A. and M. Nicolescu (2013). "Accuracy analysis of machine tools using Elastically Linked Systems." CIRP Annals - Manufacturing Technology **62**(1): 503-506.

ASME (B5.54 : 2005). Methods for performance evaluation of Computer Numerically Controlled machining centers (revision of ASME B.54-1992).

ASME (B89.4.10360.2 : 2008). Acceptance Test and Reverification Test for Coordinate Measuring Machines (CMMs). Part 2: CMMs Used for Measuring Linear Dimensions.

Ballbar, T. R. Q. (1999-2009). "Ball bar test plots." Retrieved 19.10.2015, 2015, from http://www.renishaw.com/en/ballbar-20-for-qc20-w-and-qc10--11076.

Bringmann, B. and W. Knapp (2006). "Model-based 'Chase-the-Ball' calibration of a 5-axes machining center." CIRP Annals - Manufacturing Technology **55**(1): 531-534.

Bringmann, B., A. Kung, et al. (2005). "A measuring artefact for true 3D machine testing and calibration." CIRP Annals - Manufacturing Technology **54**(1): 471-474.

Castro, H. F. F. and M. Burdekin (2003). "Dynamic calibration of the positioning accuracy of machine tools and coordinate measuring machines using a laser interferometer." International Journal of Machine Tools & Manufacture **43**(9): 947-954.

Cauchick-Miguel, P. A. and T. G. Kings (1998). "Factors which influence CMM touch trigger probe performance." International Journal of Machine Tools and Manufacture **38**(4): 363-374.

Cheng, Q., H. Zhao, et al. (2015). "Machining accuracy reliability analysis of multi-axis machine tool based on Monte Carlo simulation."

Dobosz, M. and A. Wozniak (2003). "Metrological feasibilities of CMM touch trigger probes Part II: Experimental verification of the 3D theoretical model of probe pretravel." Measurement **34**(4): 287-299.

Dobosz, M. and A. Wozniak (2005). "CMM touch trigger probes testing using a reference axis." Precision Engineering **29**(3): 281-289.

Ekinci, T. O. and J. R. R. Mayer (2007). "Relationships between straightness and angular kinematic errors in machines." International Journal of Machine Tools and Manufacture **47**(12-13): 1997-2004.

Erkan, T. and J. R. R. Mayer (2010). "A cluster analysis applied to volumetric errors of five-axis machine tools obtained by probing an uncalibrated artefact." CIRP Annals - Manufacturing Technology **59**(Compendex): 539-542.

Erkan, T., J. R. R. Mayer, et al. (2011). "Volumetric distortion assessment of a five-axis machine by probing a 3D reconfigurable uncalibrated master ball artefact." Precision Engineering **35**(1): 116-125.

Everett, L. J. and A. H. Suryohadiprojo (1988). A study of kinematic models for forward calibration of manipulators. Proceedings of the 1988 IEEE International Conference on Robotics and Automation (Cat. No.88CH2555-1), 24-29 April 1988, Washington, DC, USA, IEEE Comput. Soc. Press.

Fesperman, R. R., S. P. Moylan, et al. (2010). Methods, practices, and standards for evaluating on-machine touch trigger probing of workpieces. 25th Annual Meeting of the American Society for Precision Engineering, ASPE 2010, October 31, 2010 - November 4, 2010, Atlanta, GA, United states, American Society for Precision Engineering, ASPE.

Guiassa, R., J. R. R. Mayer, et al. (2014). "Closed door machining error compensation of complex surfaces using the cutting compliance coefficient and on-machine measurement for a milling process."

Hong, C. and S. Ibaraki (2013). "Non-contact R-test with laser displacement sensors for error calibration of five-axis machine tools." Precision Engineering **37**(1): 159-171.

Hong, C., S. Ibaraki, et al. (2011). "Influence of position-dependent geometric errors of rotary axes on a machining test of cone frustum by five-axis machine tools." Precision Engineering **35**(1): 1-11.

Hong, C., S. Ibaraki, et al. (2012). "Graphical presentation of error motions of rotary axes on a five-axis machine tool by static R-test with separating the influence of squareness errors of linear axes." International Journal of Machine Tools and Manufacture **59**: 24-33.

Ibaraki, S., T. Iritani, et al. (2012). "Calibration of location errors of rotary axes on five-axis machine tools by on-the-machine measurement using a touch-trigger probe." International Journal of Machine Tools and Manufacture **58**: 44-53.

Ibaraki, S., Y. Kimura, et al. (2015). "Formulation of influence of machine geometric errors on five-axis on-machine scanning measurement by using a laser displacement sensor." Journal of Manufacturing Science and Engineering, Transactions of the ASME **137**(2).

Ibaraki, S., M. Sawada, et al. (2010). "Machining tests to identify kinematic errors on five-axis machine tools." Precision Engineering **34**(3): 387-398.

ISO (2008). Evaluation of measurement data – Guide to the expression of uncertainty in measurement

ISO (2008). Evaluation of measurement data – Supplement 1 to the "Guide to the expression of uncertainty in measurement" – Propagation of distributions using a Monte Carlo method, ISO. JCGM 101:2008.

ISO (2012). Test Code for Machine Tools-Part 1: Geometric accuracy of machines operating under no-load or quasi-static conditions. 230-1.

ISO (10360-3 : 2000). Geometrical Product Specifications (GPS) -- Acceptance and reverification tests for coordinate measuring machines (CMM) Part 3: CMMs with the axis of a rotary table as the fourth axis.

ISO/DIS (230-10 : 2011). Test code for machine tools-Part 10: Determination of measuring performance of probing systems of numerically controlled machine tools.

ISO/DIS (230-10 : 2011). Test code for machine tools Part 10: Determination of measuring performance of probing systems of numerically controlled machine tools.

Jankowski, M. and A. Wozniak (2016). "Mechanical model of errors of probes for numerical controlled machine tools." Measurement: Journal of the International Measurement Confederation **77**: 317-326.

Jankowski, M., A. Wozniak, et al. (2014). "Machine tool probes testing using a moving inner hemispherical master artefact." Precision Engineering **38**(2): 421-427.

JCGM (102:2011). Evaluation of measurement data – Supplement 2 to the "Guide to the expression of uncertainty in measurement" – Extension to any number of output quantities. GUM uncertainty framework.

Johnson, R. P., Y. Qingping, et al. (1998). Dynamic error characteristics of touch trigger probes fitted to coordinate measuring machines. IMTC/98 Conference. IEEE Instrumentation and Measurement Technology Conference. Where Instrumentation is Going (Cat. No.98CH36222), 18-21 May 1998, USA, IEEE.

Khan, A. W. and W. Chen (2011). "A methodology for systematic geometric error compensation in five-axis machine tools." International Journal of Advanced Manufacturing Technology **53**(Compendex): 615-628.

Lei, W. T. and Y. Y. Hsu (2002). "Accuracy test of five-axis CNC machine tool with 3D probe-ball. Part I: Design and modeling." International Journal of Machine Tools and Manufacture **42**(10): 1153-1162.

Lei, W. T. and Y. Y. Hsu (2002). "Accuracy test of five-axis CNC machine tool with 3D probe-ball. Part II: Errors estimation." International Journal of Machine Tools and Manufacture **42**(10): 1163-1170.

Lei, W. T. and Y. Y. Hsu (2003). "Error measurement of five-axis CNC machines with 3D probe–ball." Journal of Materials Processing Technology **139**(1-3): 127-133.

Mayer, J. R. R. (2012). "Five-axis machine tool calibration by probing a scale enriched reconfigurable uncalibrated master balls artefact." CIRP Annals - Manufacturing Technology **61**(1): 515-518.

Mir, Y. A., J. R. R. Mayer, et al. (2002). "Tool path error prediction of a five-axis machine tool with geometric errors." Proceedings of the Institution of Mechanical Engineers, Part B: Journal of Engineering Manufacture **216**(5): 697-712.

Mou, J. and C. R. Liu (1995). "Adaptive methodology for machine tool error correction." Journal of Engineering for Industry, Transactions of the ASME **117**(3): 389-399.

Rahman, M. M. and J. R. R. Mayer (2015). "Five axis machine tool volumetric error prediction through an indirect estimation of intra- and inter-axis error parameters by probing facets on a scale enriched uncalibrated indigenous artefact." Precision Engineering **40**(0): 94-105.

Ramesh, R., M. A. Mannan, et al. (2000). "Error compensation in machine tools - a review. Part I: Geometric, cutting-force induced and fixture-dependent errors." International Journal of Machine Tools and Manufacture **40**(9): 1235-1256.

Ramesh, R., M. A. Mannan, et al. (2000). "Error compensation in machine tools - a review. Part II: Thermal errors." International Journal of Machine Tools and Manufacture **40**(9): 1257-1284.

Schwenke, H., W. Knapp, et al. (2008). "Geometric error measurement and compensation of machines—An update." CIRP Annals - Manufacturing Technology **57**(2): 660-675.

Shaowei, Z., D. Guofu, et al. (2012). "Integrated geometric error modeling, identification and compensation of CNC machine tools." International Journal of Machine Tools & Manufacture **52**(1): 24-29.

Slamani, M., J. R. R. Mayer, et al. (2011). "Modeling and Experimental Validation of Machine Tool Motion Errors Using Degree Optimized Polynomial Including Motion Hysteresis." Experimental Techniques **35**(1): 37-44.

Srivastava, A. K., S. C. Veldhuis, et al. (1995). "Modelling geometric and thermal errors in a five-axis CNC machine tool." International Journal of Machine Tools and Manufacture **35**(9): 1321-1337.

Suh, S.-H., E.-S. Lee, et al. (1998). "Error modelling and measurement for the rotary table of five-axis machine tools." International Journal of Advanced Manufacturing Technology **14**(9): 656-663.

Tsutsumi, M. and A. Saito (2003). "Identification and compensation of systematic deviations particular to 5-axis machining centers." International Journal of Machine Tools & Manufacture **43**(8): 771-780.

Tsutsumi, M. and A. Saito (2004). "Identification of angular and positional deviations inherent to 5-axis machining centers with a tilting-rotary table by simultaneous four-axis control movements." International Journal of Machine Tools & Manufacture **44**(12-13): 1333-1342.

Veldhuis, S. C. and M. A. Elbestawi (1995). "A Strategy for the Compensation of Errors in Five-Axis Machining." CIRP Annals - Manufacturing Technology **44**(1): 373-377.

Verma, M. R., E. Chatzivagiannis, et al. (2014). Comparison of the measurement performance of high precision multi-axis metal cutting machine tools. International Conference on Digital Enterprise Technology - DET 2014 Disruptive Innovation in Manufacturing Engineering towards the 4th Industrial Revolution, March 25, 2014 - March 28, 2014, Stuttgart, Germany, Elsevier.

Weckenmann, A. and J. Lorz (2005). Monitoring coordinate measuring machines by calibrated parts. Seventh International Sympsoium on Measurement Technology and Intelligent Instruments, 6-8 Sept. 2005, UK, IOP Publishing.

Weikert, S. and W. Knapp (2004). "R-test, a new device for accuracy measurements on five axis machine tools." CIRP Annals - Manufacturing Technology **53**(1): 429-432.

Wozniak, A. and M. Dobosz (2003). "Metrological feasibilities of CMM touch trigger probes. Part I: 3D theoretical model of probe pretravel." Measurement **34**(4): 273-286.

Wozniak, A. and M. Dobosz (2005). "Factors influencing probing accuracy of a coordinate measuring machine." IEEE Transactions on Instrumentation and Measurement **54**(6): 2540-2548.

Wozniak, A. and M. Dobosz (2005). "Influence of measured objects parameters on CMM touch trigger probe accuracy of probing." Precision Engineering **29**(3): 290-297.

Zargarbashi, S. H. H. and J. R. R. Mayer (2006). "Assessment of machine tool trunnion axis motion error, using magnetic double ball bar." International Journal of Machine Tools and Manufacture **46**(14): 1823-1834.

Zargarbashi, S. H. H. and J. R. R. Mayer (2009). "Single setup estimation of a five-axis machine tool eight link errors by programmed end point constraint and on the fly measurement with Capball sensor." International Journal of Machine Tools and Manufacture **49**(Compendex): 759-766.